**Technical Report Documentation Page**

| 1. Report No. | 2. Government Accession No. | 3. Recipients's Catalog No. |
|---|---|---|
| 4. Title and Subtitle<br>Quasi Static and Dynamic Roof Crush Testing | | 5. Report Date<br>June 1998<br>6. Performing Organization Code<br>NRD-23 |
| 7. Author(s)<br>Glen C. Rains and Michael A. Van Voorhis | | 8. Performing Organization Report No.<br>VRTC-82-0197/VRTC-86-0391 |
| 9. Performing Organization Name and Address<br>National Highway Traffic Safety Administration<br>Vehicle Research and Test Center<br>P.O. Box 37<br>East Liberty, OH 43319 | | 10. Work Unit No. (TRAIS)n code<br>11. Contract of Grant No. |
| 12. Sponsoring Agency Name and Address<br>National Highway Traffic Safety Administration<br>400 Seventh Street, S.W.<br>Washington, DC 20590 | | 13. Type of Report and Period Covered<br>Final Report<br>14. Sponsoring Agency Code |
| 15. Supplementary Notes | | |

16. Abstract

A study was conducted at the Vehicle Research and Test Center to investigate roof crush resistance in passenger vehicles. The objective was to determine the correlation between roof crush performance measured quasi-statically and dynamically. Currently, FMVSS No. 216 sets requirements for roof crush resistance using a quasi-static load applied to the vehicle roof. This load application is not representative of real-world loading rates of roof structures in a rollover collision. A series of tests comparing quasi-static roof loading versus dynamic roof loading was conducted to determine how static and dynamic tests can be correlated and if static test can be transformed to a dynamically equivalent result.

Nine vehicles were selected for the quasi-static tests. Subsets of this group were subject to 1) FMVSS 216 test procedure, 2) incremental crush testing, and 3) modified crush angle (roll and pitch.) Each vehicle was then ranked for performance, based on roof strength and stiffness .

Based on the roof structure performance of the quasi-static tests, six vehicles were tested by dropping them on their roofs (dynamic drop test.) Dynamic force vs. crush and energy vs. crush were plotted. The slope of the dynamic energy vs. crush plots were compared to the static tests. The slopes of the dynamic test were 1.1 to 1.6 times the static crush slopes for all six vehicles.

A multiple regression of static and dynamic testing was performed to develop an equation for predicting a dynamic energy slope from static data. The equation had a correlation coefficient of 0.94. To validate the equation, another vehicle was selected and the vehicle roof crushed quasi-statically. The equation was then used to predict the dynamic performance. The same vehicle type was then drop tested at two drop heights to obtain actual dynamic roof crush data. An 8% and 17% error was found in the predicted dynamic energy slope.

| 17. Key Words | | 18. Distribution Statement | |
|---|---|---|---|
| FMVSS 216<br>Roof Crush | | Document is available to the public through the National Technical Information Service, Springfield, VA 22161 | |
| 19. Security Classif. (of this report)<br>Unclassified | 20. Security Classif. (of this page)<br>Unclassified | 21. No of Pages | 22. Price |

**Form DOT F1700.7 (8-72)** **Reproduction of completed page authorized**

**Metric Conversion Factors**

## TABLE OF CONTENTS

**Section** **Page**


Technical Report Documentation Page . . . . . i

Metric Conversion Factors . . . . . ii

TABLE OF CONTENTS . . . . . iii

LIST OF FIGURES . . . . . v

LIST OF TABLES . . . . . ix

LIST OF EQUATIONS . . . . . ix

1.0 INTRODUCTION . . . . . 1
- 1.1 Background . . . . . 1
- 1.2 Objective . . . . . 3

2.0 Static Tests . . . . . 3
- 2.1 Test Set-up . . . . . 4
- 2.2 Test Matrix . . . . . 6
- 2.3 Static roof Crush results . . . . . 9

3.0 Drop Tests onto Floor . . . . . 21
- 3.1 Approach . . . . . 23
- 3.2 Test Matrix for Vehicles Dropped onto Floor . . . . . 25
- 3.3 Floor Drop Results . . . . . 25

4.0 Drop Tests onto Load Plate . . . . . 31
- 4.1 Approach . . . . . 31
- 4.2 Test Matrix . . . . . 33
- 4.3 Load Plate Drop Test Results for 6 Vehicles . . . . . 33

5.0 Static and Dynamic Test Comparison . . . . . 34
- 5.1 Crush Energy . . . . . 34
- 5.2 Statistical Analysis . . . . . 41
- 5.3 Validating Regression Model . . . . . 48

6.0 Summary and Conclusions: . . . . . 50

7.0 References . . . . . 55

**TABLE OF CONTENTS**
**(Continued)**

**Section** **Page**

Appendix A . . . . . 57

Appendix B . . . . . 70

Appendix C . . . . . 79

Appendix D . . . . . 92

Appendix E . . . . . 105

## LIST OF FIGURES

**Page**

**Figure 1**-Test device location and application to the roof. . . . . 4
**Figure 2** Grid layout for roof profiles . . . . . 5
**Figure 3**-Post test photograph of Nissan pickup in quasi-static test device. . . . . 8
**Figure 4**-Photo showing head form used to measure headroom reduction . . . . . 9
**Figure 5**-Overlaid plots of test data before it is concatenated. . . . . 10
**Figure 6**-Force/crush plot for the Nissan pickup tested quasi-statically. . . . . 12
**Figure 7**-Energy/crush plot and regression line for the Nissan pickup. . . . . 12
**Figure 8**-Force/crush plot for the Dodge Colt tested quasi-statically. . . . . 13
**Figure 9**-Energy/crush and regression line plot for Dodge Colt tested quasi-statically. . . . . 13
**Figure 10**-Roof profiles for the Nissan pickup tested quasi-statically. . . . . 14
**Figure 11**-Roof profiles for Dodge Colt tested quasi-statically. . . . . 15
**Figure 12**-Corridor for static force deflection curves. . . . . 19
**Figure 13**-Corridor for static energy deflection curves. . . . . 20
**Figure 14**-Corridor for normalized static energy deflection curves. . . . . 20
**Figure 15**-Illustration of floor drop procedure. . . . . 24
**Figure 16**-Pre-test photo of floor drop test. . . . . 26
**Figure 17**-Photo showing placement of accelerometers used in the floor drop tests. . . . . 26
**Figure 18**-Post test photo of the Nissan. . . . . 28
**Figure 19**-Roof profile of the Nissan. . . . . 28
**Figure 20(a)**-Plot for drop angle analysis . . . . . 30
**Figure 20(b)**-Plot for drop angle analysis . . . . . 30
**Figure 20(c)**-Plot for drop angle analysis . . . . . 30
**Figure 20(d)**-Plot for drop angle analysis . . . . . 30
**Figure 21**-Load plate. . . . . 32
**Figure 22**-Setup. . . . . 32
**Figure 23**-Load plate layout. . . . . 32
**Figure 24**-Force/crush curve for the Nissan drop test onto the load plate. . . . . 35
**Figure 25**-Energy/crush curve for the Nissan drop test onto the load plate. . . . . 35
**Figure 26**-Force/crush curve for the Colt drop test onto the load plate. . . . . 36
**Figure 27**-Energy/crush curve for the Colt drop test onto the load plate. . . . . 36
**Figure 28**-Quasi-static vs. Dynamic drop for force/crush data. . . . . 38
**Figure 29**-Quasi-static vs. Dynamic drop for energy/crush data. . . . . 39
**Figure 30**-Quasi-static vs. Dynamic drop for regression data. . . . . 40
**Figure 31**-Caprice drop height comparison of force/crush. . . . . 45
**Figure 32**-Cavalier drop height comparison of force/crush. . . . . 45
**Figure 33**-Caprice drop height comparison of energy/crush. . . . . 46
**Figure 34**-Cavalier drop height comparison of energy/crush. . . . . 46
**Figure 35**-Caprice drop height comparison for regressions. . . . . 47
**Figure 36**-Cavalier drop height comparison for regressions. . . . . 47
**Figure 37**-Dodge Neon force/crush curve for quasi-static test. . . . . 48

## LIST OF FIGURES
## (Continued)


**Page**

**Figure 38**-Dodge Neon energy/crush and regression curves for quasi-static test. . . . . 49
**Figure 39**-Dodge Neon regression lines for quasi-static test vs. predicted. . . . . 49
**Figure 40**-Dodge Neon regression lines for predicted vs. actual at 2 heights. . . . . 50
**Figure A(1)**-Nissan #1 quasi-static tests roof crush profiles. . . . . 58
**Figure A(2)**-Nissan #2 quasi-static tests roof profiles. . . . . 59
**Figure A(3)**-Dodge Colt #1 quasi-static tests roof crush profiles. . . . . 60
**Figure A(4)**-Dodge Colt #2 quasi-static tests roof crush profiles. . . . . 61
**Figure A(5)**-Chevy Cavalier #1 quasi-static tests roof profiles. . . . . 62
**Figure A(6)**-Honda Accord quasi-static tests roof profiles. . . . . 63
**Figure A(7)**-Chevy Caprice #1 quasi-static tests roof crush profiles. . . . . 64
**Figure A(8)**-Ford Explorer #1 quasi-static tests roof crush profiles. . . . . 65
**Figure A(9)**-Chevy CK-1500 quasi-static tests roof crush profiles. . . . . 66
**Figure A(10)**-Ford Taurus #1 quasi-static tests roof crush profiles. . . . . 67
**Figure A(11)**-Ford Taurus #2 quasi-static tests roof crush profiles. . . . . 68
**Figure A(12)**-Dodge Neon #1 quasi-static tests roof crush profiles. . . . . 69
**Figure B(1)**-Nissan #4 floor drop test roof crush profiles. . . . . 71
**Figure B(2)**-Nissan #5 multiple floor drop tests roof crush profiles. . . . . 72
**Figure B(3)**-Nissan #7 floor drop test roof crush profiles. . . . . 73
**Figure B(4)**-Nissan #8 multiple floor drop tests roof crush profiles. . . . . 74
**Figure B(5)**-Dodge Colt #3 floor drop test roof crush profiles. . . . . 75
**Figure B(6)**-Dodge Colt #4 multiple floor drop tests roof crush profiles. . . . . 76
**Figure B(7)**-Dodge Colt #5 floor drop test roof crush profiles. . . . . 77
**Figure B(8)**-Dodge Colt #6 multiple floor drop tests roof crush profiles. . . . . 78
**Figure C(1)**-Nissan #10 load plate drop test roof profiles. . . . . 80
**Figure C(2)**-Dodge Colt #7 load plate drop test roof crush profiles. . . . . 81
**Figure C(3)**-Chevy Cavalier #2 load plate drop test roof crush profiles. . . . . 82
**Figure C(4)**-Chevy Cavalier #3 load plate drop test roof crush profiles. . . . . 83
**Figure C(5)**-Chevy Cavalier #4 load plate drop test roof crush profiles. . . . . 84
**Figure C(6)**-Ford Taurus #3 load plate drop test roof crush profiles. . . . . 85
**Figure C(7)**-Chevy Caprice #2 load plate drop test roof crush profiles. . . . . 86
**Figure C(8)**-Chevy Caprice #3 load plate drop test roof crush profiles. . . . . 87
**Figure C(9)**-Chevy Caprice #4 load plate drop test roof crush profiles. . . . . 88
**Figure C(10)**-Ford Explorer #2 load plate drop test roof crush profiles. . . . . 89
**Figure C(11)**-Plymouth Neon #2 load plate drop test roof crush profiles. . . . . 90
**Figure C(12)**-Plymouth Neon #3 load plate drop test roof crush profiles. . . . . 91
**Figure D(1)**-Nissan #1 quasi-static test force/crush curve. . . . . 93
**Figure D(2)**-Nissan #1 quasi-static test energy/crush curve. . . . . 93
**Figure D(3)**-Nissan #2 quasi-static test force/crush curve. . . . . 94
**Figure D(4)**-Nissan #2 quasi-static test energy/crush curve. . . . . 94

## LIST OF FIGURES
## (Continued)


Page

**Figure D(5)**-Dodge Colt #1 quasi-static test force/crush curve. . . . . 95
**Figure D(6)**-Dodge Colt #1 quasi-static test energy/crush curve. . . . . 95
**Figure D(7)**-Dodge Colt #2 quasi-static test force/crush curve. . . . . 96
**Figure D(8)**-Dodge Colt #2 quasi-static test energy/crush. curve . . . . . 96
**Figure D(9)**-Chevy Cavalier #1 quasi-static test force/crush curve. . . . . 97
**Figure D(10)**-Chevy Cavalier #1 quasi-static test energy/crush curve. . . . . 97
**Figure D(11)**-Honda accord quasi-static test force/crush curve. . . . . 98
**Figure D(12)**-Honda Accord quasi-static test energy/crush curve. . . . . 98
**Figure D(13)**-Chevy Caprice #1 quasi-static test force/crush curve. . . . . 99
**Figure D(14)**-Chevy Caprice #1 quasi-static test energy/crush curve. . . . . 99
**Figure D(15)**-Ford Explorer #1 quasi-static test force/crush curve. . . . . 100
**Figure D(16)**-Ford Explorer #1 quasi-static test energy/crush curve. . . . . 100
**Figure D(17)**-Chevy CK-1500 PU quasi-static test force/crush curve. . . . . 101
**Figure D(18)**-Chevy CK-1500 PU quasi-static test energy/crush curve . . . . . 101
**Figure D(19)**-Ford Taurus #1 quasi-static test force/crush curve. . . . . 102
**Figure D(20)**-Ford Taurus #1 quasi-static test energy/crush curve. . . . . 102
**Figure D(21)**-Ford Taurus #2 quasi-static test force/crush curve. . . . . 103
**Figure D(22)**-Ford Taurus #2 quasi-static test energy/crush curve. . . . . 103
**Figure D(23)**-Dodge Neon #1 quasi-static test force/crush curve. . . . . 104
**Figure D(24)**-Dodge Neon #1 quasi-static test energy/crush curve. . . . . 104
**Figure E(1)**-Nissan #10 load plate drop test force/crush curve. . . . . 106
**Figure E(2)**-Nissan #10 load plate drop test energy/crush curve. . . . . 106
**Figure E(3)**-Plymouth Colt #7 load plate drop test force/crush curve. . . . . 107
**Figure E(4)**-Plymouth Colt #7 load plate drop test energy/crush curve. . . . . 107
**Figure E(5)**-Chevy Cavalier #2 load plate drop test force/crush curve. . . . . 108
**Figure E(6)**-Chevy Cavalier #2 load plate drop test energy/crush curve. . . . . 108
**Figure E(7)**-Chevy Cavalier #3 load plate drop test force/crush curve. . . . . 109
**Figure E(8)**-Chevy Cavalier #3 load plate drop test energy/crush curve. . . . . 109
**Figure E(9)**-Chevy Cavalier #4 load plate drop test force/crush curve. . . . . 110
**Figure E(10)**-Chevy Cavalier #4 load plate drop test energy/crush curve . . . . . 110
**Figure E(11)**-Ford Taurus #3 load plate drop test force/crush curve. . . . . 111
**Figure E(12)**-Ford Taurus #3 load plate drop test energy/crush curve. . . . . 111
**Figure E(13)**-Ford Explorer #2 load plate drop test force/crush curve . . . . . 112
**Figure E(14)**-Ford Explorer #2 load plate drop test energy/crush curve. . . . . 112
**Figure E(15)**-Chevy Caprice #2 load plate drop test force/crush curve. . . . . 113
**Figure E(16)**-Chevy Caprice #2 load plate drop test energy/crush curve. . . . . 113
**Figure E(17)**-Chevy Caprice #3 load plate drop test force/crush curve. . . . . 114
**Figure E(18)**-Chevy Caprice #3 load plate drop test energy/crush curve. . . . . 114
**Figure E(19)**-Chevy Caprice #4 load plate drop test force/crush curve. . . . . 115
**Figure E(20)**-Chevy Caprice #4 load plate drop test energy/crush curve. . . . . 115

**LIST OF FIGURES**
**(Continued)**

**Page**

**Figure E(21)-** Plymouth Neon #2 load plate drop test force/crush curve. . . . . 116
**Figure E(22)-** Plymouth Neon #2 load plate drop test energy/crush curve. . . . . 116
**Figure E(23)-** Plymouth Neon #3 load plate drop test force/crush curve . . . . . 117
**Figure E(24)-** Plymouth Neon #3 load plate drop test energy/crush curve . . . . . 117

## LIST OF TABLES

**Page**

**Table 1**-Quasi-static test matrix. . . . . 7
**Table 2**-Results from test at different load plate angles for the Nissan and the Colt. . . . . 16
**Table 3**-Summary of crush characteristics for test at 5° Pitch, 25° Roll angle. . . . . 17
**Table 4**-Summary showing crush at head contact results. . . . . 18
**Table 5**-Summary of vehicle ranking from quasi-static testing. . . . . 22
**Table 6**-Test matrix for floor drop tests. . . . . 27
**Table 7**-Summary of roof crush measurements for drop tests. . . . . 29
**Table 8**-Test matrix for drop tests onto load plate. . . . . 33
**Table 9**-Summary of vehicle ranking using dynamic data. . . . . 37
**Table 10**-Data used in statistical analysis. . . . . 42
**Table 11**-Results of statistical analysis. . . . . 42
**Table 12**-Results from application of the prediction equation. . . . . 43
**Table 13**-Test matrix for drop height analysis testing. . . . . 44

## LIST OF EQUATIONS

**Page**

**[1]** Head Room Reduction . . . . . 6
**[2]** Drop Height . . . . . 23
**[3]** C. G. Location . . . . . 24
**[4]** Dynamic Slope Prediction . . . . . 41

## 1.0 INTRODUCTION

### 1.1 Background

In the 1990 fatal automobile reporting system (FARS), there were over 15,000 single-vehicle automobile crash fatalities [1]*. Of those, over half were from rollover crashes. Although large portions of the fatal injuries are caused by ejection, rollover safety for non-ejected occupants is also of great concern.

The current Federal Motor Vehicle Safety Standard (FMVSS) No. 216 [2] requires that a passenger car roof withstand a load of 1.5 times the vehicle's unloaded weight in kilograms multiplied by 9.8 or 22,240 Newtons, whichever is less, to either side of the forward edge of the vehicle's roof with no more than 125 mm of crush. The same standard also applies to light trucks and vans (LTV's) with a GVWR of 2,722 kilograms or less, without the 22,240 Newton force limit. This standard has been criticized for being a static test which does not represent real-world rollover events.

In an effort to reduce the fatalities and injuries to non-ejected occupants by roof intrusion, the NHTSA is investigating the possibility of upgrading FMVSS No. 216. The NHTSA has previously investigated various concepts that would improve roof intrusion resistance. A historical perspective is presented below.

From the mid-80's to early 90's a series of tests were conducted with a rollover cart [3]. This rollover cart was propelled at 30 mph and brought to a stop. As the cart was brought to a stop, the vehicle was propelled by pneumatic cylinders with its roll axis perpendicular to the motion of the rollover device. The tests were conducted to measure the roof integrity and failure modes in a rollover event. This test proved to be very severe and difficult to use to discriminate between good and bad performing roof structures. Additionally, these rollovers were inherently non-repeatable, leading to a dead-end in the possible development of an improved roof crush standard based on dynamic rollover testing.

Several studies by Wright Patterson Air Force Base (WPAFB) were also initiated to simulate the rollover dynamics of rollover tests and actual rollover crashes. An Articulated Total Body (ATB) computer model was used to simulate the roll kinematics from a real-world rollover crash resulting in occupant injury [4]. The ATB model proved to be useful in re-creating the vehicle motion from the crash investigation information and predicting occupant ejection.

Countermeasures to roof intrusion were investigated in a series of tests with a modified Nissan Pick-up [5]. The Nissan pick-up was chosen since it had the most repeatable rollover with the rollover cart. Countermeasures involving foam reinforcements in the joints between the roof header, side rails and A- and B-pillars were first investigated. Further enhancements to the roof structure strength were added through additional steel reinforcements. Substantial improvement to the roof integrity was found, however the severity of the rollover test made it difficult to prevent severe intrusion.

In each of these studies, the primary objectives were to investigate possible countermeasures to prevent severe roof crush and ways to test for roof crush strength. Each study involved full-scale rollover tests or real-world crashes in their investigations. While these are good research tools, the use of a full-scale rollover test would not be repeatable enough to incorporate into a federal regulation to improve roof crush strength.

Since a full-scale rollover test has yet to be shown to be repeatable, NHTSA began investigating other possible test procedures for upgrading the FMVSS No. 216. One option to upgrade FMVSS No. 216 is to continue using a static test that is set to some dynamically equivalent severity. A static test is advantageous by its repeatability. Roof structure failure modes are also similar to rollover tests and real-world collisions [8]. However, it may not be representative of real-world dynamic performance. A dynamic drop test onto the vehicle roof may be an intermediary step that adds a dynamic load to the roof, but does not introduce rollover forces. This test would introduce a difficult procedure for turning the vehicle upside down to drop on its roof, would not be as repeatable as a static test, but would be more repeatable than a full-scale rollover test.

## 1.2 Objective

This report examines the current characteristics of the roof structure when loaded quasi-statically and dynamically in a drop test. The primary objective was to determine the characteristics of a quasi-static test and a dynamic drop test. If the static test results can be transformed to dynamically equivalent test results, FMVSS No. 216 could be upgraded using a more repeatable and simpler static test.

## 2.0 STATIC TESTS

A test plan was developed to examine the roof strength characteristics for vehicles in production. Nine vehicle models were selected that had high sales volume and represented the various vehicle classes (passenger cars and LTV's) and domestic and foreign manufacturers. Each vehicle was tested by quasi-statically crushing the roof to different crush levels and different load angles. The objective of these tests were to:

1. Conduct a fleet study of vehicle roof stiffness, strength and energy when a quasi-static load is applied.

2. Examine angles of the test plate and their effect on roof strength and stiffness when a quasi-static load is applied.

3. Characterize the roof failure characteristics when a quasi-static load is applied.

## 2.1 Test Set-up

The test procedure and devices for quasi-static roof crush testing are described in FMVSS No. 216, Roof Crush Resistance. The quasi-static load on the roof was applied with a rigid, unyielding flat rectangular plate, 762 mm x 1829 mm (30" x 72"). This plate was oriented at a longitudinal angle of 5° below horizontal and a lateral angle of 25° below the horizontal, as shown in Figure 1. The plate was positioned above each vehicle so that the first contact point on the roof was on the longitudinal centerline of the plate at a point 254 mm (10") behind the forward most edge of the plate. This procedure is intended to simulate the roof contact with the ground in an actual rollover event. A quasi-static load was then applied to the roof at a rate of 13 mm (.5") per second and in a direction normal to the load plate surface.

Each vehicle roof was marked at specific intervals and digitized into X, Y, and Z coordinates to generate a roof profile prior to testing (Figure 2). This grid layout was constructed using the dimensions of the pillars and rooftop to determine the number of points needed to accurately construct the roof profile. Each pillar was defined by 5 points with spacing between each point

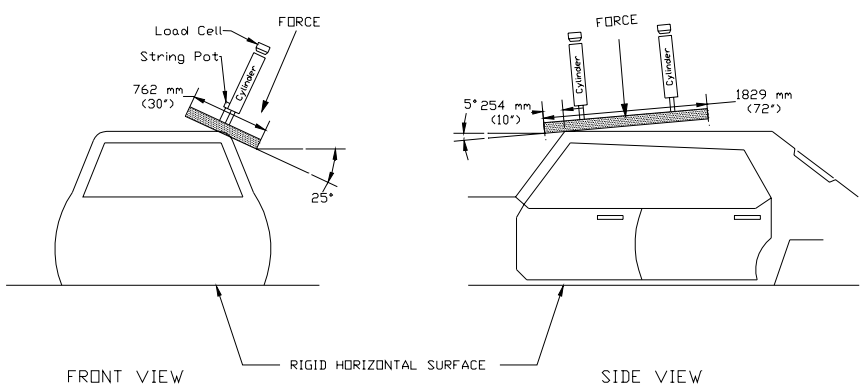


**Figure 1**-Test device location and application to the roof.

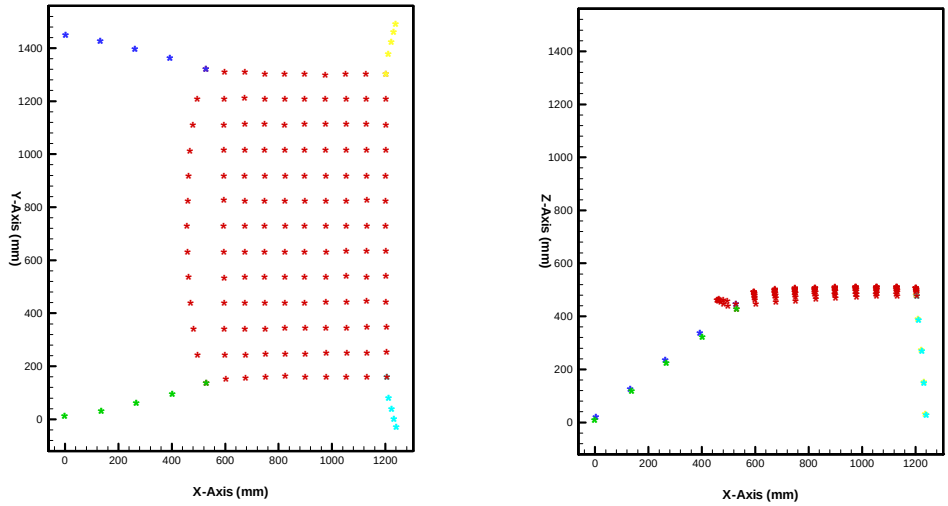


**Figure 2**-Grid layout for roof profiles.

being 1/4 the measured length of the pillar. The points of the rooftop grid were spaced at 100 mm (4") intervals in the X and Y directions.

To ensure accurate measurements each vehicle was secured to the sub frame of the test fixture, which required removing the wheels and securing the vehicles frame with chains and turn buckles. Force data was collected with 2 load cells placed at the end of the hydraulic cylinders and connected to the top of the test device (Figure 1). Each load cell (manufactured by Interface™) had a 111,205 N (25,000 lbs) rating. Deflection of the roof was measured with string pots connected to each of the cylinders, as shown in Figure 1. The string pots (manufactured by Celesco™ and Rayelco™) and each had a full scale rating of 1321 mm (52"). The data was collected using a Metraplex™ data acquisition system at a 20 Hz sample rate.

A 50$^{th}$ percentile male dummy head form was placed in the occupant compartment to mark the point during roof crush where the occupants head was contacted by the roof. The head form was positioned so that its CG was at a predetermined distance and angle from the H-point. The H-point for the driver was determined for each vehicle using the dimensions found from the procedure described by SAE standard J826, "Devices for use in defining and measuring vehicle seating

accommodations for a 50th percentile male HIII dummy." Head room is defined for the purposes of this paper as the vertical space between the top of an occupants head and the roof when normally seated. When roof crush takes place, the head room is reduced. Percent headroom reduction is then

$$HRR = \frac{RC * \cos\beta * \cos\theta}{HR} * 100\% \qquad \textbf{[1]}$$

defined as:

where,

ß = plate roll angle,

θ = plate pitch angle,

RC = load plate displacement,

HR = vertical distance from top of head to roof interior for a 50th percentile male , and

HRR = percent head room reduction for a 50th percentile male (%).

The reduction in vertical space between the occupant and roof is assumed to be equal to the vertical component of the displacement of the load plate.

## 2.2 Test Matrix

Initially, two vehicle models (1989 Dodge Colt and 1989 Nissan pickup) were tested to examine the effect of load plate angle on roof crush resistence. First, the roofs were crushed following the FMVSS 216 procedures. That is, the load plate angles were set at 5° pitch and 25° roll, and the roofs were crushed to a force equal to 1.5 times the vehicle weight. Three additional tests were then performed on each vehicle. In the first of these, the roof was crushed until the load plate had displaced 127 mm (5") after first contact [note: The point of first contact was defined as the point of initial contact between the load plate and the undeformed roof, prior to the FMVSS 216 type test]. The next test crushed the roof until the plate had displaced a total of 254 mm (10") from

first contact, and the last test crushed the roof until the plate had displaced a total of 381 mm (15") from first contact. After each test, the roof was unloaded and the roof profile was digitized to record the post-test roof crush profile. A second Dodge Colt and Nissan Pickup were then used in another series of tests, identical to the first, except that the load plate angles were set to 0° pitch and 15° roll (see Table 1).

**Table 1 -- Quasi-Static Test Matrix**

| Vehicle | Crush Level | Angle |
|---|---|---|
| 89 Nissan Pickup #1 | FMVSS216, 127 mm, 254 mm, 381 mm | 5° Pitch, 25° Roll |
| 89 Dodge Colt #1 | FMVSS216, 127 mm, 254 mm, 381 mm | 5° Pitch, 25° Roll |
| 89 Dodge Colt #2 | FMVSS216, 127 mm, 254 mm, 381 mm | 0° Pitch, 15° Roll |
| 89 Nissan Pickup #2 | FMVSS216, 127 mm, 254 mm, 381 mm | 0° Pitch, 15° Roll |
| 90 Chevy Cavalier #1 | 127 mm, 254 mm, 381 mm | 5° Pitch, 25° Roll |
| 90 Honda Accord #1 | 127 mm, 254 mm, 381 mm | 5° Pitch, 25° Roll |
| 91 Chevrolet Caprice #1 | 127 mm, 254 mm, 381 mm | 5° Pitch, 25° Roll |
| 91 Ford Explorer #1 | 127 mm, 254 mm, 381 mm | 5° Pitch, 25° Roll |
| 90 Chevrolet CK1500 PU | 127 mm, 254 mm, 381 mm | 5° Pitch, 25° Roll |
| 89 Ford Taurus #1 | 127 mm, 254 mm, 381 mm | 5° Pitch, 25° Roll |
| 92 Ford Taurus #1 | 127 mm, 254 mm, 381 mm | 5° Pitch, 25° Roll |

Further testing of seven additional vehicle models was conducted with the test plate at the standard 5° pitch 25° roll setting, and crushed to 381 mm (15") in 127 mm (5") increments. No FMVSS 216 tests were performed on these vehicles. The total list of tested vehicles and the test configurations are shown in Table 1.

Videos of each test were taken as well as pre-test and post-test photographs. Figure 3 is a pre-test photograph showing the 1989 Nissan pickup chassis fixed rigidly in position to the roof crush device's lower platform. The photograph in Figure 4 shows the Nissan pickup and its orientation with respect to the load plate for a test with plate roll angle at 25° and pitch angle of 5°. Figure 4 also shows the head form used to measure HR (headroom) in Equation 1.

**Figure 3**-Pre-test photograph of Nissan pickup in quasi-static test device.

**Figure 4**-Photo showing head form used to measure headroom reduction.

## 2.3 Static Roof Crush Results

The multiple roof crush tests performed on each vehicle were concatenated to create a single load vs. crush plot. Figure 5 shows an overlay of the tests before the data was concatenated. Although there are some discontinuities between successive tests, the results appear to be a reasonable force/crush history of the vehicles roof crush performance up to 381 mm (15").

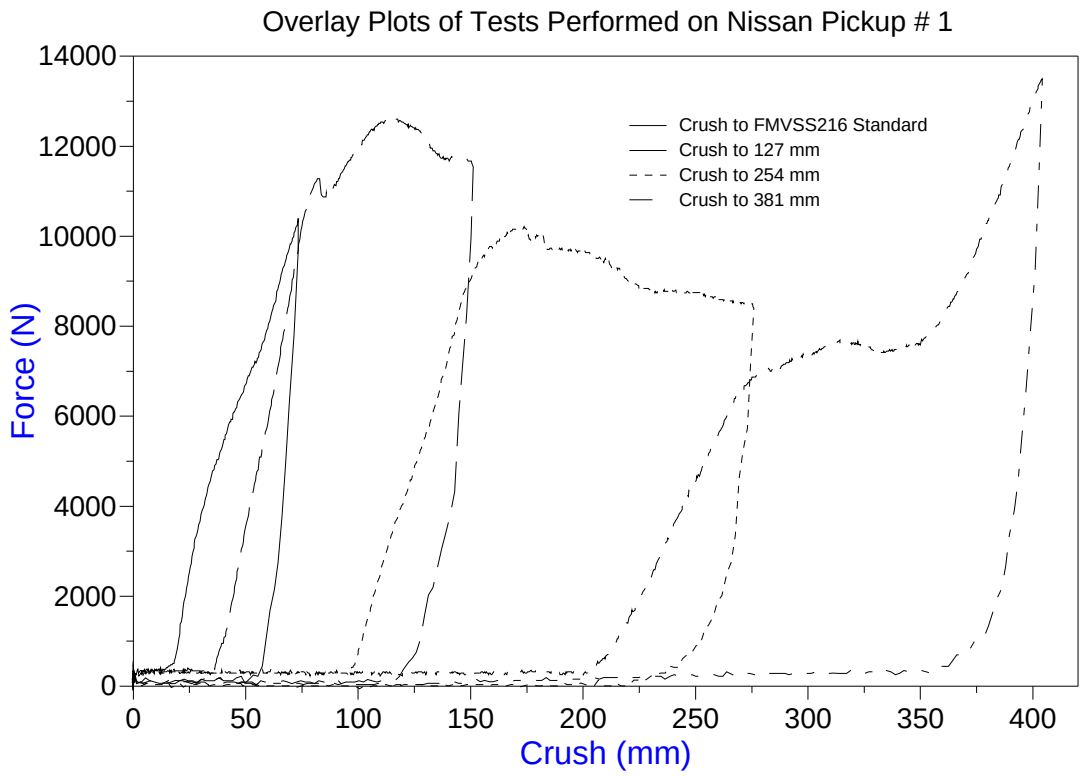


**Figure 5**-Overlaid plots of test data before it is concatenated.

Figures 6 through 9 are the force vs. crush and energy vs. crush plots for the concatenated 127 mm (5"), 254 mm (10") and 381 mm (15") static crush tests of the 1989 Nissan pickup and 1989 Dodge Colt with the 5° pitch and 25° roll load plate angle. Energy is calculated by integration of the force vs. crush data. The energy vs. crush plots (Figures 7 & 9) are highly linear. A linear regression was conducted on the data which created a best-fit line with an $R^2 = 0.99$ in both cases. Consequently, the energy absorbed in the roof as a function of roof crush was accurately fitted to a straight line. Force and energy vs. crush plots for all vehicles tested statically can be found in Appendix D.

Roof profile plots of the Nissan pickup and the Dodge Colt are shown in Figures 10 and 11. Figures 10a and 11a are the profile plots of the roof after testing to the FMVSS No. 216 requirements. Figures 10b, 11b, 10c, 11c, 10d and 11d are profile plots of the roof after 127 mm (5"), 254 mm (10"), and 381 mm (15") of roof crush, respectively. A complete set of roof crush profiles for vehicles listed in Table 1 appear in Appendix A.

Table 2 shows the results when testing the Nissan and Colt at different load plate angles. The following observances can be made:

1. Under loading equal to 1 ½ times the vehicle weight, absolute roof crush was higher with the 5° pitch, 25° roll plate angle. This corresponds to the application of a load more transverse to the length of the A-pillar.

2. Under loading equal to 1 ½ times the vehicle weight, HRR was less at 0° pitch, 15° roll angles for the Nissan pickup while the Dodge Colt was more.

3. The energy slope was higher with the 0° pitch, 15° roll angles. This again appears to give the roof more energy absorbing capability by directing the load more closely along the length of the A-pillar.

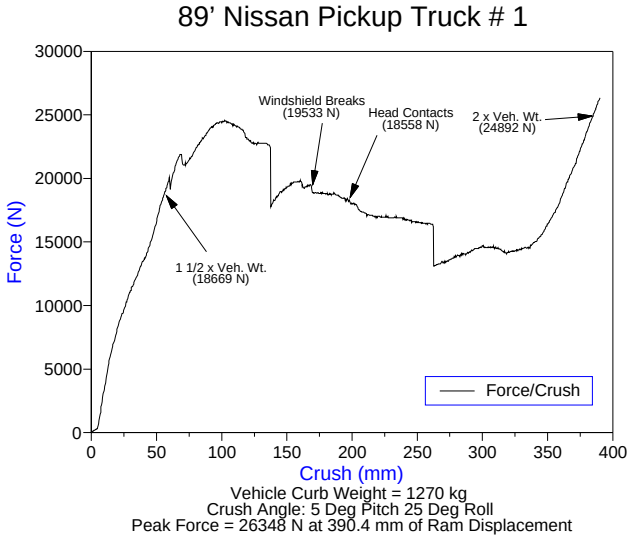


**Figure 6**-Force/crush plot for the Nissan pickup tested quasi-statically.

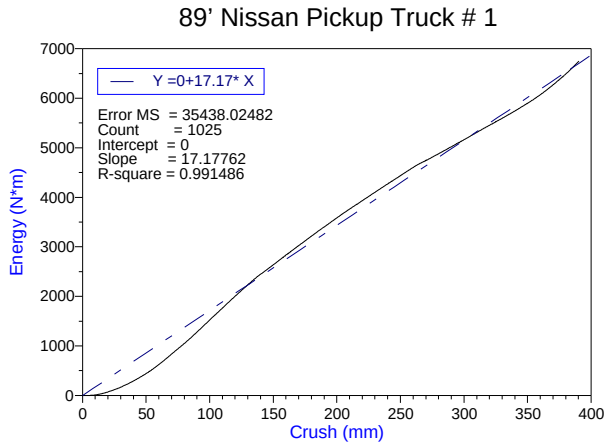


**Figure 7**-Energy/crush plot and regression line for the Nissan pickup.

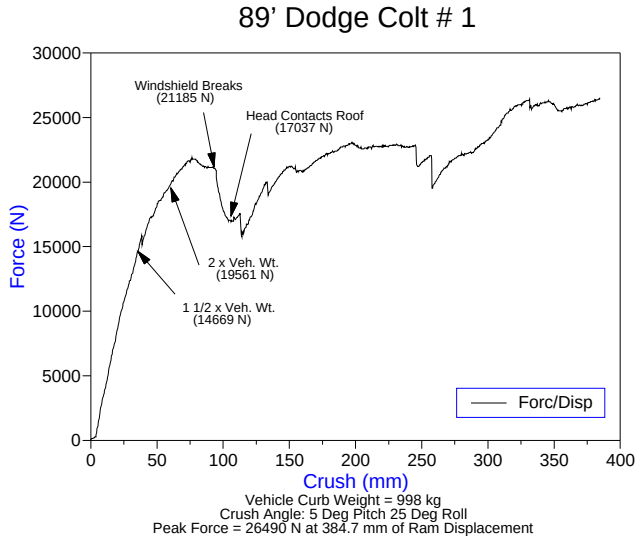


**Figure 8**-Force/crush plot for the Dodge Colt tested quasi-statically.

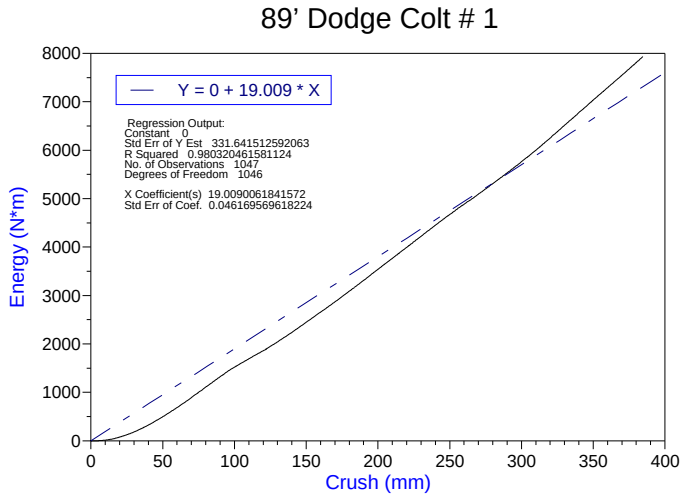


**Figure 9**-Energy/crush and regression line plot for Dodge Colt tested quasi-statically.

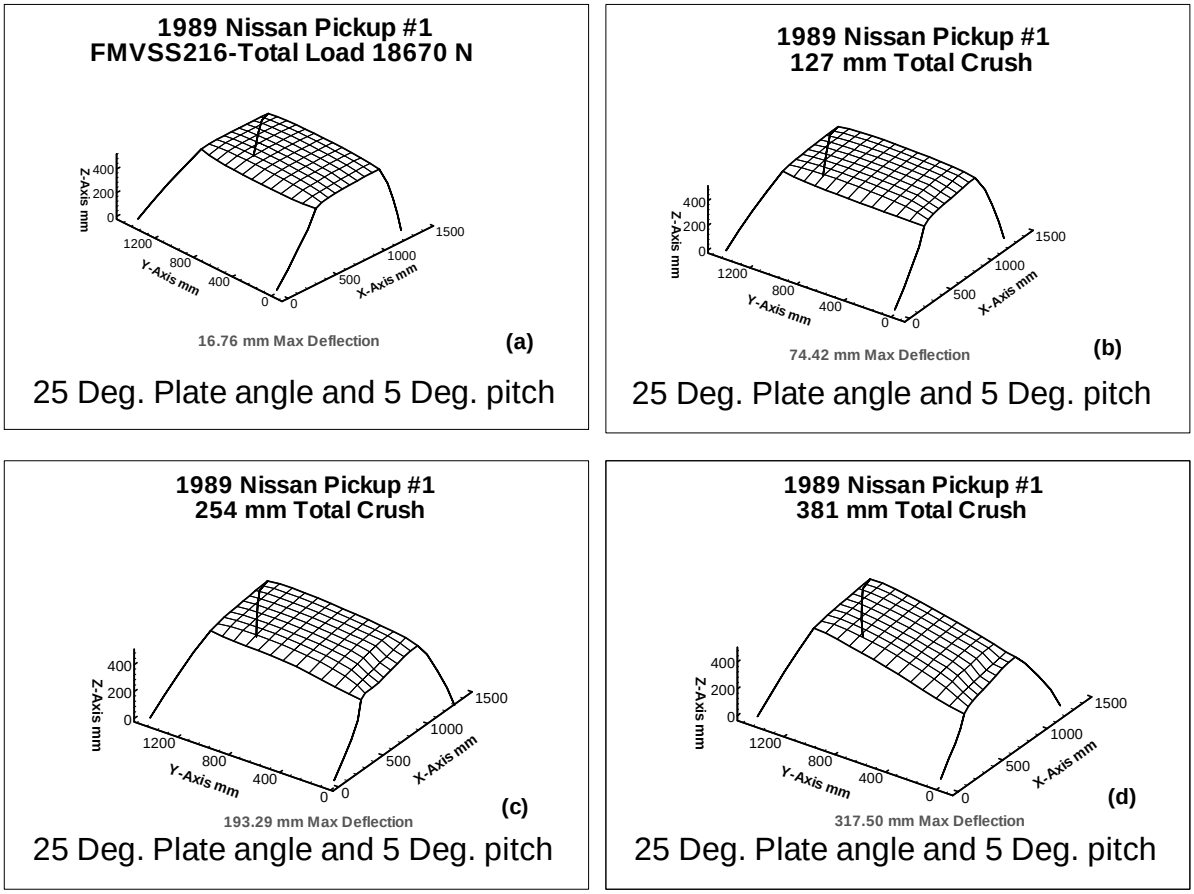


**Figure 10**-Roof profiles for the Nissan pickup tested quasi-statically.

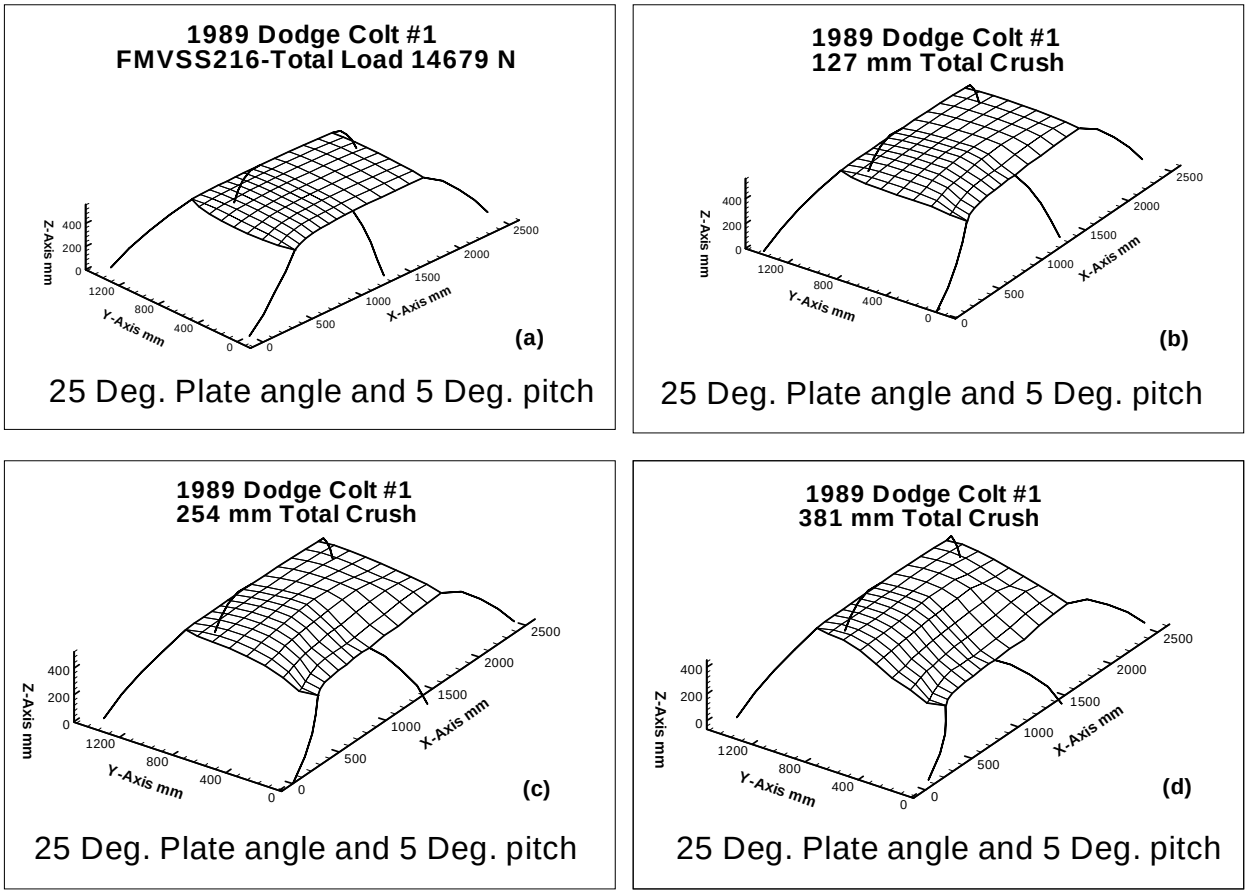


**Figure 11**-Roof profiles for Dodge Colt tested quasi-statically.

| Table 2 - Results from test at different load plate angles for the Nissan and the Colt | | | | |
|---|---|---|---|---|
| | Dodge Colt 5°, 25° | Dodge Colt 0°, 15° | Nissan PU 5°, 25° | Nissan PU 0°, 15° |
| Roof crush at 1½ vehicle wt. (mm) | 35.7 | 32.0 | 55.5 | 34.8 |
| HRR at 1½ vehicle wt. (%) | 21.1 | 30.4 | 26.3 | 15.6 |
| Force at 127 mm roof crush (N) | 18757 | 24250 | 22652 | 27883 |
| Force at 254 mm roof crush (N) | 21851 | 22075 | 16531 | 14619 |
| Force at 381 mm roof crush (N) | 26357 | 30267 | 23797 | 24683 |
| Linearized energy slope (N*m/mm) | 19.01 | 21.05 | 17.18 | 19.22 |
| $R^2$ | .980 | .985 | .991 | .993 |

4. Roof energy absorption can be estimated with a straight line with a high level of accuracy. Using least mean squares regression of energy vs. crush data, a linear fit gave an $R^2$ at or above .98 in all cases.

Table 3 summarize the roof crush and energy characteristics for the nine vehicles loaded at the 5° pitch and 25° roll angles.

All vehicles tested were within the requirements of FMVSS No. 216 with an average roof crush of 56 mm at 1 ½ times the vehicle weight. The average HRR at a load on the roof of 1 ½ times the vehicle weight, was 27%. In real-world rollover collisions percent headroom reduction averaged 69% for injured occupants who were belted [7].

Table 4 summarizes the load plate force after 127 mm (5"), 254 mm (10") and 381 mm (15") of roof crush, respectively, for all 9 vehicles tested. The table shows the energy equation and $R^2$ values for each of the vehicles. These values are derived from the linear regressions of the energy plots created by the integration of the force versus crush data. The data indicates the energy equations to be highly accurate in predicting the amount of energy absorbed at specific levels of roof crush($R^2$ ranged from .963 to 0.993).

| Table 3 - Summary of crush characteristics for test at 5° Pitch, 25° Roll angle | | | | | |
|---|---|---|---|---|---|
| **Test Vehicle Ranked by Headroom Reduction** | **Crush Angle** | **Vehicle Weight (kg)** | **Force @ 1 ½ x Vehicle Weight (N)** | **Roof Crush @ 1 ½ x Vehicle Weight (mm)** | **% HRR @ 1 ½ vehicle weight** |
| 89 Nissan Pickup #1 | 5° Pitch, 25° Roll | 1270 | 18669 | 55.5 | 26.3 % |
| 90 Chevrolet CK-1500 PU | 5° Pitch, 25° Roll | 1679 | 24681 | 64.3 | 20.8 % |
| 91 Ford Explorer #1 | 5° Pitch, 25° Roll | 1632 | 23990 | 51.6 | 21.0 % |
| 89 Dodge Colt #1 | 5° Pitch, 25° Roll | 998 | 14671 | 35.7 | 21.1 % |
| 91 Chevy Caprice #1 | 5° Pitch, 25° Roll | 1698 | 24961 | 82.2 | 32.5 % |
| 90 Chevy Cavalier #1 | 5° Pitch, 25° Roll | 1089 | 16008 | 54.4 | 24.2 % |
| 89 Ford Taurus #1 | 5° Pitch, 25° Roll | 1411 | 20742 | 47.8 | 28.3 % |
| 90 Honda Accord #1 | 5° Pitch, 25° Roll | 1259 | 18507 | 61.1 | 29.0 % |
| 92 Ford Taurus #1 | 5° Pitch, 25° Roll | 1411 | 20742 | 49.8 | 35.4 % |
| Average | | 1383 | 20330 | 55.8 | 26.5% |
| Std. Dev. | | 253 | 3723 | 12.9 | 5.3% |

| Table 4 - Summary showing crush at head contact results | | | | | | |
|---|---|---|---|---|---|---|
| **Test Vehicle** | **Crush Angle** | **Roof Crush @Head Roof Contact (mm)** | **Force @ 127 mm (5") Roof Crush (N)** | **Force @ 254 mm (10") Roof Crush (N)** | **Force @ 381 mm (15") Roof Crush (N)** | **Energy Equations $R^2$** |
| 89 Nissan Pickup #1 | 5° Pitch, 25° Roll | 191 | 22652 | 16531 | 23797 | Y=0+17.17762*X .991 |
| 89 Dodge Colt #1 | 5° Pitch, 25° Roll | 152 | 18757 | 21851 | 26357 | Y=0+19.00900*X .980 |
| 90 Chevy Cavalier #1 | 5° Pitch, 25° Roll | 203 | 24587 | 23780 | 40199 | Y=0+21.03836*X .970 |
| 90 Honda Accord #1 | 5° Pitch, 25° Roll | 190 | 18017 | 21500 | 44072 | Y=0+20.84463*X .963 |
| 91 Chevy Caprice #1 | 5° Pitch, 25° Roll | 229 | 28987 | 18855 | 32657 | Y=0+22.50828*X .984 |
| 91 Ford Explorer #1 | 5° Pitch, 25° Roll | 222 | 25817 | 23645 | 30059 | Y=0+22.92578*X .993 |
| 90 Chevrolet CK-1500 PU | 5° Pitch, 25° Roll | 279 | 40300 | 15300 | 13500 | Y=0+23.33228*X .974 |
| 89 Ford Taurus #1 | 5° Pitch, 25° Roll | 152 | 31310 | 31210 | 40280 | Y=0+24.40990*X .984 |
| 92 Ford Taurus #2 | 5° Pitch, 25° Roll | 127 | 27264 | 27319 | 50794 | Y=0+23.92925*X .971 |
| Average | | 193.89 | 26410 | 22221 | 33235 | |
| Std. Dev. | | 46.58 | 6811 | 5044 | 34573 | |

Figure 12 was created from the force / crush data of the nine vehicles tested with a plate angle of 5° pitch and 25° roll. The corridor between the minimum and maximum forces (using 5 mm increments) represents the range at which the 9 vehicles performed. An average force displacement curve was created from the mean values of force calculated for each of the 5 mm increments measured.

The load carrying capacity for all nine vehicles were very close up to approximately 40 mm of roof crush. At that point the forces began to diverge for any given roof crush. The range of forces on the roof at 127 mm of crush was higher than at 254 mm of crush. Loads began increasing after

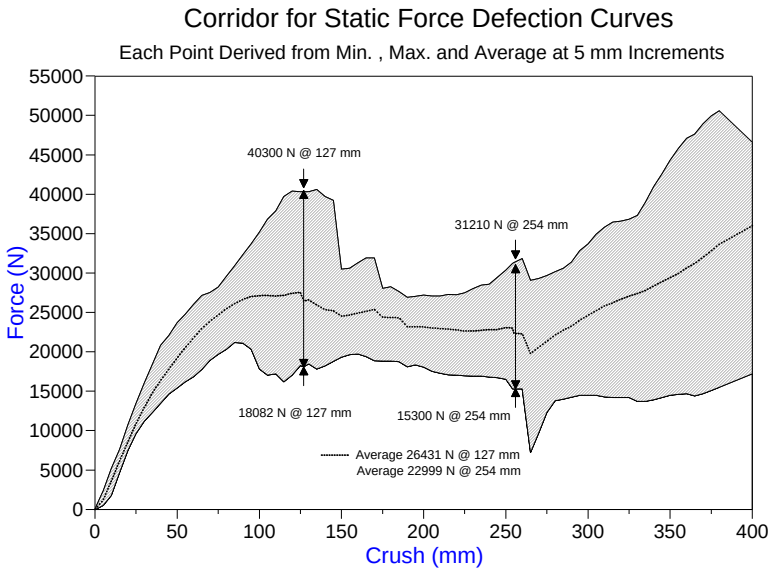


**Figure 12-**Corridor for static force deflection curves.

300 mm (11.8") of crush because the roof structures began to pick up some of the vehicles' structures below the A-pillar.

Each force vs. crush curve was integrated to produce an energy vs. crush curve. The range of energy is shown in Figure 13. At approximately 50-100 mm, the range of energy was quite narrow. At that point, the range widened and vehicle roof crush energy varied substantially. Figure 14 shows the range of normalized[1] energy data for the static roof crush tests. Energy absorption varied less when normalized by the vehicle weight. Consequently these vehicles may perform similarly when rolled or dropped on the roof, up to several millimeters of crush. Again, as vehicle structures other than the roof get loaded (headrest, etc...), the energy absorption began to diverge significantly.

[1] Normalized energy was found by dividing data by the weight of the vehicle.

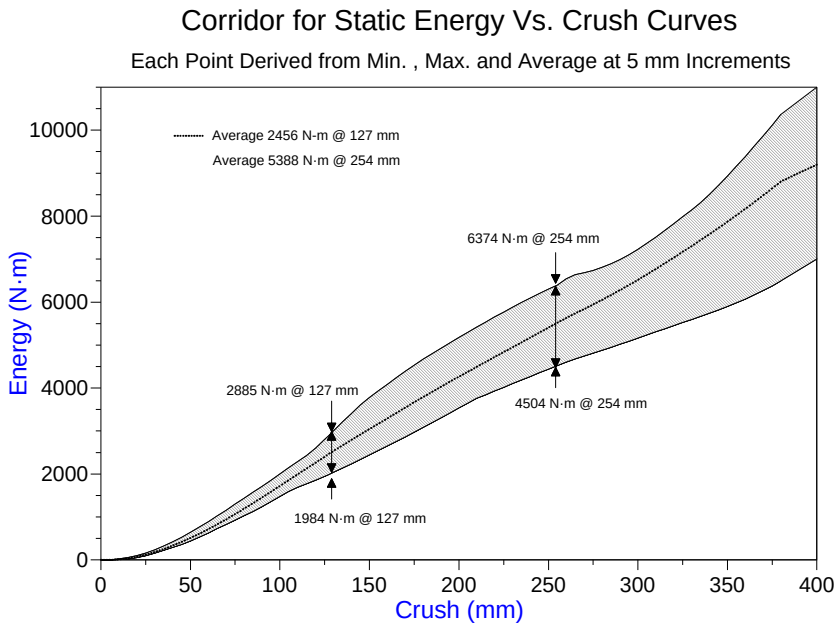


**Figure 13**-Corridor for static energy deflection curves.

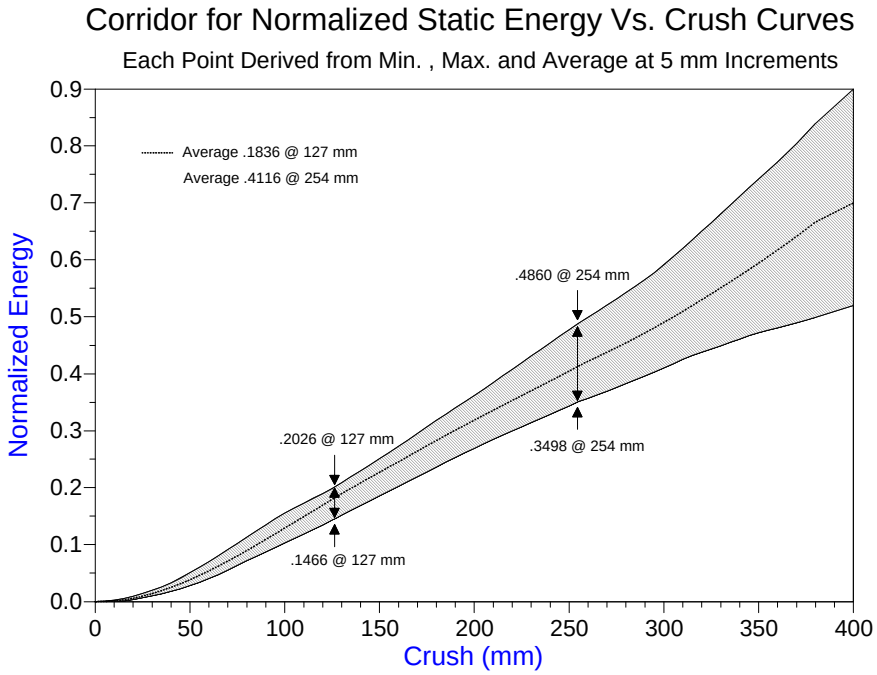


**Figure 14**-Corridor for normalized static energy deflection curves.

A summary of the force vs. crush and energy vs. crush results for all vehicles tested is given in the top portion of Table 5. The roof crush resistance was measured in terms of absolute roof crush strength (peak force), roof stiffness (force vs. crush in pseudo-elastic range) and energy absorbed by the roof after 254 mm (10") of crush. The roof crush resistance was then normalized by vehicle weight and results shown in the lower portion of Table 5. The vehicles are listed by decreasing levels of energy absorbed by the roof at 254 mm (10") of crush. The corresponding rankings by strength and stiffness are also shown.

The 1990 CK-1500 pickup was the best performer on an absolute roof strength and stiffness basis (Table 5). The worst were the Dodge Colt and the Chevy Cavalier. However, when normalizing by vehicle weight; the Colt and the Cavalier move up to become two of the better performers. Normalized data indicates the Dodge Colt had the best overall roof energy management and the Chevrolet Caprice had the worst. Therefore, using the absolute roof strength may be misleading in ranking vehicle roof strength. This is one reason why roof crush resistance is measured by deflection after applying a load of 1 ½ times the vehicle weight. These rankings were subsequently used to assist in vehicle selection for dynamic drop testing.

## 3.0 DROP TESTS ONTO FLOOR

The 1989 Nissan pickup and the Dodge Colt were chosen to conduct dynamic roof crush tests. These two vehicles' roof structures are average performers based on Table 5 in section 1.1.3. The objectives of these tests were:

1. Devise a dynamic procedure for roof crush testing,

2. Examine roof profile measurements after dynamic loading of the different roof structures, and

3. Examine roof performance at different drop angles.

| Table 5 - Summary of vehicle ranking from quasi-static testing | | | | | |
|---|---|---|---|---|---|
| **Vehicles Ranked in Order of Energy at 254 mm (10") of Crush** | **Energy at 254 mm (10") of Crush** | **Stiffness (N/mm)** | **Peak Force (N)** | **Ranking by Stiffness** | **Ranking by Peak Force** |
| 1990 Chevrolet CK-1500 Pickup | 6374 | 325 | 40,600 | 1 | 1 |
| 1989 Ford Taurus #1 | 6351 | 324 | 32,270 | 2 | 2 |
| 1991 Ford Explorer #1 | 5880 | 263 | 29,936 | 5 | 4 |
| 1991 Chevrolet Caprice #1 | 5796 | 207 | 30,104 | 7 | 3 |
| 1992 Ford Taurus #1 | 5733 | 316 | 29,585 | 3 | 5 |
| 1990 Chevy Cavalier #1 | 5042 | 188 | 25,876 | 9 | 7 |
| 1990 Honda Accord #1 | 5038 | 189 | 28,746 | 8 | 6 |
| 1989 Dodge Colt #1 | 4758 | 299 | 21,906 | 4 | 9 |
| 1989 Nissan Pickup #1 | 4504 | 246 | 24,576 | 6 | 8 |
| **Average** | **5388** | **254** | **27875** | | |
| **Standard Deviation** | **641** | **56** | **3438** | | |
| **Vehicles Ranked in Order of Normalized Energy at 254 mm (10") of Crush** | **Normalized Energy at 254 mm (10") of Crush** | **Normalized Stiffness (N/mm)** | **Normalized Peak Force (N)** | **Ranking by Normalized Stiffness** | **Ranking by Normalized Peak Force** |
| 1989 Dodge Colt #1 | 0.486 | 0.0306 | 2.240 | 1 | 5 |
| 1990 Chevy Cavalier #1 | 0.472 | 0.0176 | 2.425 | 6 | 2 |
| 1989 Ford Taurus #1 | 0.460 | 0.0234 | 2.334 | 2 | 3 |
| 1992 Ford Taurus #1 | 0.414 | 0.0229 | 2.140 | 3 | 6 |
| 1990 Honda Accord #1 | 0.408 | 0.0153 | 2.330 | 8 | 4 |
| 1990 Chevrolet CK1500 Pickup | 0.387 | 0.0198 | 2.468 | 5 | 1 |
| 1991 Ford Explorer #1 | 0.367 | 0.0164 | 1.872 | 7 | 8 |
| 1989 Nissan Pickup #1 | 0.362 | 0.0198 | 1.975 | 4 | 7 |
| 1991 Chevrolet Caprice #1 | 0.350 | 0.0124 | 1.809 | 9 | 9 |
| **Average** | **0.412** | **0.01980** | **2.177** | | |
| **Standard Deviation** | **0.051** | **0.00536** | **0.242** | | |

## 3.1 Approach

Inverted vehicles were dropped onto a piece of 3/4" plywood covering an area of 12 square meters (128 $ft^2$). The plywood was used to prevent damage to the laboratory floor. Drop heights were calculated based on energy at 381 mm (15"), 254 mm (10") and 127 mm (5") of roof crush in the quasi-static roof crush tests. The potential energy was set equal to the energy of a particular static roof crush level and drop height was calculated as follows:

$$DH = E_s \times \left( \frac{1}{V_w \times g} \right) \qquad \textbf{[2]}$$

where,

$DH$=Drop Height, (m),
$E_S$=Static roof crush energy at a particular crush level ,(N*m),
$V_W$=Vehicle mass, (kg), and
$g$= Gravity 9.8 $m/s^2$.

Drop height, pitch and roll measurements are shown in Figure 15. The vehicles were supported with the roof toward the floor and positioned to the desired height and roll and pitch angles using special wheel adapters, two fork lifts and an overhead crane. Vehicle orientation was selected to load the roof at the same orientation as the load plate in the static test: 5° pitch, 25° roll and 0° pitch, 15° roll.

Vehicle instrumentation for this series included a three axis accelerometer array located at the CG of each vehicle. For the y-axis, the C.G. was through the longitudinal centerline of vehicle. For the z-axis the C.G. was estimated to be 39.5 % of the distance from the ground to the roof top. [6] For the x-axis, the C.G. locations were estimated using Equation 3:

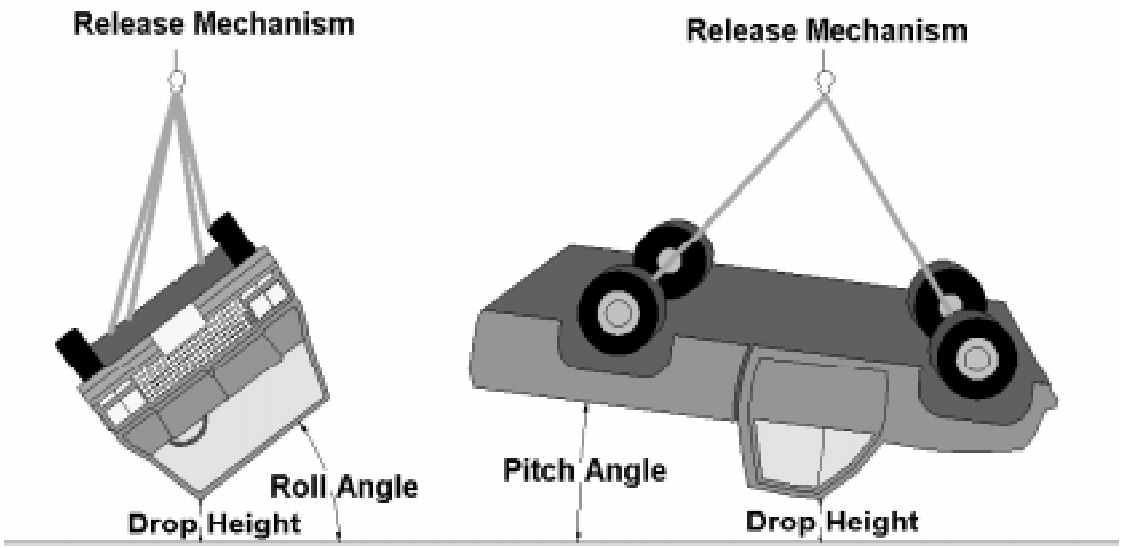


**Figure 15**-Illustration of floor drop procedure.

$$l_f = \frac{\frac{w_r}{w_f} \times lwb}{1 + \frac{w_r}{w_f}} \qquad \textbf{[3]}$$

Where:

$l_f$ = Length from front axle to CG (m),

$w_r$ = Rear axle weight (kg),

$w_f$ = Front axle weight (kg), and

lwb = Distance between the front and rear axles (m).

A contact switch was used to record time of impact after the vehicle was released. High speed film and video of each drop was taken as well as pre and post test photographs. Roof profile measurements were taken prior to and after each drop.

A photograph showing the Nissan pickup inverted and ready to drop is shown in Figure 16. A stadia rod marked with inch tape and used in the high speed film and video analysis is shown. Figure 17 is a photograph of the location of the 3-axis accelerometer array at the CG of vehicle.

## 3.2 Test Matrix for Vehicles Dropped onto Floor

The test matrix of vehicles dropped onto the floor is shown in Table 6. The table also shows the static crush data and drop heights calculated for each test. The tests were run in four sets of four tests each. For example, the first Dodge Colt (Colt #3) was dropped at a height that set the potential energy equivalent to 381 mm of static crush energy. The second Dodge Colt (Colt #4) was then dropped three times in the following order. Colt #4 was first dropped at the height calculated using Equation 2 with the input potential energy ($E_s$) equal to the 127 mm (5") static crush test. Two additional drops with the Colt #4 added energy to the roof that was equivalent to 254 mm (10") and 381 mm (15") of static crush; consequently for drop #2, the static roof crush energy at 254 mm of crush was subtracted from crush energy at 127 mm and the results used to calculate the drop height. Similarly, drop #3 was calculated by subtracting the energy at 381 mm of roof crush from the energy of 254 mm of roof crush. This procedure was repeated for both load plate angle settings on the Dodge Colts and the Nissan Pickups.

## 3.3 Floor Drop Results

Analyses of the dynamic roof strength from the floor drop tests were performed from roof profile measurements, film, video, photographs and general observation. A photograph of the Nissan pickup after the 228.6 mm (9") drop and a computer generated roof profile of that same Nissan are

**Figure 16**-Pre-test photo of floor drop test.

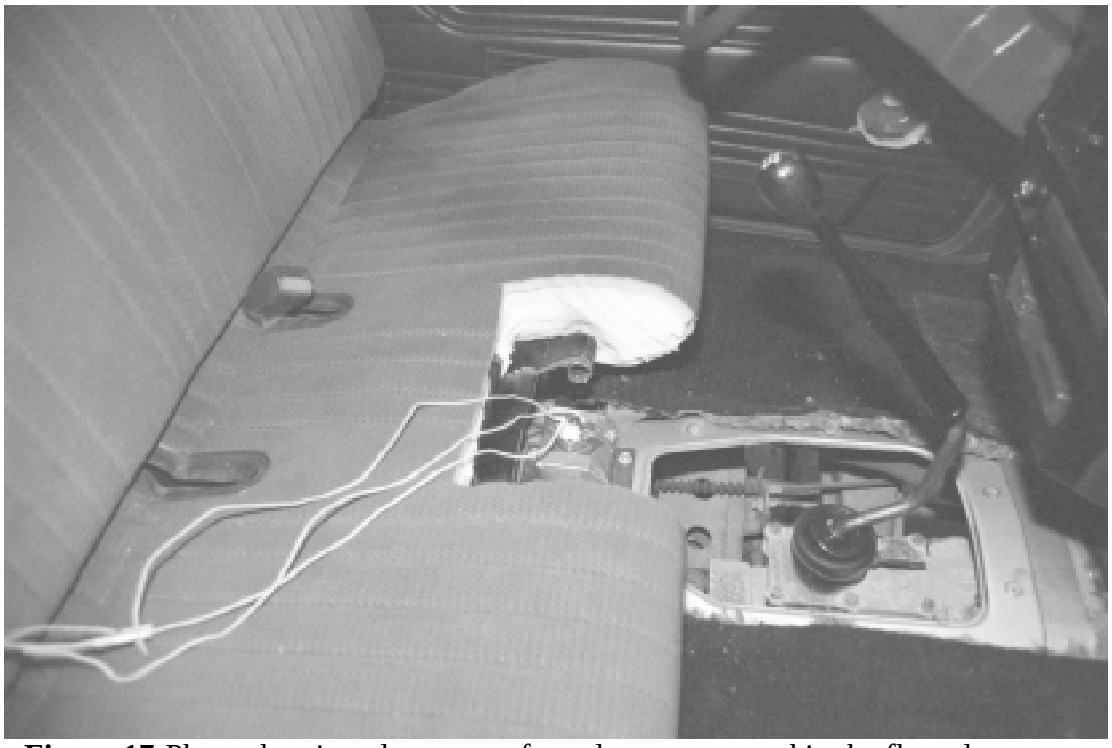

**Figure 17**-Photo showing placement of accelerometers used in the floor drop tests.

| Table 6 - Test matrix for floor drop tests | | | | |
|---|---|---|---|---|
| Static Test | Drop Angle | Static Crush Level (mm) | Static Energy at Specified Static Crush Level (N*m) | Calculated Drop Height (mm) Equation 2 |
| Colt #3 | 5º Pitch, 25º Roll | 381 | 7844.9 | 812.8 |
| Colt #4 | 5º Pitch, 25º Roll | 127 | 1984.0 | 215.9 |
| Colt #4 | 5º Pitch, 25º Roll | 254 - 127 | 2772.6 | 279.4 |
| Colt #4 | 5º Pitch, 25º Roll | 381 - 254 | 3080.7 | 330.2 |
| Colt #5 | 0º Pitch, 15º Roll | 381 | 8634.3 | 939.8 |
| Colt #6 | 0º Pitch, 15º Roll | 127 | 2367.6 | 254 |
| Colt #6 | 0º Pitch, 15º Roll | 254 - 127 | 2771.1 | 304.8 |
| Colt #6 | 0º Pitch, 15º Roll | 381 - 254 | 3496.2 | 393.7 |
| Nissan #7 | 5º Pitch, 25º Roll | 381 | 6507.9 | 596.9 |
| Nissan #8 | 5º Pitch, 25º Roll | 127 | 2158.2 | 190.5 |
| Nissan #8 | 5º Pitch, 25º Roll | 254 - 127 | 2349.0 | 203.2 |
| Nissan #8 | 5º Pitch, 25º Roll | 381 - 254 | 1995.6 | 196.8 |
| Nissan #4 | 0º Pitch, 15º Roll | 381 | 7276.2 | 660.4 |
| Nissan #5 | 0º Pitch, 15º Roll | 127 | 2632.2 | 228.6 |
| Nissan #5 | 0º Pitch, 15º Roll | 254 - 127 | 2238.5 | 190.5 |
| Nissan #5 | 0º Pitch, 15º Roll | 381 - 254 | 2411.5 | 241.3 |

shown in Figures 18 and 19 respectively. A complete set of the roof profile measurements for the dynamic drop tests on the floor is contained in Appendix B.

**Figure 18**-Post test photo of the Nissan.

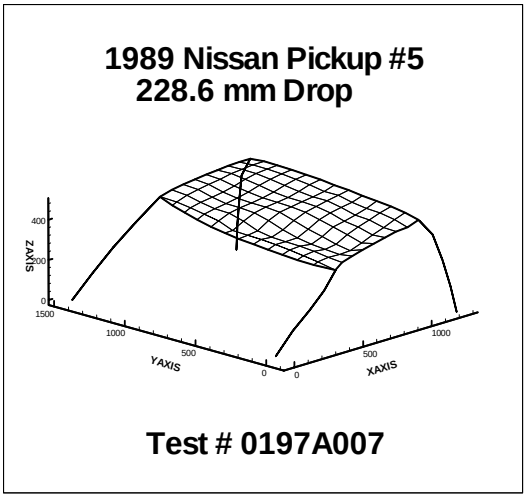


**Figure 19**-Roof profile of the Nissan.

A summary of the peak roof deflections in the floor drop test is given in Table 7. The table shows the difference between the static peak roof crush (this is the crush value used to calculate dynamic drop height). Some of the peak roof crush measurements in the dynamic case are less than the static. This can be partially attributed to the rotation of the vehicle out of its set 216 angles after impact. The rotation changed the direction of the roof load and affected peak crush. High speed film of the Dodge Colt shows an interaction between the front-end of the vehicle and the floor in the dynamic test. The data indicates that some of the load shifted from the roof which reduced the force of the drop.

The full drop test was compared to the third drop of the multiple drops with the second vehicle. The third drop should theoretically have the same energy input to its roof as the full drop test in the first vehicle. Consequently Colt #3 was compared to the third drop test of Colt #4. In this case, the peak roof crush was only 6 mm different. Colt #5 and Colt #6 were 13 mm different. The Nissan comparison was not as good. The difference between Nissan#4 and #5 was 17 mm and that for Nissan #7 and #8 was 37 mm. Again, vehicle rotation during impact and front-end interaction can alter the test results and reduce values of a comparison between tests.

| Table 7 - Summary of roof crush measurements for drop tests | | | |
|---|---|---|---|
| **Vehicles Tested** | **Static Crush** | **Dynamic Crush** | **Difference** |
| Colt #3 at 5° pitch and 25° roll | 381 mm | 248 mm | 133 mm |
| Colt #4 at 5° pitch and 25° roll | 127 mm | 135 mm | -8 mm |
| Colt #4 at 5° pitch and 25° roll | 254 mm | 193 mm | 61 mm |
| Colt #4 at 5° pitch and 25° roll | 381 mm | 242 mm | 139 mm |
| Colt #5 at 0° pitch and 15° roll | 381 mm | 221 mm | 160 mm |
| Colt #6 at 0° pitch and 15° roll | 127 mm | 76 mm | 51 mm |
| Colt #6 at 0° pitch and 15° roll | 254 mm | 149 mm | 105 mm |
| Colt #6 at 0° pitch and 15° roll | 381 mm | 208 mm | 173 mm |
| Nissan #7 at 5° pitch and 25° roll | 381 mm | 289 mm | 92 mm |
| Nissan #8 at 5° pitch and 25° roll | 127 mm | 172 mm | -45 mm |
| Nissan #8 at 5° pitch and 25° roll | 254 mm | 297 mm | -43 mm |
| Nissan #8 at 5° pitch and 25° roll | 381 mm | 326 mm | 55 mm |
| Nissan #4 at 0° pitch and 15° roll | 381 mm | 345 mm | 36 mm |
| Nissan #5 at 0° pitch and 15° roll | 127 mm | 179 mm | -52 mm |
| Nissan #5 at 0° pitch and 15° roll | 254 mm | 298 mm | -44 mm |
| Nissan #5 at 0° pitch and 15° roll | 381 mm | 362 mm | 19 mm |

The difference in dynamic roof crush when dropping at the two impact angles was also investigated. For a visual comparison, overlay plots were generated showing roof profiles of the Nissan and the Colt at the 5° pitch, 25° roll and 0° pitch, 15° roll (Figure 20 b & 20 d), respectively. Although the profiles of the Nissan are similar in shape, there is a difference of 56 mm (2.2") between the maximum roof crush values. The difference in peak crush for the Colt was 27 mm. The Nissan crushed more at the 0° pitch, 15° roll angles while the Colt crushed more at the 5° pitch, 25° roll angles. When the roof profiles at the different drop angles were compared statistically, (see Figures 20 a and 20 c) the results indicated a strong relationship exists between the shape of the roof crush profiles (Note: if the roof crush profiles were identical, the points would form a diagonal line which would yield a $R^2 = 1$, a slope of 1.0, and an intercept of 0).

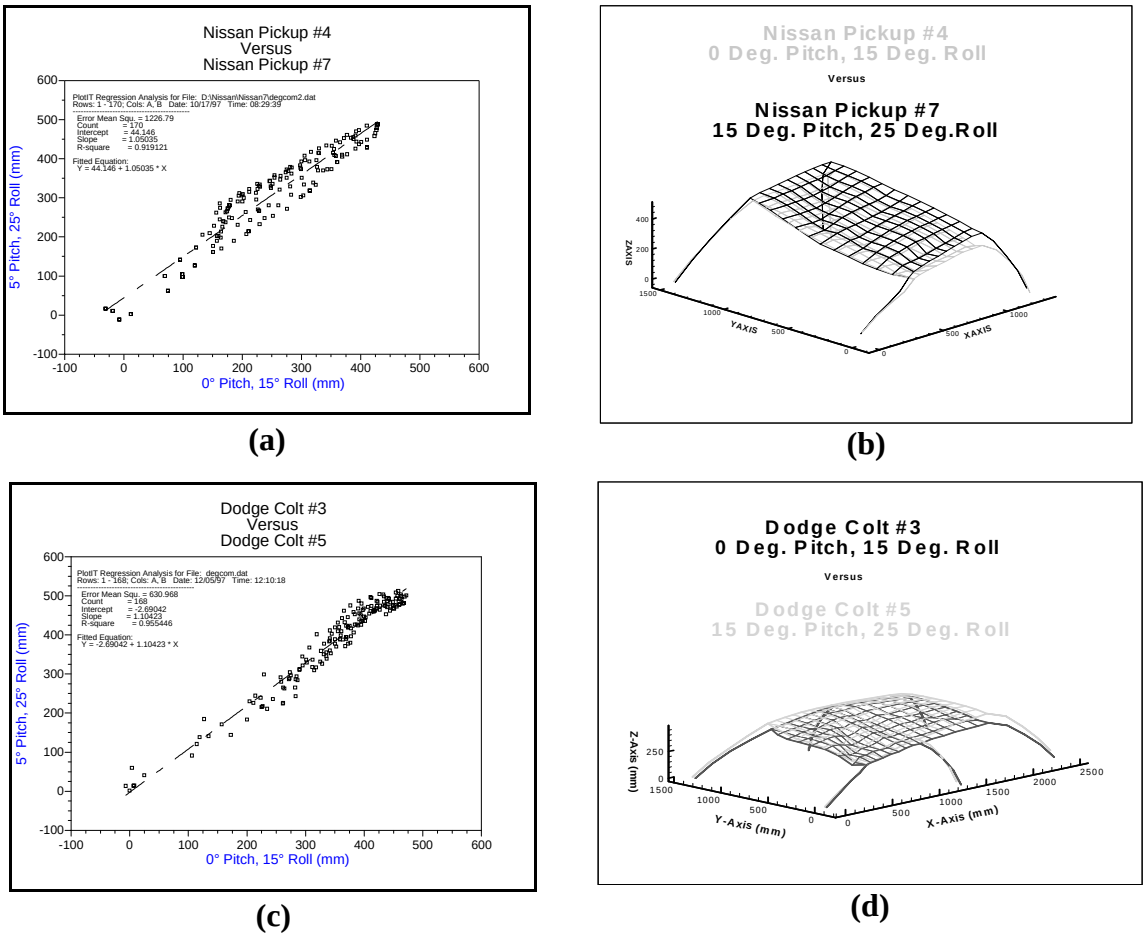


**Figure 20**-Plots for drop angle analysis.

## 4.0 DROP TESTS ONTO LOAD PLATE

To directly compare the static force and energy vs. crush plots to dynamic results, a procedure was devised to measure the dynamic force and deflection of the roof drop test.

The objectives of this study were:

1. Devise a method to accurately measure force and crush of the inverted drop test previously implemented.
2. To rank a fleet representation matrix of vehicles in order of roof crush performance, when tested dynamically.

### 4.1 Approach

A load plate (Figure 21) was constructed using the NHTSA's load cell crash barrier and laid horizontal so that force could be recorded as the vehicle was dropped. Extra rows of load cells and load plates were added to accommodate roof areas of the various vehicles. Figure 23 shows the layout used for placement of the different size load cells. The 50,000 lb load cells are in the area most likely to see the most impact force. A string pot (Figure 22) was attached to the A-pillar at the roof and front header interface to measure the maximum roof crush. As with the floor drop test, a three axis accelerometer array was placed at the cg and an additional four accelerometers were placed at the junction of the left A-pillar and rooftop near the first contact point. The other three were placed on the left front door in a three-axis array.

Six drops were initially conducted, one each on 1991 Caprice, 1990 Cavalier, 1992 Taurus, 1991 Explorer, 1990 Nissan Pickup, and the 1989 Dodge Colt. These vehicles represented three relatively good performers (Colt, Cavalier, Taurus) and three relatively bad performers (Caprice, Nissan Pickup, Explorer) in the static roof crush test performance when judged by the overall strength and stiffness ranking of each vehicle in Table 5. The drop heights were calculated to set potential energy of the suspended vehicle equal to the static test energy after 254 mm (10") of roof crush. Each vehicle was dropped at the 5° pitch and 25° roll angle onto the load plate at a height equivalent to 254 mm (10") static crush energy.

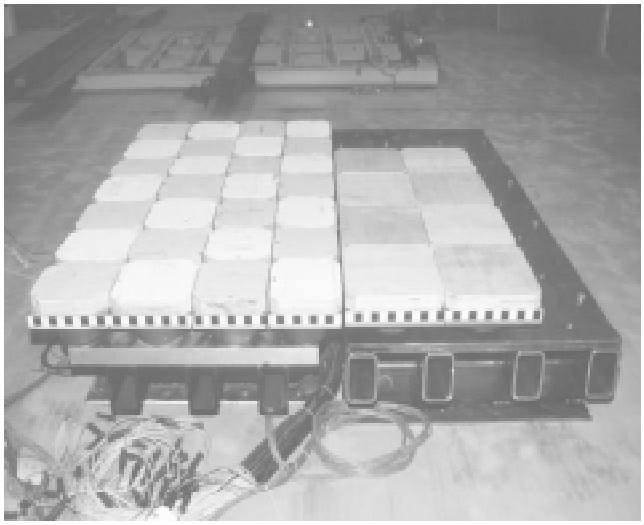

**Figure 21**-Load plate.

**Figure 22**-Setup.

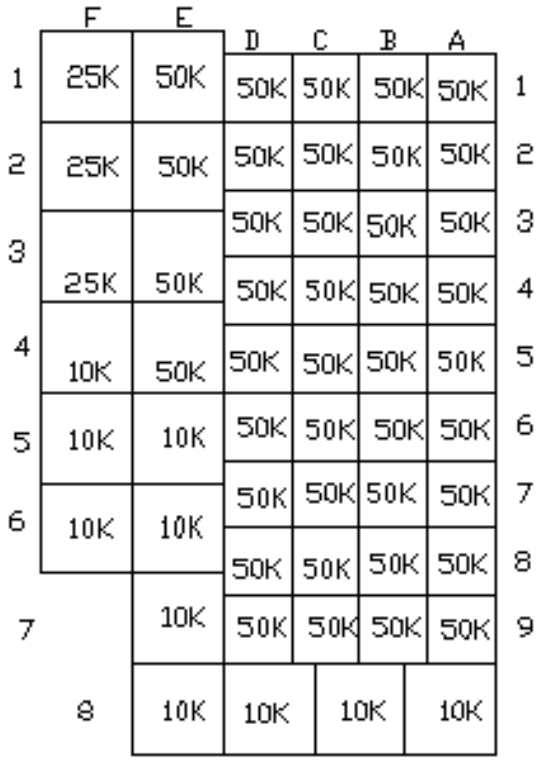


**Figure 23**-Load plate layout.

## 4.2 Test Matrix

Table 8 summarizes the test matrix of vehicle drops onto the load plate. The table also shows the static crush data and calculations made for drop height. The actual drop height used differs slightly from the calculated value because of the limited adjustment of the overhead crane. As for the Taurus, the difference is significant (33 mm) and can only be explained as an error in calculating the drop height or taking the needed measurement. Each vehicle roof profile was measured before and after each test. A complete set of vehicle profiles from drop tests onto the load plate can be found in Appendix C. High speed video and film were taken as well as pre and post- test photographs.

**Table 8 - Test matrix for drop tests onto load plate**

| Test Vehicle | Static Crush (mm) | Static Energy from E Curve (N*m) | Calculated Drop Height (mm) Equation 2 | Drop Height Used (mm) | Drop Angle |
|---|---|---|---|---|---|
| Caprice #2 | 254 | 5781.7 | 343.7 | 342.9 | 5º Pitch, 25º Roll |
| Cavalier #2 | 254 | 5055.5 | 473.4 | 472.4 | 5º Pitch, 25º Roll |
| Nissan #10 | 254 | 4995.5 | 400.9 | 400.5 | 5º Pitch, 25º Roll |
| Colt #7 | 254 | 5109.0 | 521.8 | 520.7 | 5º Pitch, 25º Roll |
| Taurus #3 | 254 | 6183.1 | 467.8 | 434.3 | 5º Pitch, 25º Roll |
| Explorer #2 | 254 | 5906.1 | 353.9 | 353.1 | 5º Pitch, 25º Roll |

## 4.3 Load Plate Drop Test Results for 6 Vehicles

The load cell array data were summed to create a total force-time history from each drop test. Plotting this versus the roof crush, as measured by the string potentiometer, produced a force vs. crush curve for each vehicle dropped. Those for the Nissan Pickup and Dodge Colt are shown in

Figures 24 and 26. The force vs. crush curves were then integrated to obtain energy vs. crush curves. Those for the Nissan pickup and the Dodge Colt are shown in Figures 25 and 27. A linear regression was performed on the energy vs. crush data to produce an equation to predict energy at specific crush levels (see Figures 25 and 27). As for the static crush results, strong correlations were obtained. The force and energy vs. crush curves for the remaining vehicles, including the linear regression results, are in Appendix E.

Table 9 ranks the vehicle strengths using the dynamic data. When normalized by weight, the Dodge Colt performed well on a stiffness and peak force (strength) basis. The Chevy Caprice performed poorly.

## 5.0 STATIC AND DYNAMIC TEST COMPARISON

The primary objective of this study was to understand the differences and similarities between static and dynamic roof crush. In the previous three sections, the results of a static and dynamic roof crush series were reported. The results of the static and dynamic tests are compared here to determine whether static roof crush test results can be used to determine a dynamically equivalent result.

### 5.1 Crush Energy

The force vs. crush plots for the first six drop tests onto a load plate are compared to the static tests in Figure 28. As can be seen, the dynamic forces are consistently higher than the static results. This is attributable to the higher dynamic loading rate. This also results in consistently higher roof energy absorption at any given roof deflection, as seen in the comparison of energy vs. crush plot for the static and dynamic tests in Figure 29.

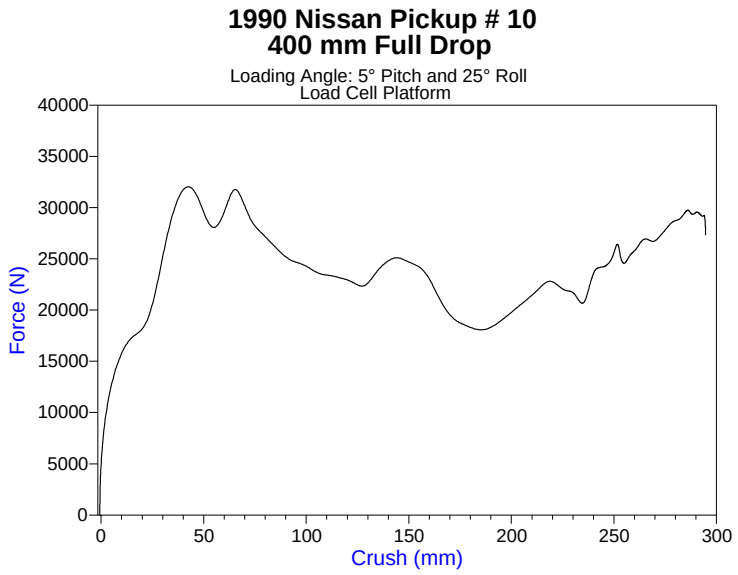


**Figure 24**-Force/crush curve for the Nissan drop test onto the load plate.

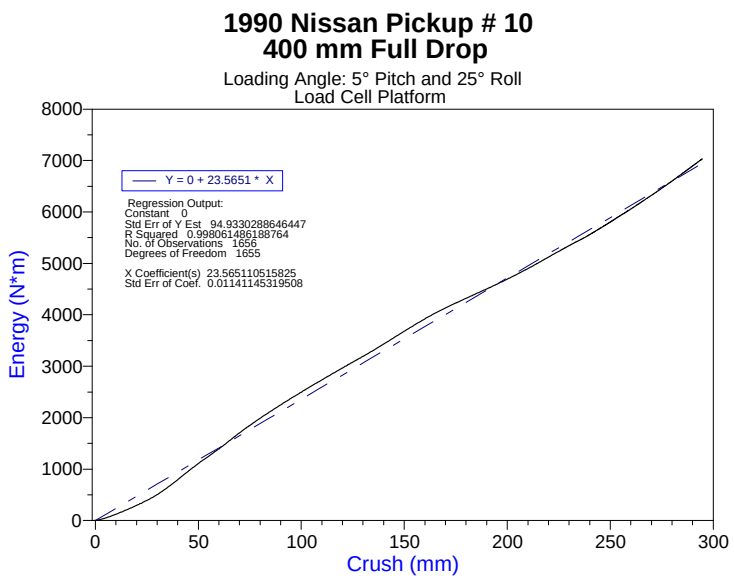


**Figure 25**-Energy/crush curve for the Nissan drop test onto the load plate.

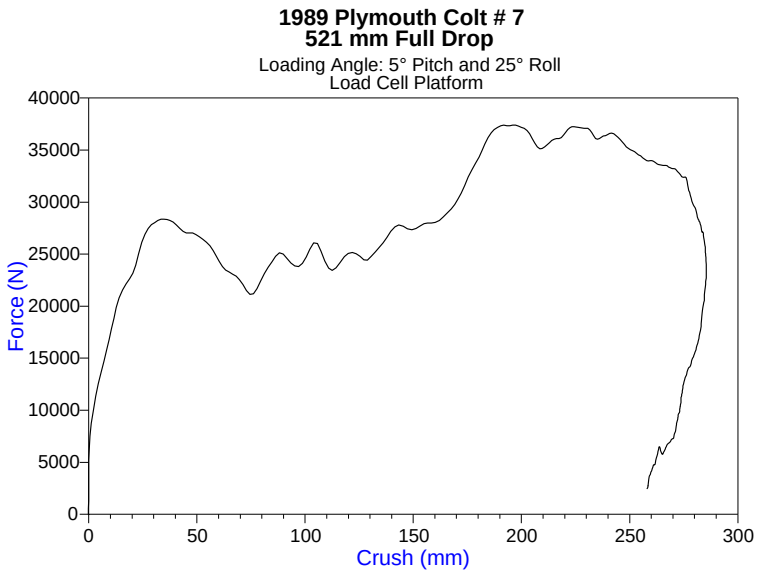


**Figure 26**-Force/crush curve for the Colt drop test onto the load plate.

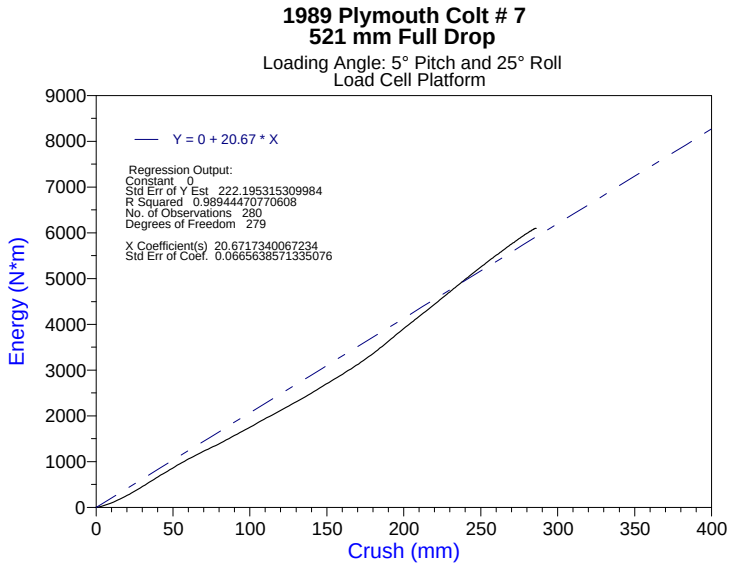


**Figure 27**-Energy/crush curve for the Colt drop test onto the load plate.

| Table 9 - Summary of vehicle ranking using dynamic data | | | | | | |
|---|---|---|---|---|---|---|
| **Vehicles Ranked by Energy** | **Energy @ 254 mm (N*m)** | **Energy $R^2$** | **Stiffness (N/mm)** | **Peak Force (N)** | **Ranking by Stiffness** | **Ranking by Peak Force** |
| Taurus #3 | 10146 | 0.98 | 689 | 36292 | 4 | 2 |
| Caprice #2 | 8925 | 1 | 389 | 34590 | 6 | 3 |
| Explorer #2 | 8433 | 0.99 | 602 | 45748 | 5 | 1 |
| Cavalier #2 | 5984 | 1 | 1057 | 20760 | 1 | 6 |
| Nissan #10 | 5880 | 1 | 865 | 32040 | 2 | 4 |
| Colt #7 | 5357 | 0.99 | 805 | 28366 | 3 | 5 |
| **Average** | **7454** | **0.99** | **735** | **32966** | | |
| **Standard Deviation** | **1970** | **0.01** | **230** | **8344** | | |
| | | | | | | |
| **Vehicles Ranked by Normalized Energy** | **Normalized Energy @ 254 mm (N*m)** | | **Normalized Stiffness (N/mm)** | **Normalized Peak Force (N)** | **Ranking by Normalized Stiffness** | **Ranking by Normalized Peak Force** |
| Taurus #3 | 0.769 | | 0.0522 | 2.749 | 4 | 3 |
| Colt #7 | 0.588 | | 0.0883 | 3.112 | 2 | 1 |
| Cavalier #2 | 0.561 | | 0.0990 | 1.945 | 1 | 6 |
| Caprice #2 | 0.531 | | 0.0231 | 2.058 | 6 | 5 |
| Nissan #10 | 0.517 | | 0.0761 | 2.818 | 5 | 2 |
| Explorer #2 | 0.506 | | 0.0361 | 2.744 | 3 | 4 |
| **Average** | **0.678** | | **0.0703** | **2.931** | | |
| **Standard Deviation** | **0.128** | | **0.0255** | **0.257** | | |

The dynamic and static energy vs. crush curves were fit to straight lines using least squares regression (Figure 30). The resulting correlation coefficient ($R^2$), was very high in each case (>.95). The dynamic roof crush energy had a higher slope than the static roof crush energy in each case, which lends support to using energy as a metric for comparing the static and dynamic roof crush. The dynamic energy slope can be set equal to the static energy slope times an amplification factor. When this was done, the amplification factor for the six tests here ranged from 1.1 to 1.6. Consequently, dynamic energy cannot be predicted as a linear function of static energy alone.

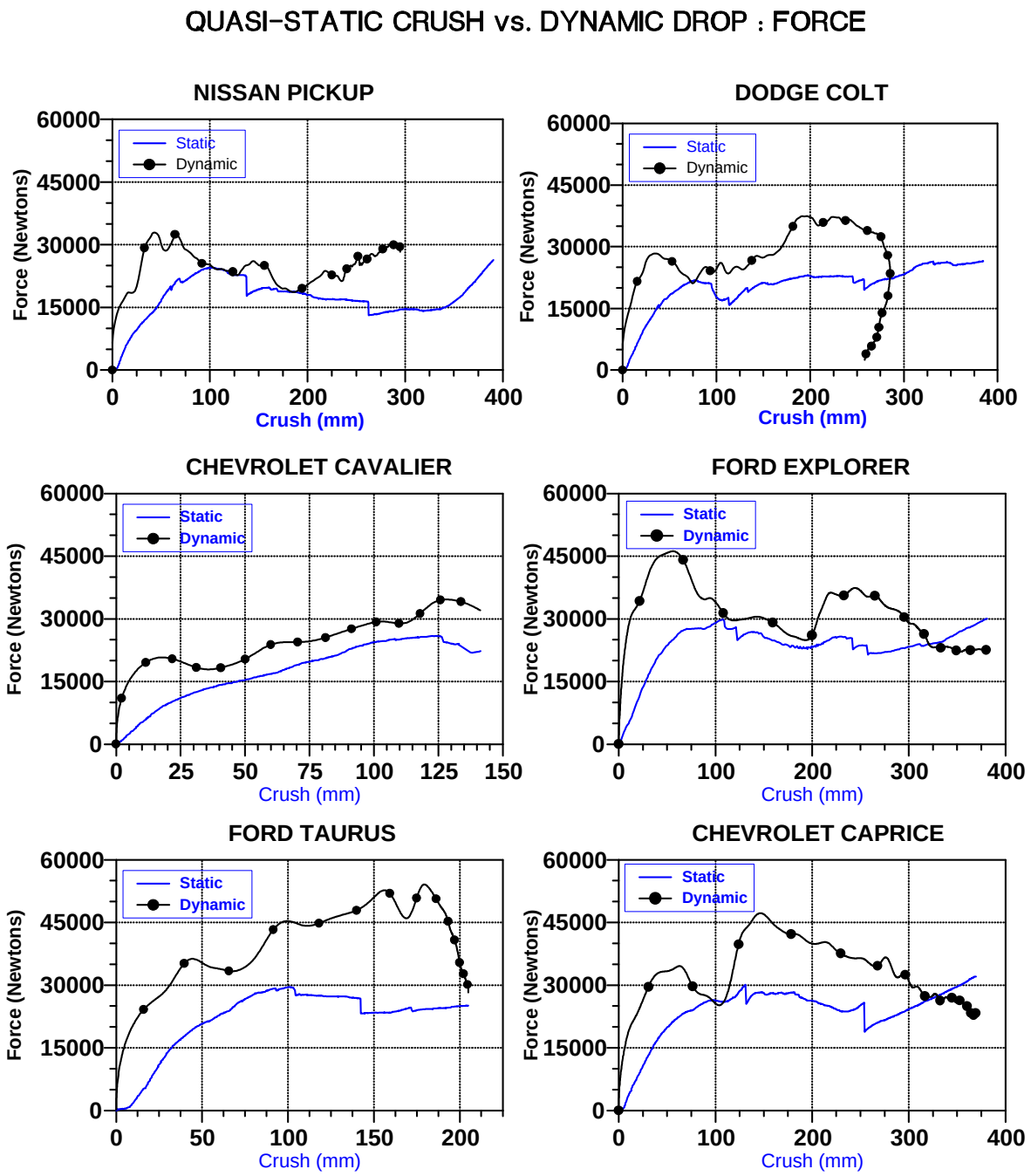


**Figure 28**-Quasi-static vs. Dynamic drop for force/crush data.

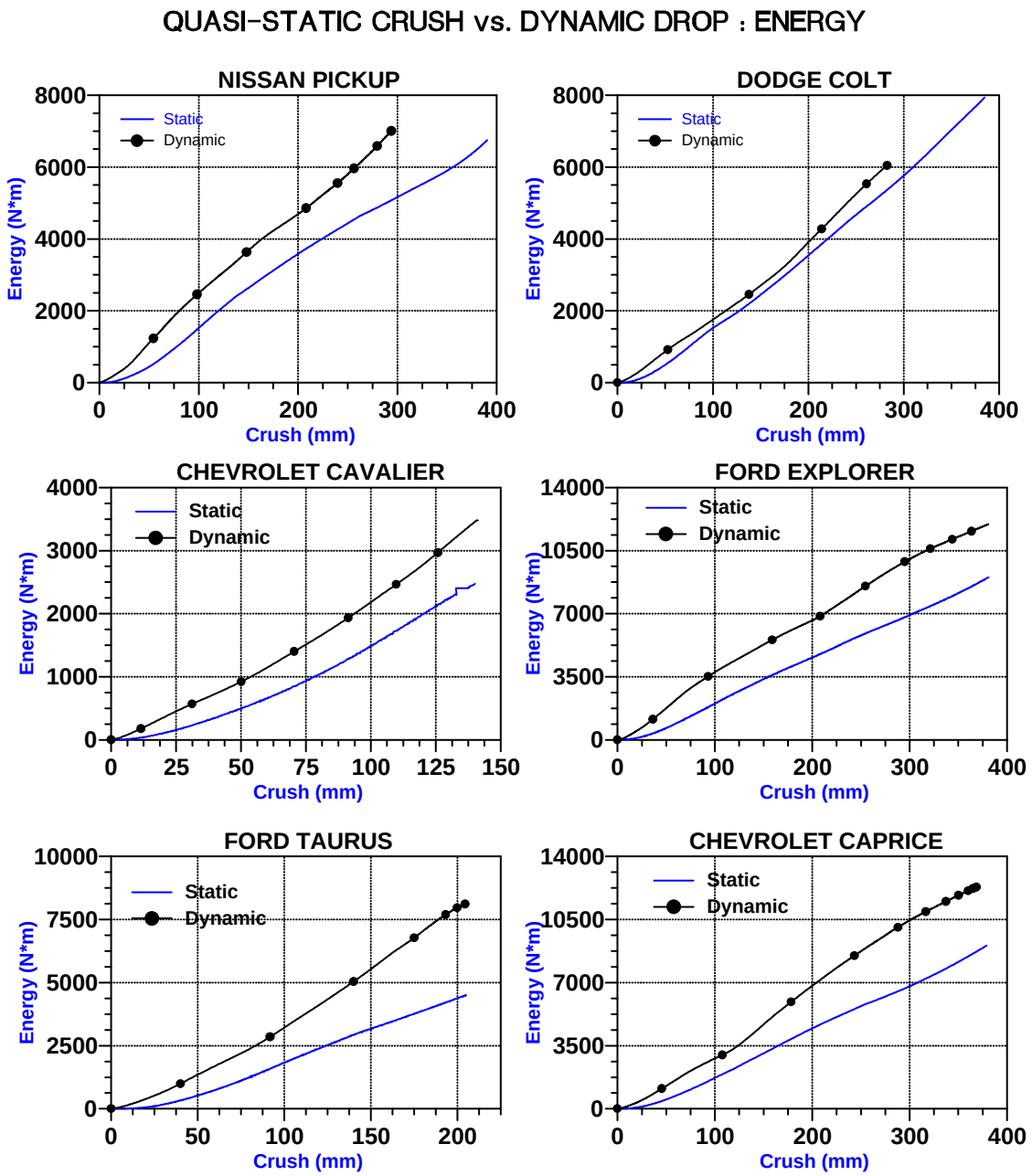


**Figure 29**-Quasi-static vs. Dynamic drop for energy/crush data.

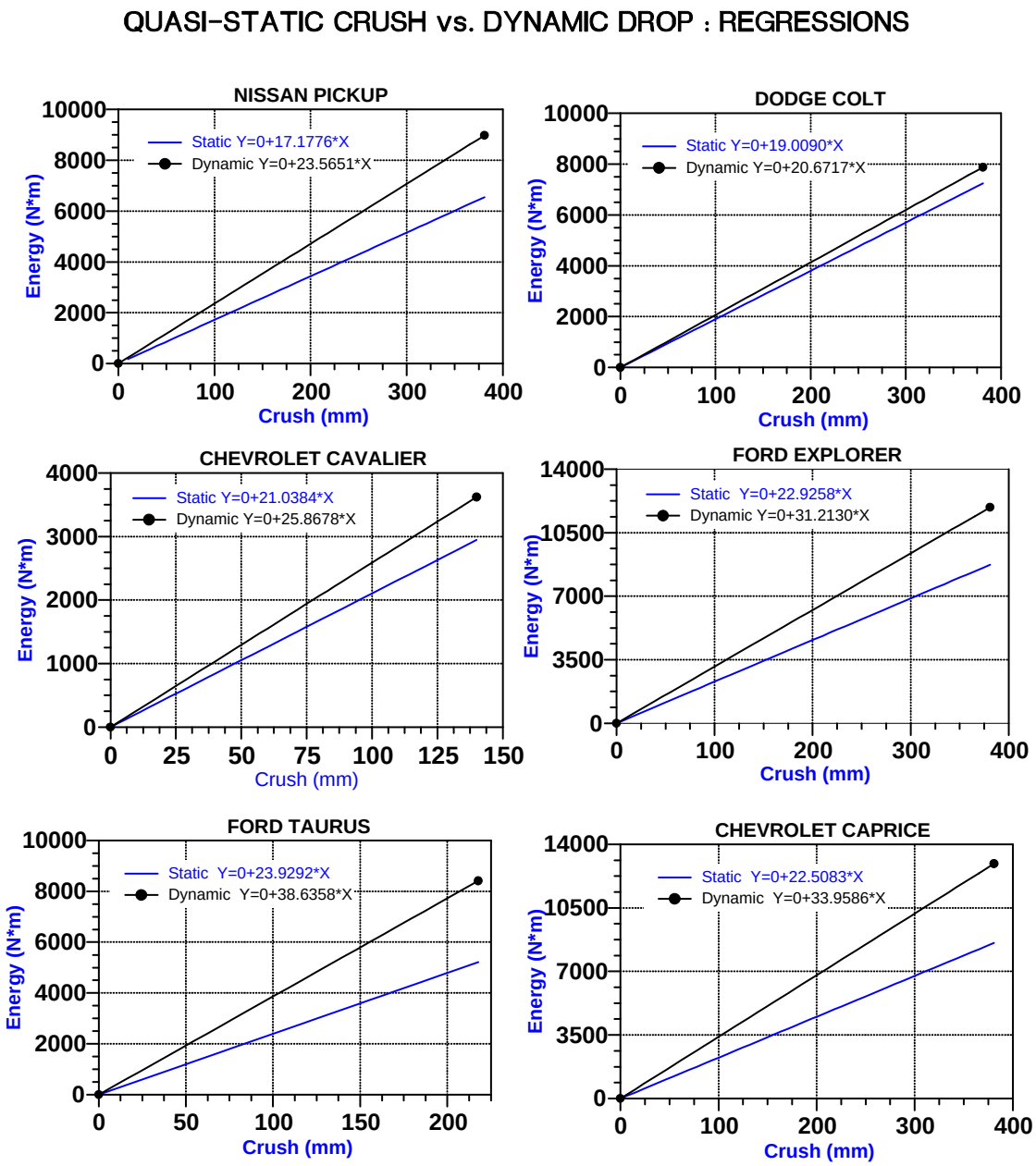


**Figure 30**-Quasi-static vs. Dynamic drop for regression data.

## 5.2 Statistical Analysis

A statistical analysis was conducted to determine if the slope of the dynamic energy vs. roof crush could be predicted from static test results and vehicle dependent parameters. A multiple linear regression was conducted using the SAS program to predict the dynamic energy slope based on the static energy slope, A-pillar length, roof area, and front/rear weight ratio of the vehicle (Table 10). Using the SAS regression procedure, variables were added and dropped from the model based on their statistical significance to the prediction of the dynamic energy slope. Using the parameters listed in Table 10, the static energy was the only statistically significant variable (at a 0.25 level) resulting in a $R^2$ of 0.78. Since static energy can be a squared function of crush, a new variable was added to the list of variables that was equivalent to the static energy slope squared. Table 11 shows the results of the SAS run. The model chosen to predict the dynamic energy slope was:

$$E_D = E_N \times \beta_2 + E_S \times \beta_1 + \beta_0 \qquad \textbf{[4]}$$

where, $E_D$ = Dynamic slope (N),

$E_N$ = Static slope squared $(\text{N-m/mm})^2$

$E_S$ = Static Slope (N),

$\beta_0$, $\beta_1$, and $\beta_2$ = regression constants.

The regression constants, taken from Table 11 of the SAS run results are,

$\beta_0$ =220.6

$\beta_1$ =- -21.459

$\beta_2$ =0.580

The measure of the accuracy of this equation is judged by the regression correlation coefficient ($R^2$), which was 0.94. Therefore, this equation predicts dynamic energy absorption for the vehicles and conditions tested in this study with a reasonable level of accuracy.

**Table 10 - Data used in statistical analysis**

**Data on characteristics of test cars:**

Measured from largest common roof crush

| Vehicle | Dyn. en. slope | Sta. en. slope | Ratio | Weight Front (kg) | Weight Rear (kg) | Ratio Front to Rear | "A" Pillar Length (mm) | Roof Area ($mm^2$/1000) |
|---|---|---|---|---|---|---|---|---|
| 1989 Dodge Colt | 20.67 | 19.01 | 1.09 | 632 | 351 | 1.79 | 778.76 | 1535.0 |
| 1989 Nissan Pickup | 23.56 | 17.18 | 1.37 | 684 | 496 | 1.38 | 693.17 | 880.2 |
| 1990 Chevy Cavalier* | 25.87 | 21.04 | 1.23 | 717 | 372 | 1.93 | 634.20 | 1245.4 |
| 1992 Ford Taurus | 38.64 | 23.93 | 1.61 | 889 | 458 | 1.94 | 761.24 | 1666.9 |
| 1991 Ford Explorer | 31.21 | 22.93 | 1.36 | 894 | 807 | 1.11 | 641.35 | 2652.6 |
| 1991 Chevy Caprice | 33.96 | 22.51 | 1.51 | 1007 | 708 | 1.42 | 761.75 | 1978.6 |

* - string pot broke after 140 mm of roof crush

**Table 11 - Results of statistical analysis**

The SAS System 7

Bounds on condition number: 1, 1

Step 2 Variable ES Entered R-squares = 0.93832347 C(p) = .

| | DF | Sum of Squares | Mean Square | F | Prob>F |
|---|---|---|---|---|---|
| Regression | 2 | 216.93414669 | 108.46707334 | 22.82 | 0.0153 |
| Error | 3 | 14.25920331 | 4.75306777 | | |
| Total | 5 | 231.19335000 | | | |

| Variable | Parameter Estimate | Standard Error | Type II Sum of Squares | F | Prob>F |
|---|---|---|---|---|---|
| INTERCEP | 220.57569803 | 87.17008853 | 30.43367210 | 6.40 | 0.0854 |
| EN | 0.57951949 | 0.20884548 | 36.59821772 | 7.70 | 0.0693 |
| SE | -21.45943325 | 8.58323289 | 29.71041444 | 6.25 | 0.0877 |

Bounds on condition number: 512.7974, 2051.19

All variables left in the model are significant at the 0.2500 level.
No other variable met the 0.2500 significance level for entry into the model.

The results indicate that the dynamic energy slope can be predicted for the six tests used to develop the correlation. Table 12 shows the static energy slope, actual and predicted dynamic slope, and percent difference between the actual and predicted dynamic slope. However, each of these vehicles were dropped from a height that resulted in the same energy input to the roof as the energy at 254 mm (10") of static roof crush. In the real-world, roof loading may vary significantly in the dynamics of the rollover. Therefore, unless a prescribed rollover crash severity can be established, the prediction of dynamic roof crush energy from a static test should ideally be insensitive to drop height, or more directly, impact severity.

**Table 12 - Results from application of the prediction equation**

| Vehicle | Static Slope | Predicted Dynamic Slope | Actual Dynamic Slope | % Diff. |
|---|---|---|---|---|
| Nissan Pickup | 17.18 | 23.13 | 23.59 | 2.0 % |
| Dodge Colt | 19.01 | 22.26 | 20.67 | 7.7 % |
| Cavalier | 21.04 | 25.85 | 25.87 | -0.1 % |
| Ford Explorer | 22.93 | 33.48 | 31.21 | 7.3 % |
| Taurus | 23.93 | 39.22 | 38.64 | 1.5 % |
| Caprice | 22.51 | 31.44 | 33.96 | -7.4 % |

To examine this issue further, another series of drop tests were conducted to examine the sensitivity of the roof crush force and deformation to drop height. The Chevy Caprice and Chevy Cavalier were chosen from the six vehicles as good and poor performing vehicles in the combined static and drop tests. It was judged that by using the best and worst vehicles in our study, the results should encompass the majority of vehicles in the fleet.

A total of four additional drop tests were conducted (Table 13). Two drop tests were conducted with two Chevy Caprices at drop heights of 140 mm and 241 mm. (The drop heights were set so that the potential energy of each vehicle was equal to the roof crush energy after 127 and 191

| Table 13 - Test matrix for drop height analysis testing | | | | |
|---|---|---|---|---|
| Test Vehicle | Static Crush (mm) | Static Energy From E Curve (N*m) | Calculated Drop Height (mm) Equation 2 | Drop Height Used (Mm) |
| Caprice #2 | 254 | 5781.7 | 343.7 | 343 |
| Caprice #3 | 127 | 2444.6 | 145.4 | 140 |
| Caprice #4 | 191 | 4217.7 | 250.9 | 241 |
| Cavalier #2 | 254 | 5055.5 | 473.4 | 472 |
| Cavalier #3 | 127 | 2163.5 | 202.7 | 203 |

mm of static roof crush).The resulting force vs. crush and energy vs. crush plots were over-lain with the initial drop height results (Figures 31 and 33). Two Chevy Cavaliers were tested similarly at drop heights of 203 mm and 340 mm and overlain in Figures 32 and 34.

The three drops of the Caprice reveal that the force vs. crush characteristics were very similar for all three drop heights. As a result, the energy vs. crush curves for the Caprice were all very similar (Figure 34). The force vs. crush characteristics of the three Cavaliers showed variations in the load carrying capacity of the roof after only about 20 mm of crush. As drop height increased, the force level to the first peak occurred at lower levels and at smaller amounts of crush. Therefore it appeared the rate of loading had a more significant effect on the load carrying capacity for the Cavalier when compared to the Caprice. However, differences in the force vs. crush plots did not translate to significant difference in the energy vs. crush comparison (Figure 34).

When the energy vs. crush curves were linearized for the Caprice and Cavalier, there was close agreement between the three drop heights (Figures 35 and 36). The slope of the lines for the Caprice varied from 30.4 to 34.8 N*m/mm, with the average slope equaling 33.04 (N*m/mm). The linear regression of the Cavalier energy curves yielded slopes ranging from 25.9 to 28.0 (N*m/mm), with an average slope of 26.7 (N*m/mm). The predicted dynamic energy slopes for Caprice and Cavalier were 31.44 and 25.85 (N*m/mm) , respectively.

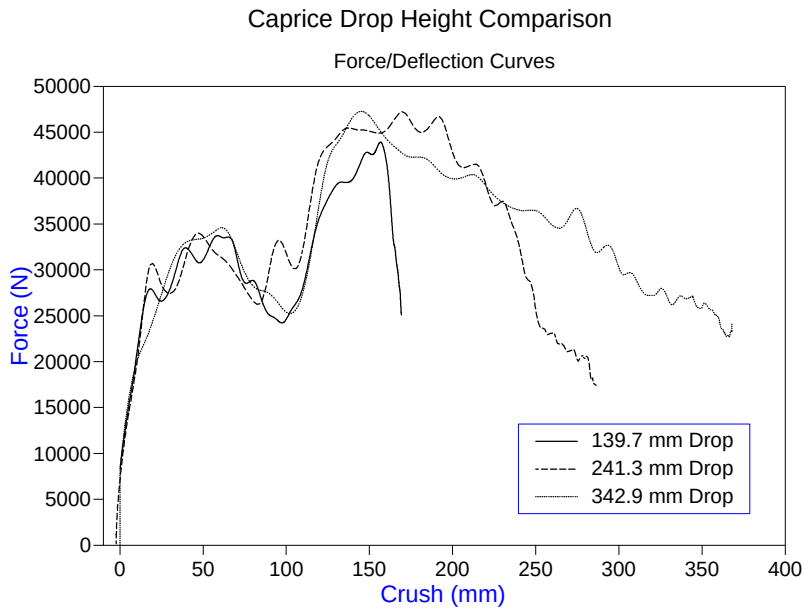


**Figure 31**-Caprice drop height comparison of force/crush.

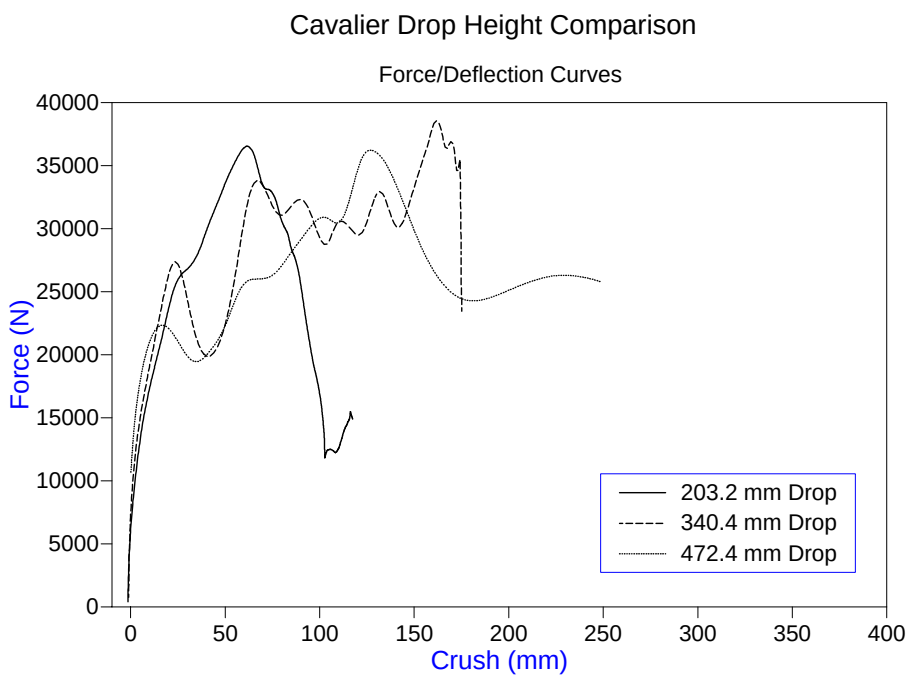


**Figure 32**-Cavalier drop height comparison of force/crush.

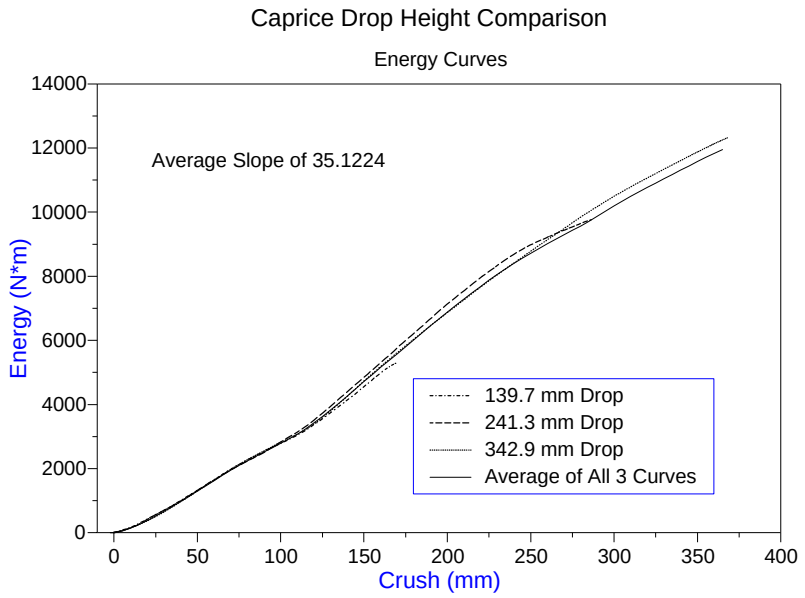


**Figure 33**-Caprice drop height comparison of energy/crush.

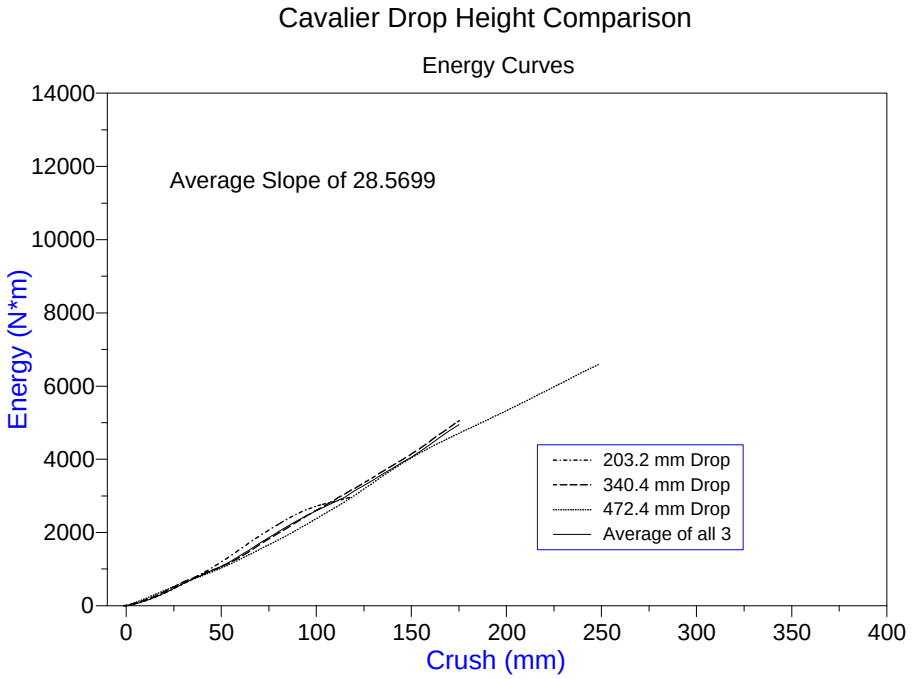


**Figure 34**-Cavalier drop height comparison of energy/crush.

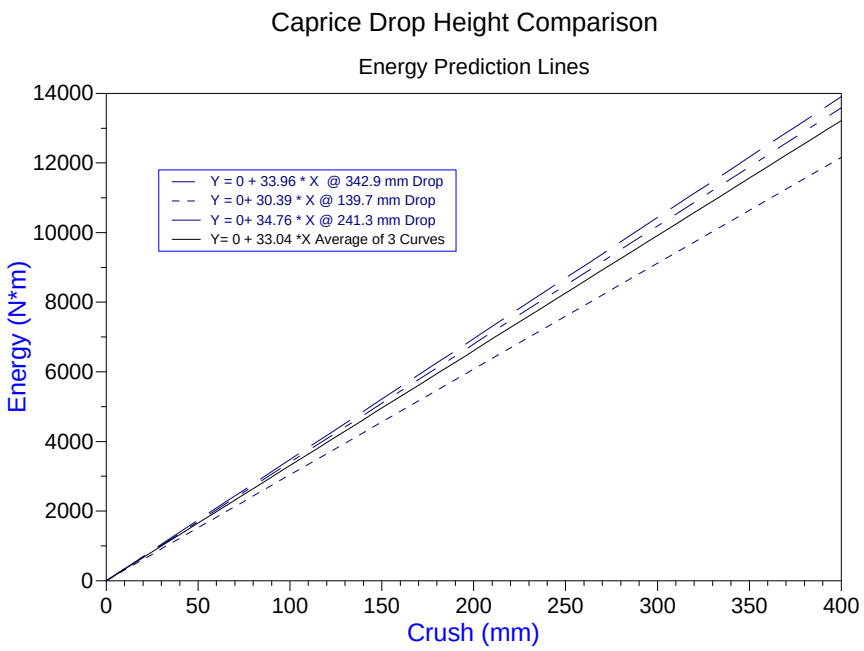


**Figure 35**-Caprice drop height comparison for regressions.

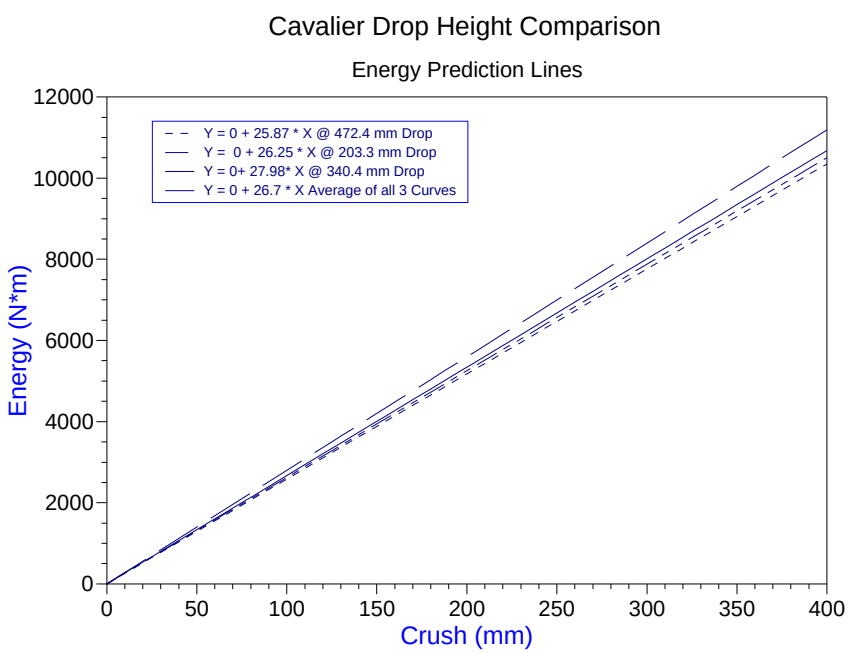


**Figure 36**-Cavalier drop height comparison for regressions.

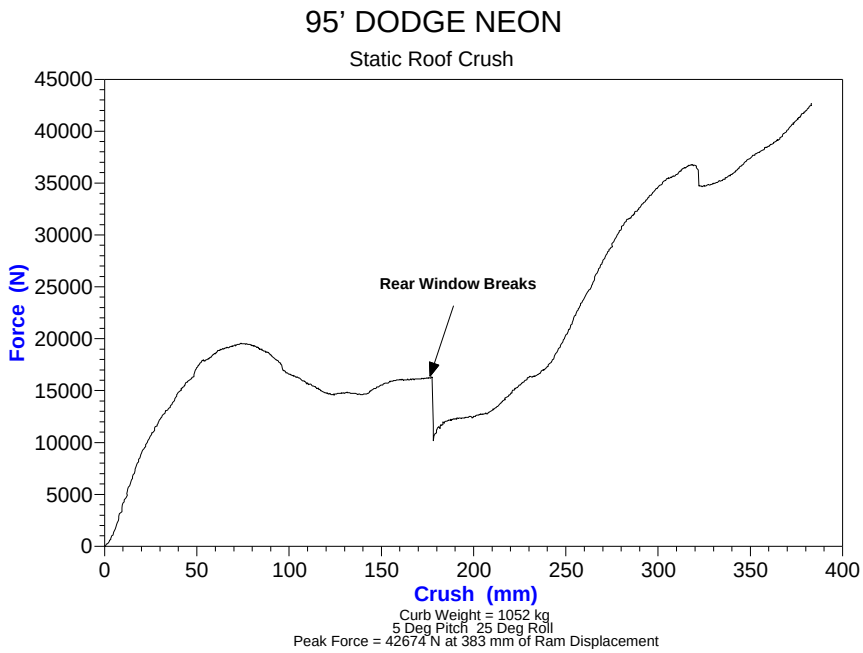


**Figure 37**-Dodge Neon force/crush curve for quasi-static test.

## 5.3 Regression Model Validation

To test the accuracy of the regression technique for calculating the dynamic energy slope, a 1995 Dodge Neon was selected for validating the model. The roof was quasi-statically crushed to 381 mm. The force vs. crush (Figure 37) was integrated to get the energy vs. crush curve (Figure 38). The energy curve was linearized, and the dynamic energy curve was then calculated using Equation 4 (Figure 39). To examine the accuracy of this prediction, additional Dodge Neons were dropped from heights equivalent to the energy input at 254 mm (10") and 127 mm (5") of static roof crush. The resulting drop heights were 343 mm (13.5") and 168 mm (6.6"). The resulting force vs. crush from the load plate was then integrated and linearized. The comparison of the predicted and actual dynamic energy vs. crush of the Neon is shown in Figure 40. The percent error between the slope of the actual and predicted values is 17.2 % for the higher drop height. The lower drop height was closer to the predicted, but still had a 8.2 % error from the test data. In this case the predictive power of the equation was degraded as drop height (severity) increased.

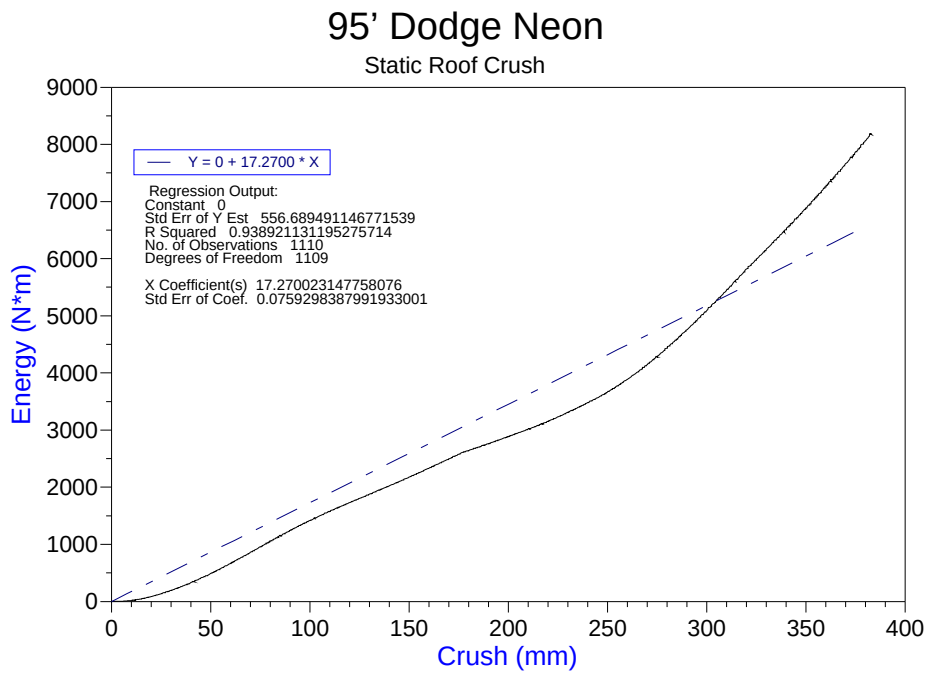


**Figure 38**-Dodge Neon energy/crush and regression curves for quasi-static test.

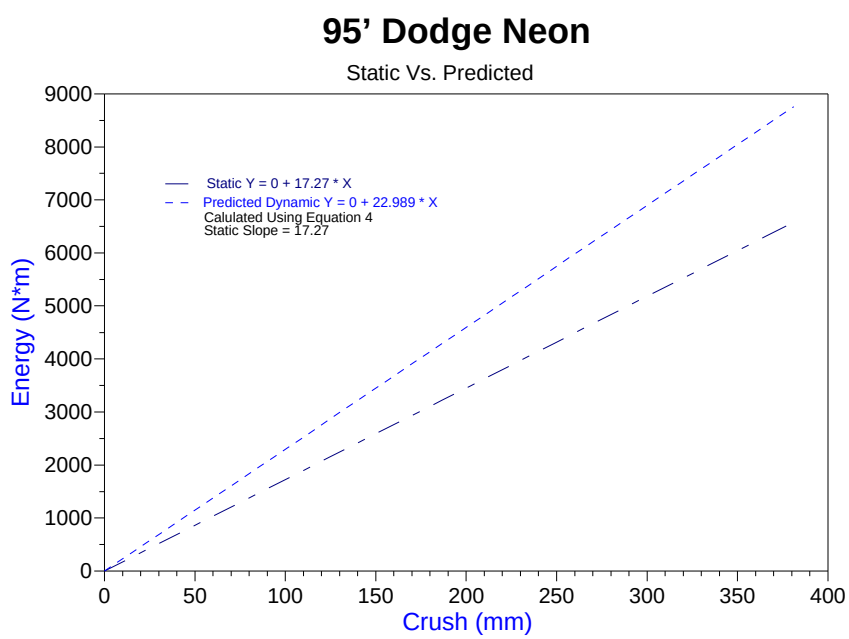


**Figure 39**-Dodge Neon regression lines for quasi-static test vs. predicted.

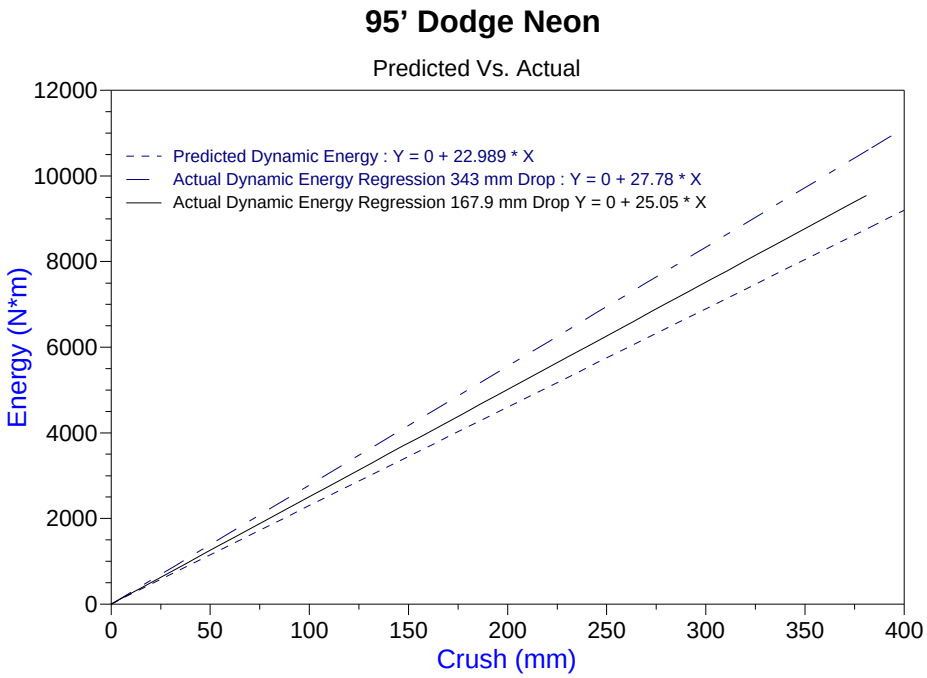


**Figure 40**-Dodge Neon regression lines for predicted vs. actual at 2 heights.

## 6.0 SUMMARY AND CONCLUSIONS:

A comprehensive study of quasi-static and dynamic loading of roof structures was conducted at the VRTC. Initially, nine vehicle roof structures were crushed quasi-statically using the test procedures and load plate in FMVSS No. 216, roof crush resistance. Roofs were crushed to 381 mm (15 inches) in 127 mm (5 inch) increments on each vehicle. Roof profile measurements were made and force and integrated energy vs crush were plotted. Each vehicle was ranked by increasing stiffness and peak plate force. Results indicated that roof strength varies from vehicle to vehicle and when made relative to the vehicle weight, apparent performance can also change. When analyzing the CK-1500 pickup stiffness, it performed better than any other vehicle. However, when

normalizing by vehicle weight it became the 5th best performer. These rankings were then used to pick vehicles for dynamic drop testing.

The effect of load plate angle on roof crush resistance was also investigated using two of the vehicle types (1990 Dodge Colt and 1989 Nissan Pickup). When loading the roof at 0° pitch and 15° roll, the roof deflected less at the same load than at the standard 216 angles (5° pitch , 25° roll). This was attributed to the load being applied at a more perpendicular angle to the A-pillar column, than in FMVSS 216 which loads the A-pillar more in bending.

A study of dynamic roof crush resistance and failure modes was then conducted. The 1989 Nissan Pickup and 1990 Dodge Colt were dropped onto their roofs at heights and angles corresponding to static crush energies in the FMVSS No. 216 procedure. Roof profile and peak deflection comparisons were made between the drop tests and the quasi-static tests. Based on profile measurements, it appeared that roof failure modes in the dynamic drop tests were identical to those measured in the profiles of the static tests. Consequently, a static test was comparable to the dynamic test in that regard. The primary difference between the static and dynamic tests was the peak roof crush measurement. Dynamic roof crush was less than the quasi-static roof crush test with the same energy input. This was attributed to the changes in load application as the vehicle rolls during roof crush, and by interaction of the vehicle hood with the floor. Therefore, some energy is absorbed by the vehicle hood and reduces the forces on the vehicle roof in the drop test. Subsequent testing onto a load plate eliminated hood interaction by raising the load plate 510 mm (20 inches) above the ground.

Based on peak strength and stiffness in the static tests, six of the nine vehicles tested quasi-statically were selected for drop tests onto a load plate (Three vehicles were relatively good

performers and three were relatively poor performers in the quasi-static test). These tests were conducted to determine the dynamic force vs. deflection characteristics of each vehicle roof when dropped at a pre-determined level. Each vehicle was dropped at a height that input energy into the roof that was equivalent to energy at 254 mm (10 inches) of roof crush in the quasi-static test. Force vs. crush and the integrated energy vs. crush were measured and calculated. Energy plots from the quasi-static testing and the dynamic testing were then compared. A statistical correlation was developed to predict the slope of the dynamic energy from the slope of the static energy as a function of roof crush. The following conclusions were derived from comparisons of the static and dynamic drop tests onto a load plate:

1. The peak force in the dynamic drop test was always higher than the peak force of the static test of the same vehicle model.

2. Both static and dynamic tests have energy vs. crush plots that can be estimated as straight lines. A least squares statistical fit was performed for each test, and the correlation coefficients ranged from .95 to .99.

3. When comparing the linearized static and dynamic energy vs. crush plots, the dynamic energy slopes ranged from 1.1 to 1.6 times the static energy slope.

4. A statistical correlation provided a good estimate of the dynamic energy slope from the static energy slope. A correlation coefficient ($R^2$) of .94 was produced.

Another series of tests were performed with the Cavalier and Caprice to determine the sensitivity of the dynamic force and energy plots to impact severity. To vary impact severity, the vehicle drop height was adjusted for each test. Two additional drops were conducted on each vehicle

type. Results showed that force vs. crush did not change significantly for the weaker roof structure (Caprice), but the peak force before the first drop-off in load carrying capacity of the Cavalier went down as the drop height increased. Consequently, the rate of loading was a factor in the resulting force vs. crush plots. The energy vs. crush results were very similar, however, for the three drops of each vehicle. The dynamic energy slopes ranged from 30.4 to 34.8 N*m/mm and 25.9 to 28.0 N*m/mm for the Caprice and Cavalier, respectively. The least squares regression predicted 31.4 and 25.8 N*m/mm for the Caprice and Cavalier, respectively. Consequently, load rate had an effect on the dynamic energy slope, but it appeared the least squares regression equation was still relatively accurate.

To validate the least squares statistical equation that predicted the slope of the dynamic energy curves, a Dodge Neon was selected and the roof quasi-statically crushed. Integrating and using Equation [4], the dynamic energy slope was predicted. Two additional Neons were then dropped onto the load cell barrier at a low and high drop height. The heights were based on the quasi-static crush energy at 127 mm (5 inches) and 254 mm (10 inches) of roof crush. The error of the predicted dynamic roof energy from the actual was 17.2 percent and 8.2 percent at the high and low drop height, respectively. Therefore, given the significant difference in the results of the predicted from the actual results, the least squares equation could not be validated to accurately predict the dynamic energy slope from the static test results.

Consequently, for a wide range of drop heights and vehicle types, the slope of the dynamic energy vs. crush slope is predictable with an error as much as 20 percent. Factors such as loading rate (drop height) significantly influence the difference in static and dynamic loading. Development of a static procedure for a FMVSS No. 216 upgrade would need to be correlated to one drop height severity, or the loading rate would need to be examined to determine if a higher rate can more readily

be compared to full-scale dynamic drop tests. If this could be done, an improved FMVSS No.216 may be realized by a static test that is transformed into a dynamically equivalent result. Based on the results of this study, the transformation could be based on a static to dynamic roof energy calculation.

The primary advantage of a static test procedure is the simplicity and repeatability of the test. It is a well known procedure and modification to the requirements, such as the limit on load plate displacement or changing the maximum plate application force would be simple to accomplish. On the other hand, it has yet to be shown that the static test procedure represents real-world rollover forces on the roof. This study set-out to show that quasi-static forces could be transformed to a dynamically equivalent load, thereby eliminating one of the primary objections to the static test. Another objection to the static test is the lack of performance based requirements that take into account dummy response to rollover forces. The static test cannot incorporate a dummy for injury measures, but could possibly use a dummy to measure roof head room reduction when the roof is crushed with the load plate.

The primary advantage of the dynamic test is that it can be related to dynamic loads that occur in real-world rollovers. The roof can be dynamically loaded and a dummy could also be added to the procedure to measure dummy response. However, the advantages in the static procedure are the disadvantages in the dynamic test. The test would be difficult to administer, particularly with a dummy, and it would be inherently less repeatable than the static test. In addition, the choice of impact severity would be difficult to determine and justify from crash data. There is currently no universally accepted measure of rollover severity. While these problems are not insurmountable, they could extend the development of an improved test procedure significantly.

## 7.0 REFERENCES


1. Rollover Prevention and Roof Crush - Congressional Report. 1992. National Highway Traffic Safety Administration; USDOT

2. Federal Motor Vehicle Safety Standard No. 216 - Roof Crush Resistance. CFR 49 571.216, October 1997.

3. Vehicle and Dummy Kinematics in a Controlled Rollover Crash. Rollover Crash Test Reports. National Crash Analysis Center, Ashburn, VA.

4. H. Cheng, A.. L. Rizer and L. A. Obergefell, "Pickup Truck Rollover Accident Reconstruction using the ATB Model, SAE 950133, 1995.

5. Design Modification for a 1989 Nissan Pick-up - Final Report. 1991. NHTSA/USDOT. DOT HS 807 925, NTIS, Springfield, Virginia, 22161.

6. W. Riley Garrot, Michael W. Monk and Jeffery P. Christos, "Vehicle Inertial Parameters - Measured Values and Approximations," SAE Paper 881767, Society of Automotive Engineers, Warrendale, PA, 1988.

7. Glen C. Rains and Joseph N. Kanianthra. "Determination of the Significance of Roof Crush on Head and Neck Injury to Passenger Vehicle Occupants in Rollover Crashes," SAE Paper 950655, Society of Automotive Engineers, Warrendale, PA, 1988.

8. Michael J. Leigh and Donald T. Willke, "Upgraded Rollover Roof Crush Protection: Rollover Test and Nass Case Analysis," Internal Event Report VRTC-81-0197, East Liberty, OH, June 1992

# APPENDIX A

(Roof profiles for all vehicles tested using the static test device.)

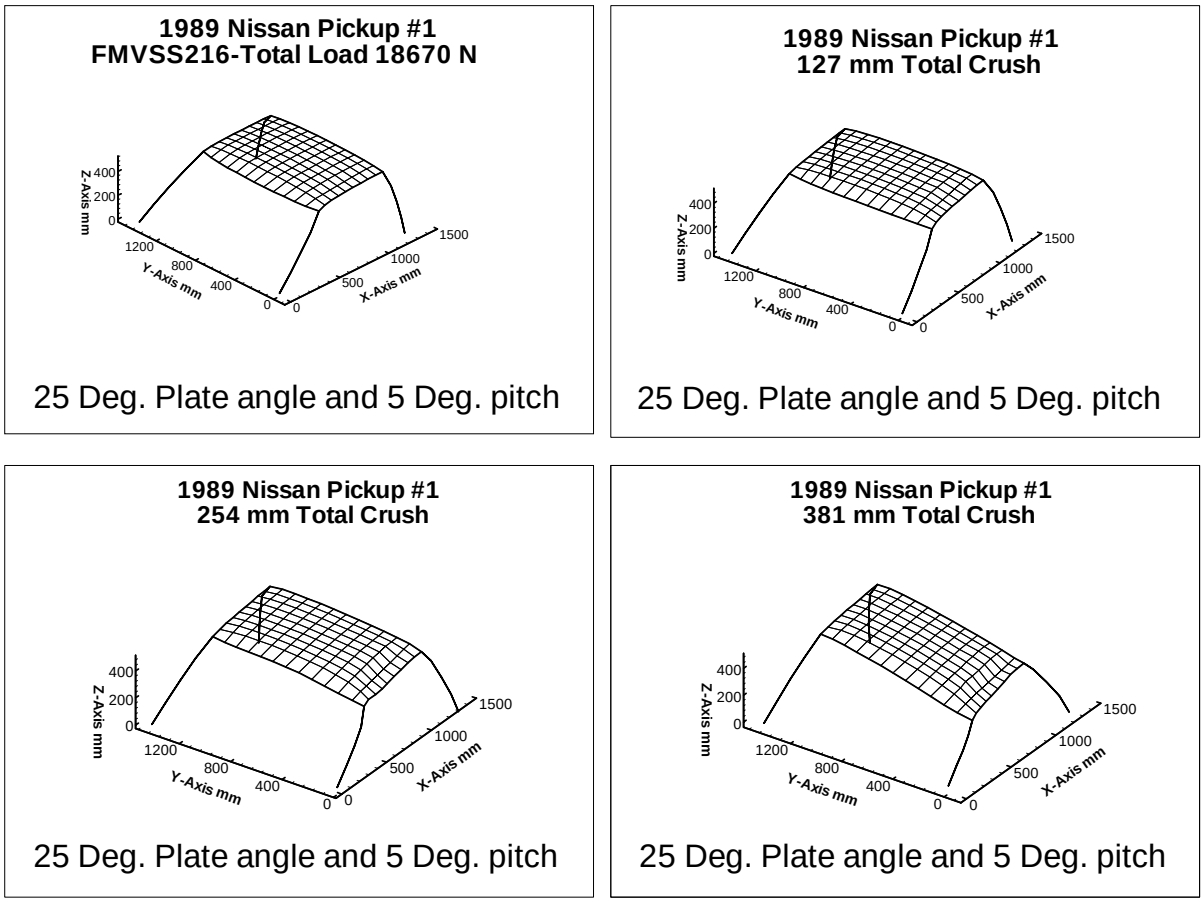


**Figure A(1)**-Nissan #1 quasi-static tests roof crush profiles.

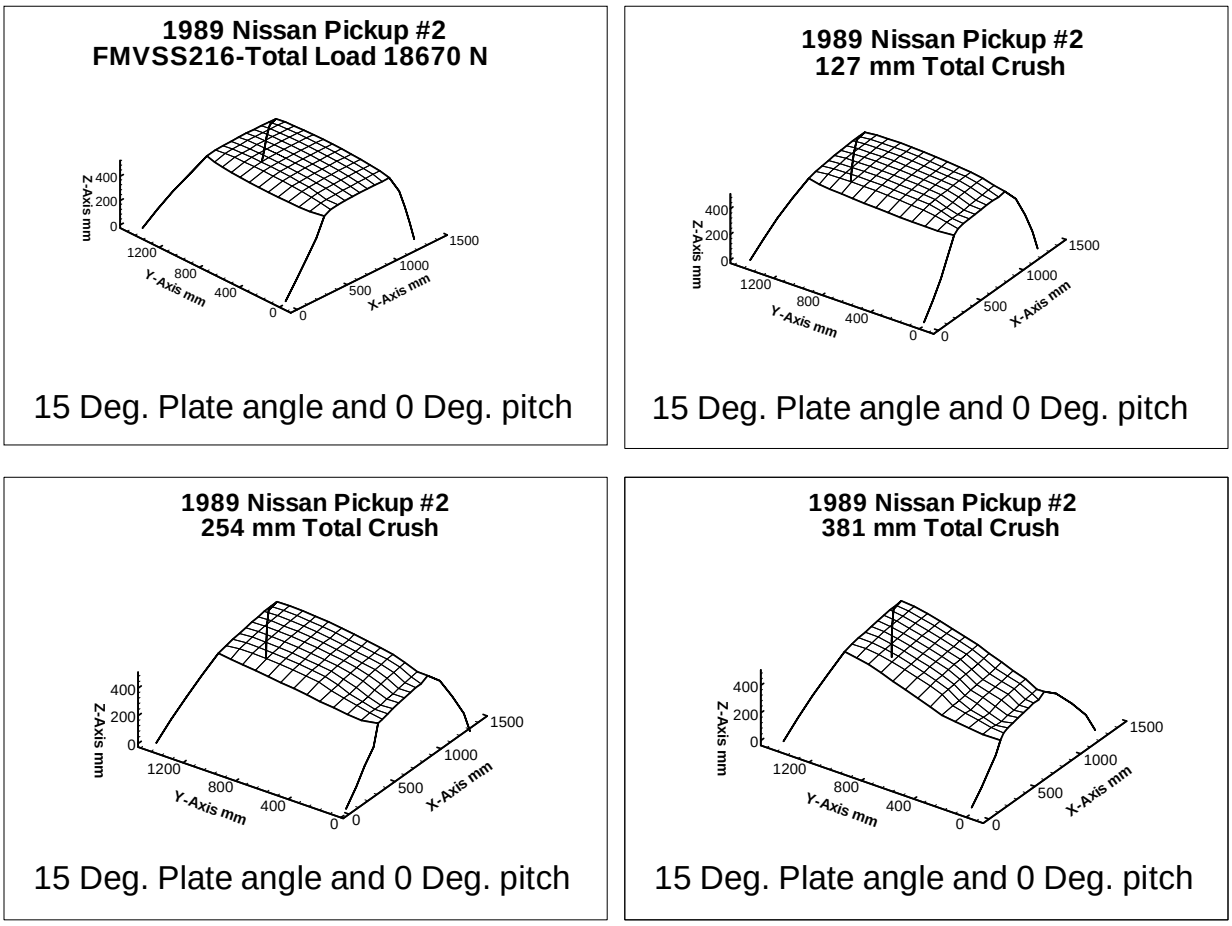


**Figure A(2)**-Nissan #2 quasi-static tests roof profiles.

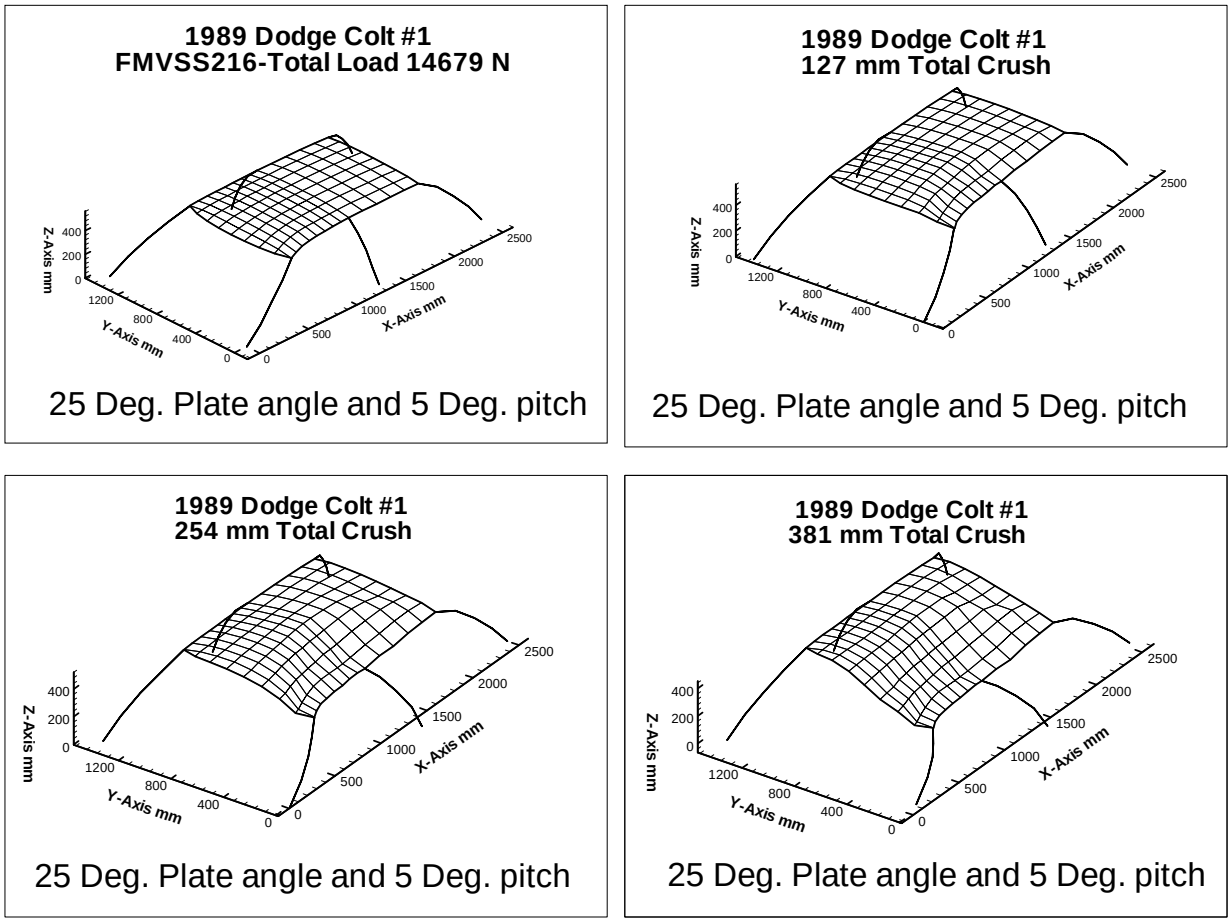


**Figure A(3)-**Dodge Colt #1 quasi-static tests roof profiles.

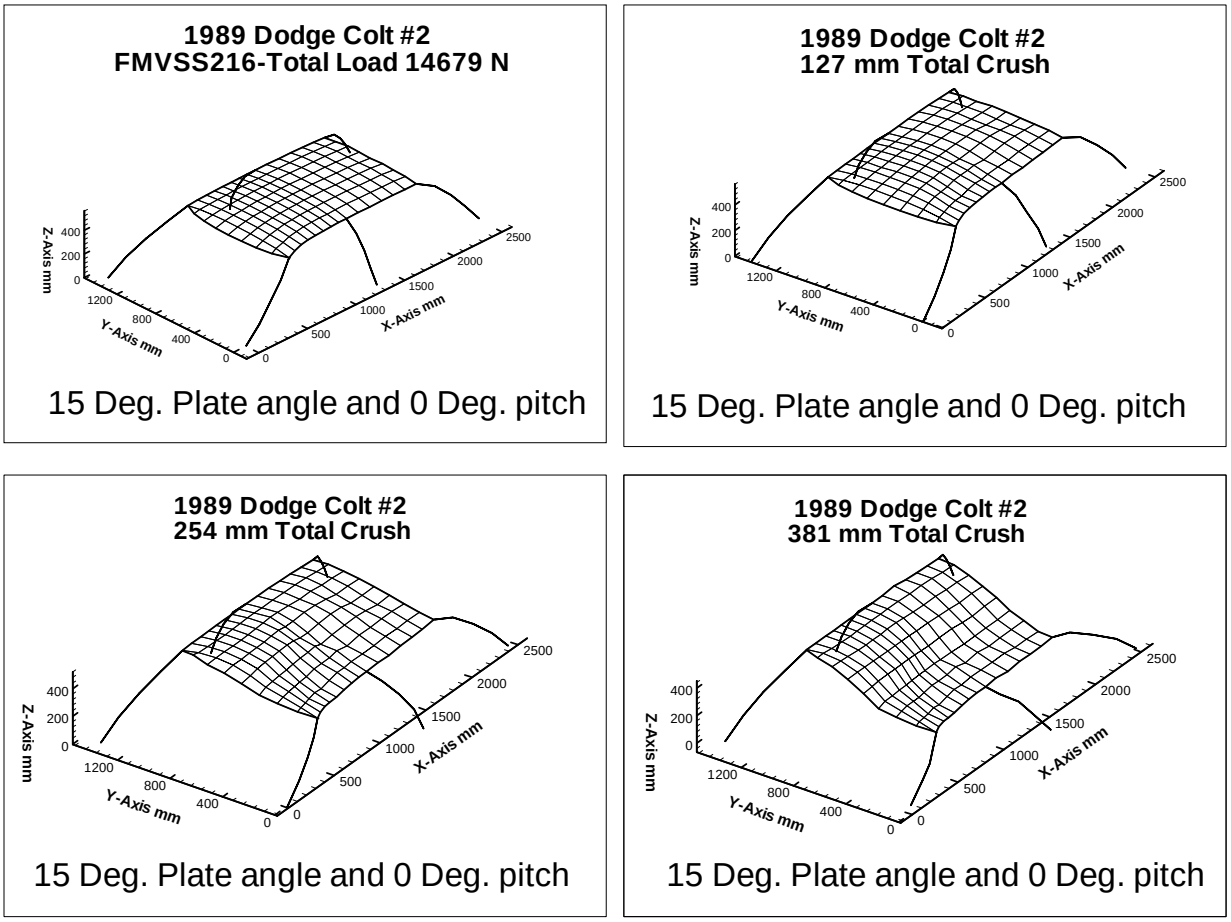


**Figure A(4)**-Dodge Colt #2 quasi-static tests roof profiles.

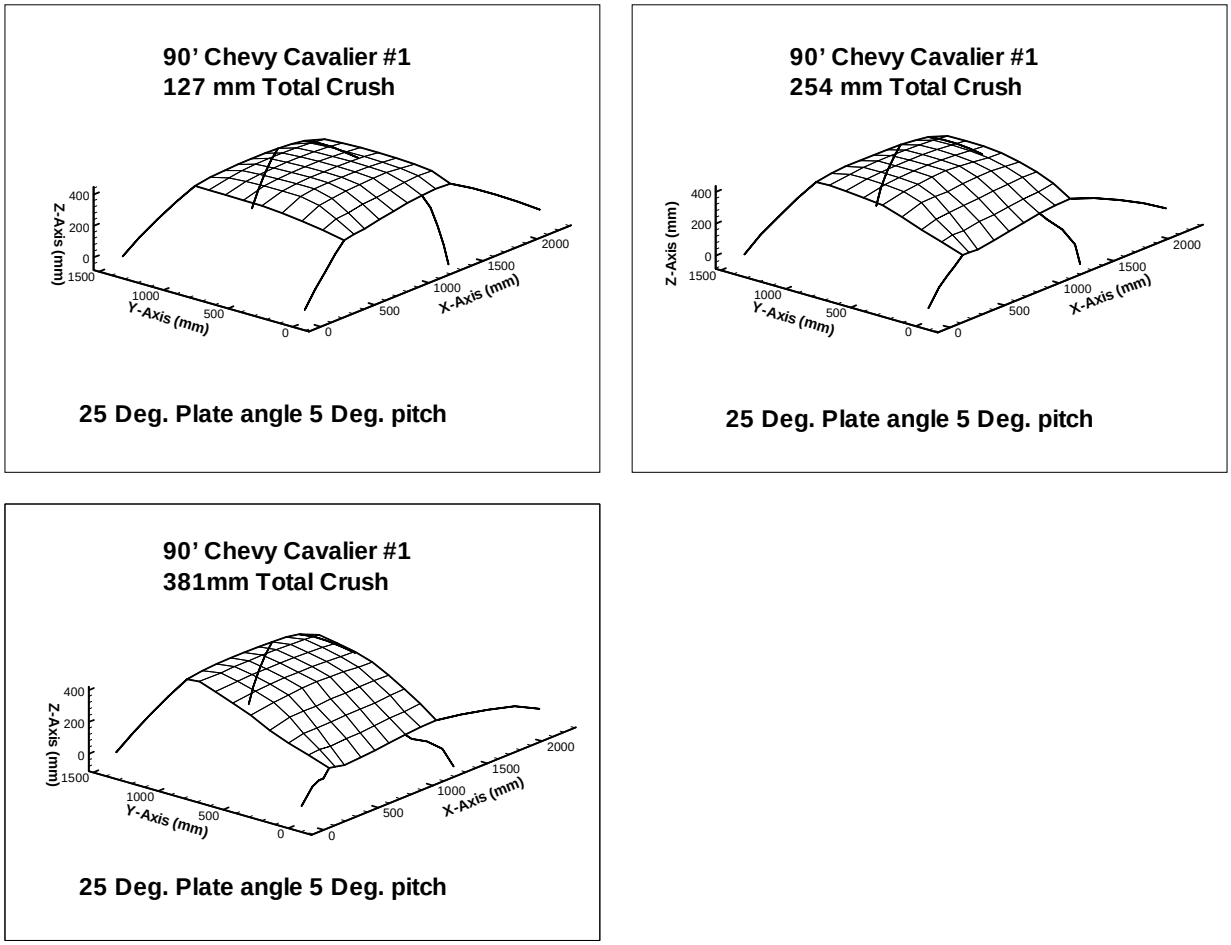


**Figure A(5)**-Chevy Cavalier #1 quasi-static tests roof profiles.

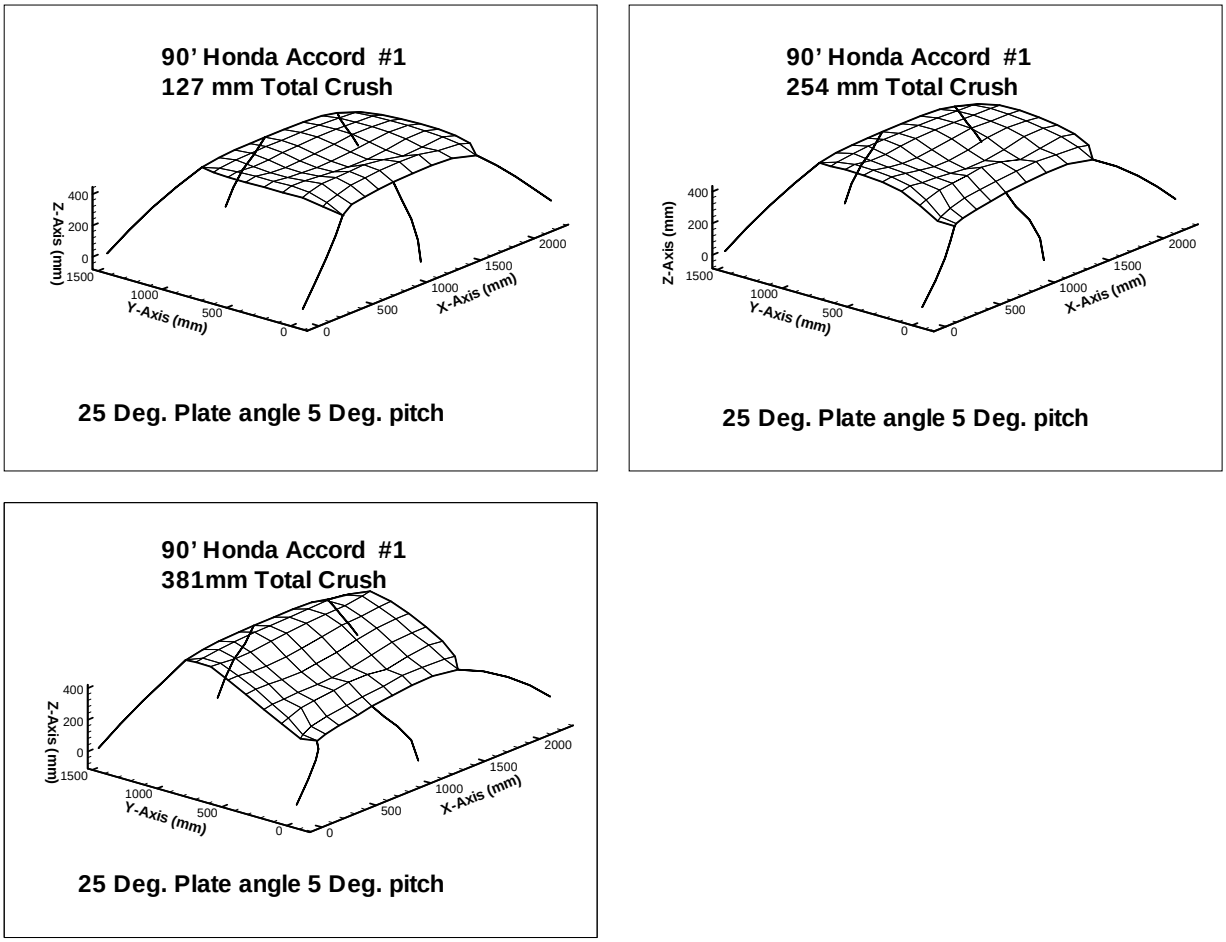


**Figure A(6)**-Honda Accord quasi-static tests roof profiles.

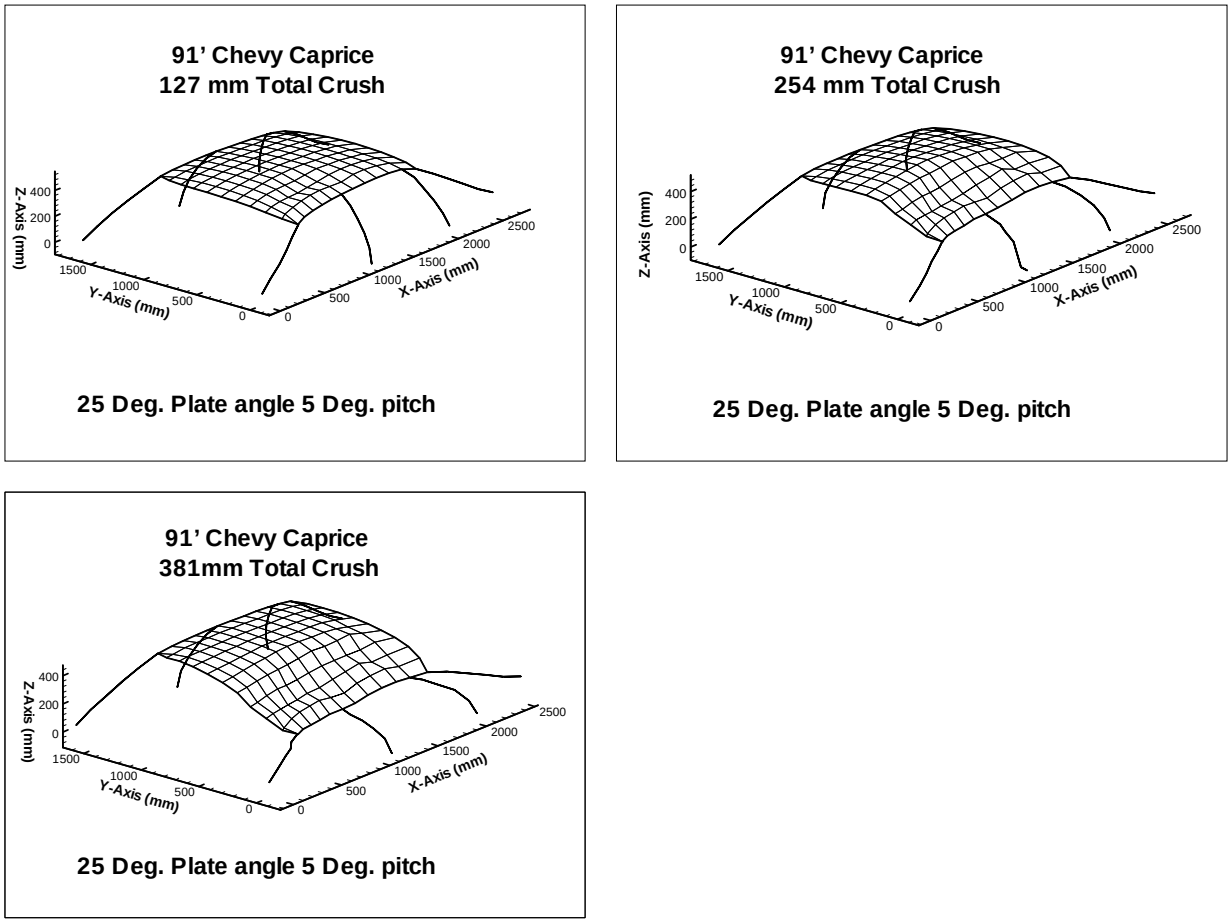


**Figure A(7)**-Chevy Caprice #1 quasi-static tests roof crush profiles.

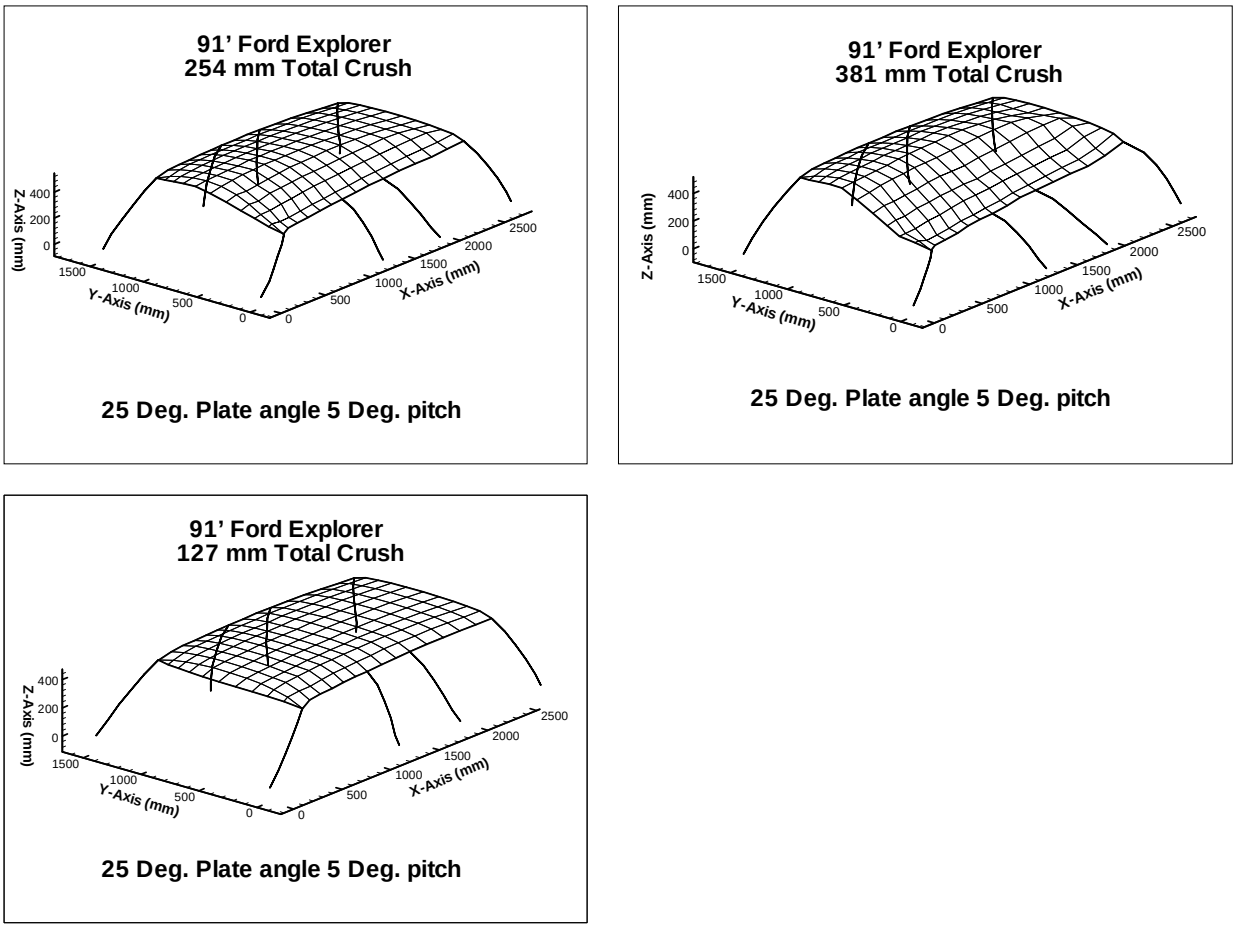


**Figure A(8)**-Ford Explorer #1 quasi-static tests roof crush profiles.

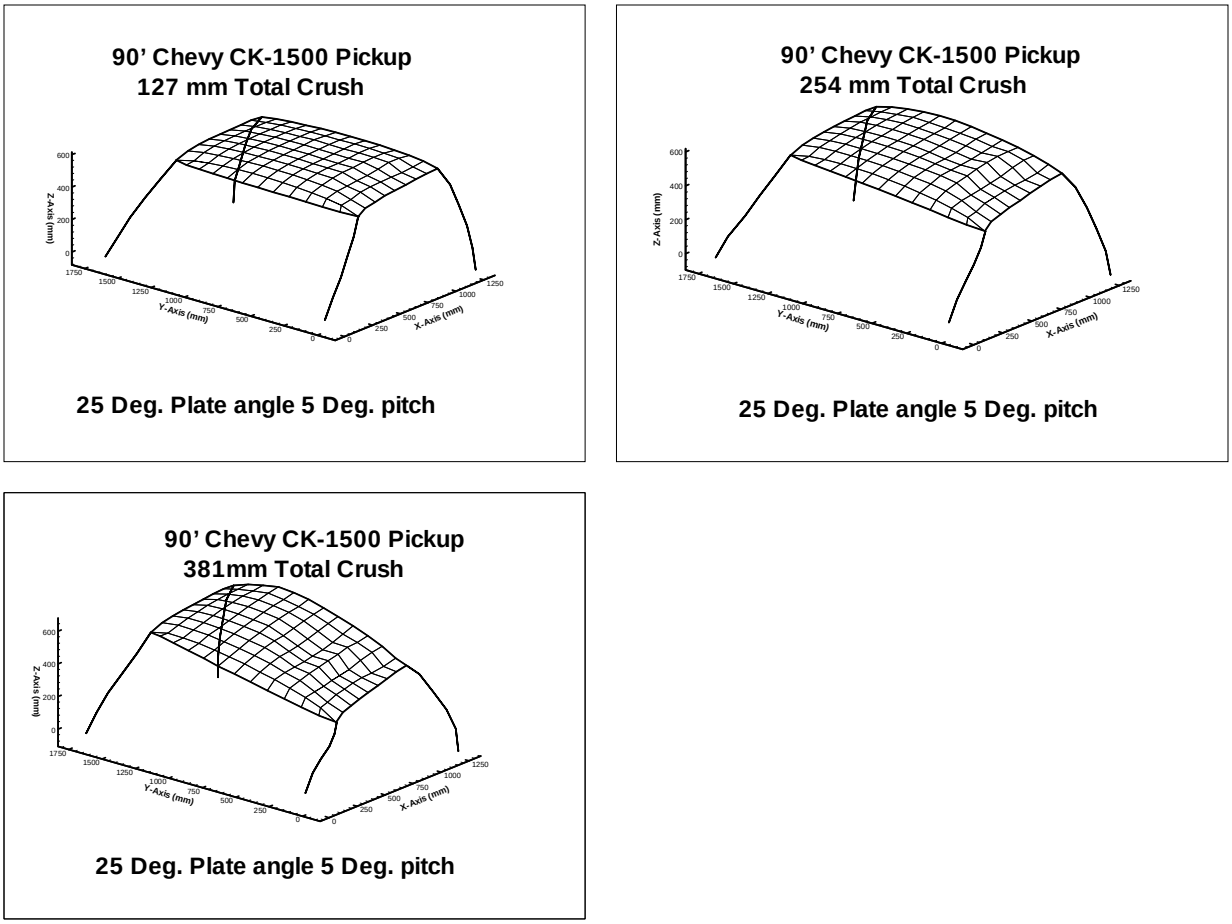


**Figure A(9)**-Chevy CK-1500 quasi-static tests roof crush profiles.

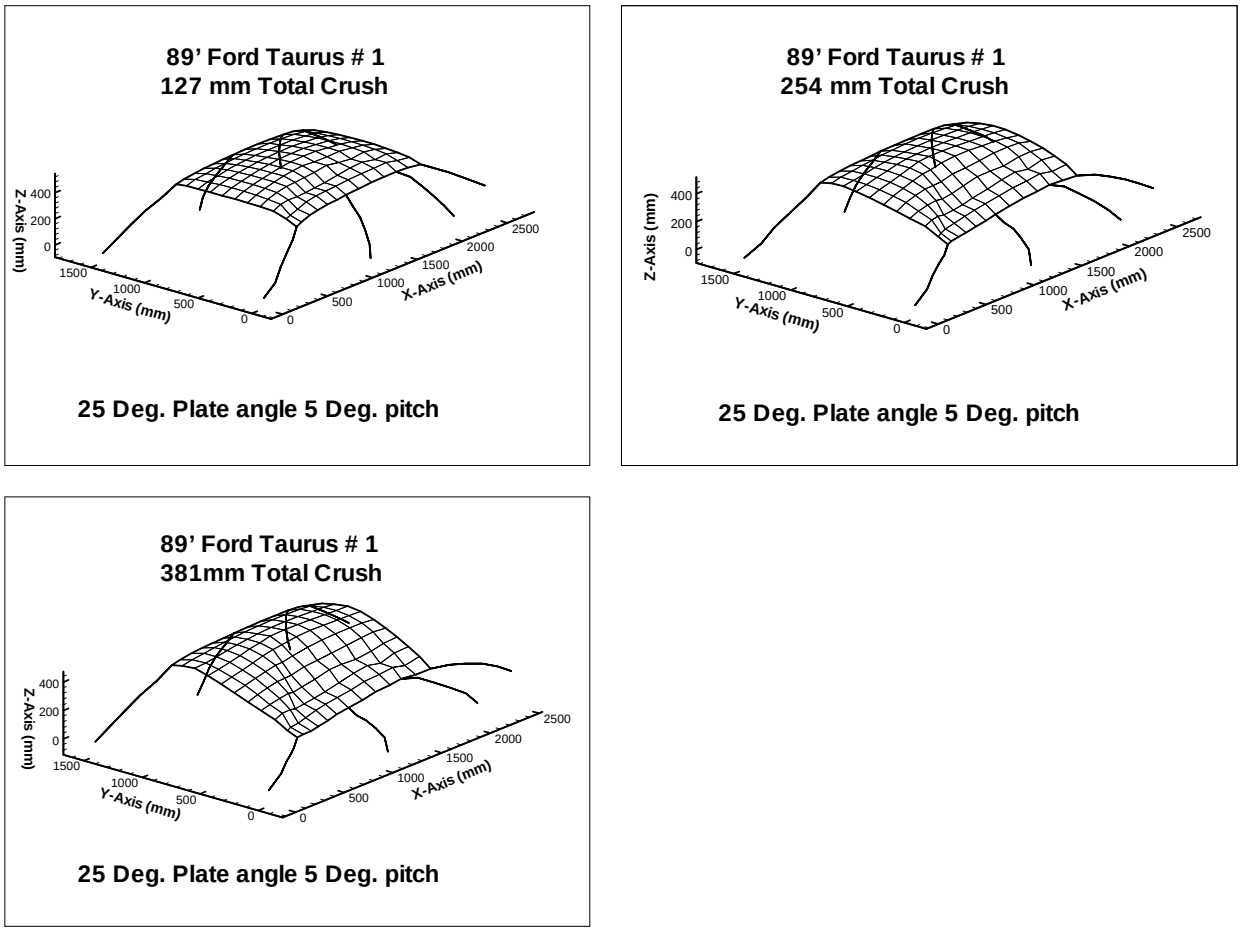


**Figure A(10)**-Ford Taurus #1 quasi-static tests roof crush profiles.

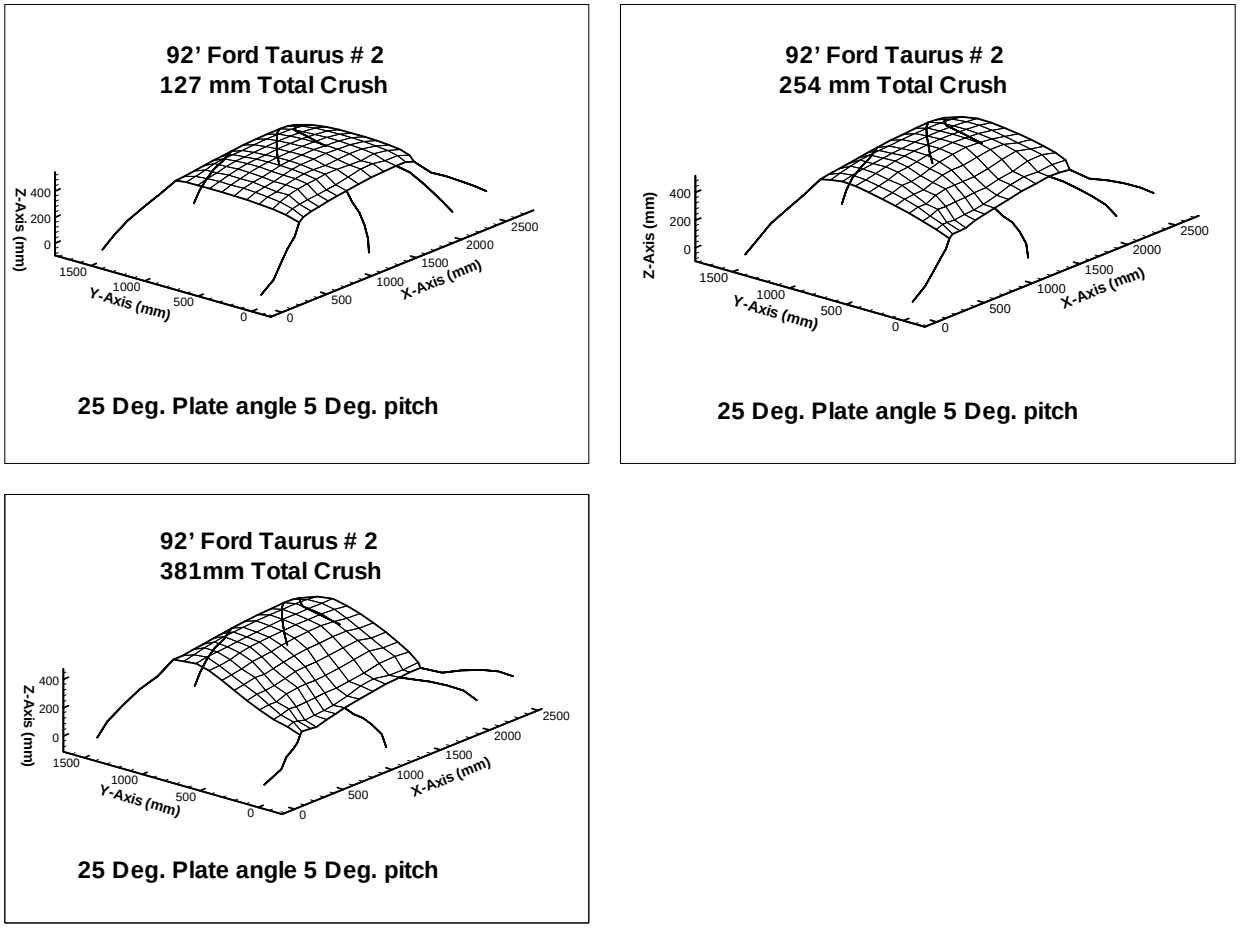


**Figure A(11)**-Ford Taurus #2 quasi-static tests roof crush profiles.

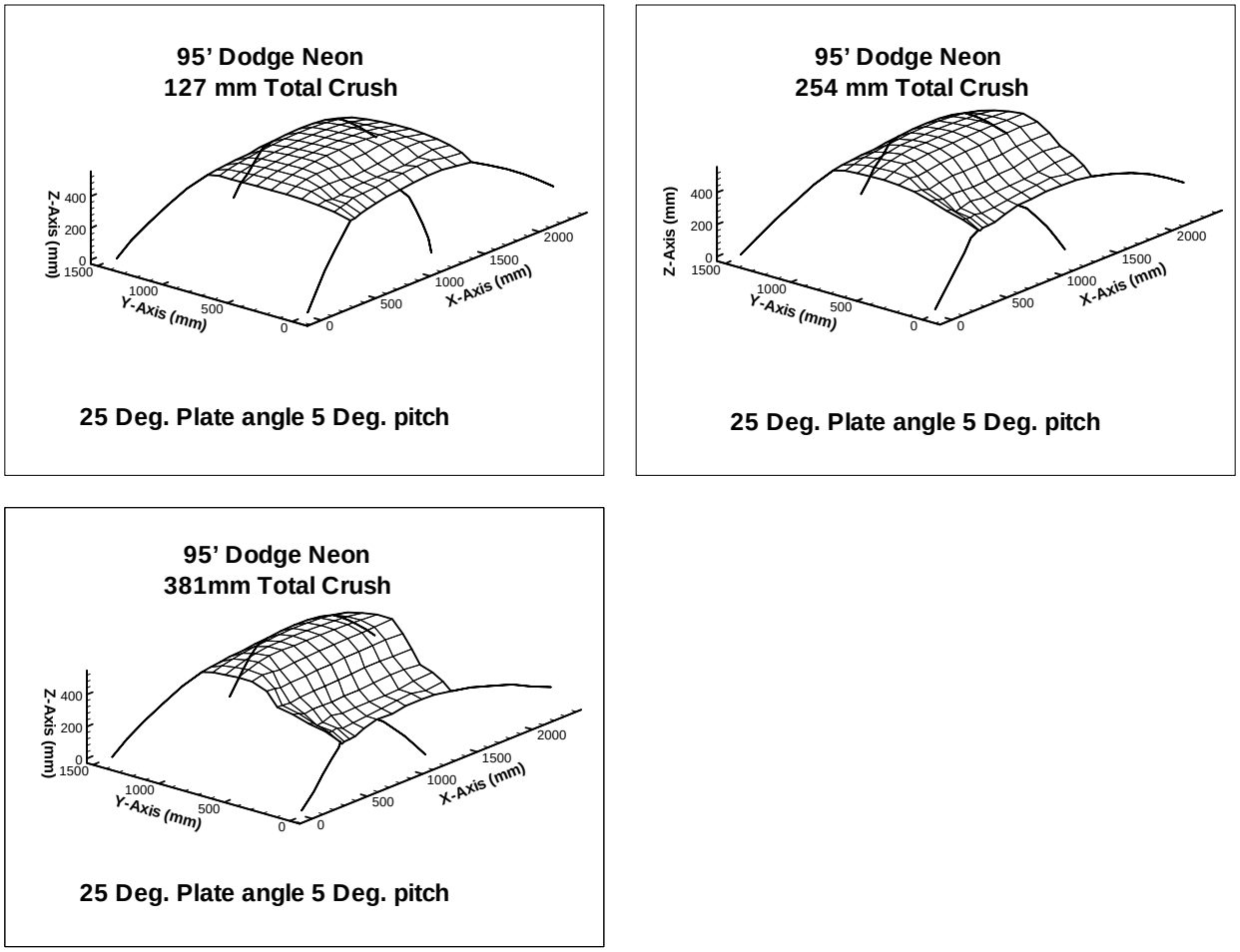


**Figure A(12)-**Dodge Neon #1 quasi-static tests roof crush profiles.

## Appendix B

(Roof profiles  for all vehicles drop tested onto floor.)

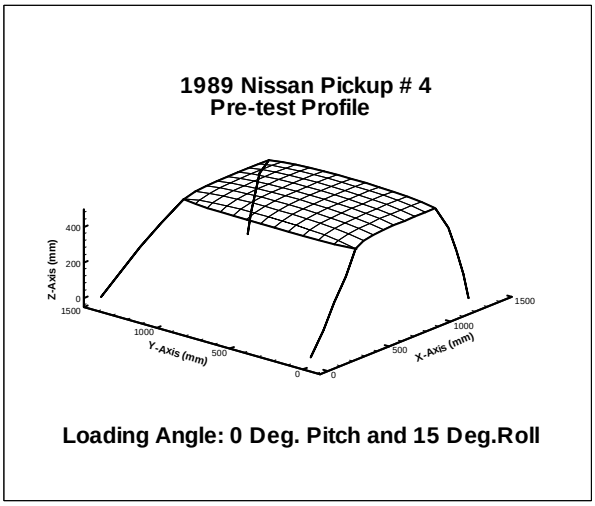


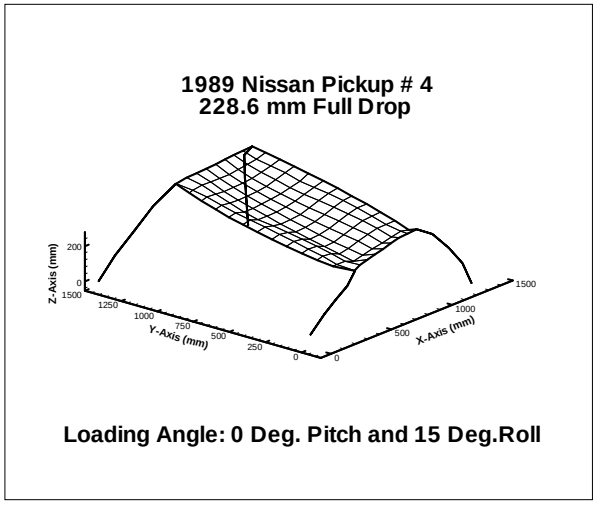


**Figure B(1)-**Nissan #4 floor drop test roof crush profiles.

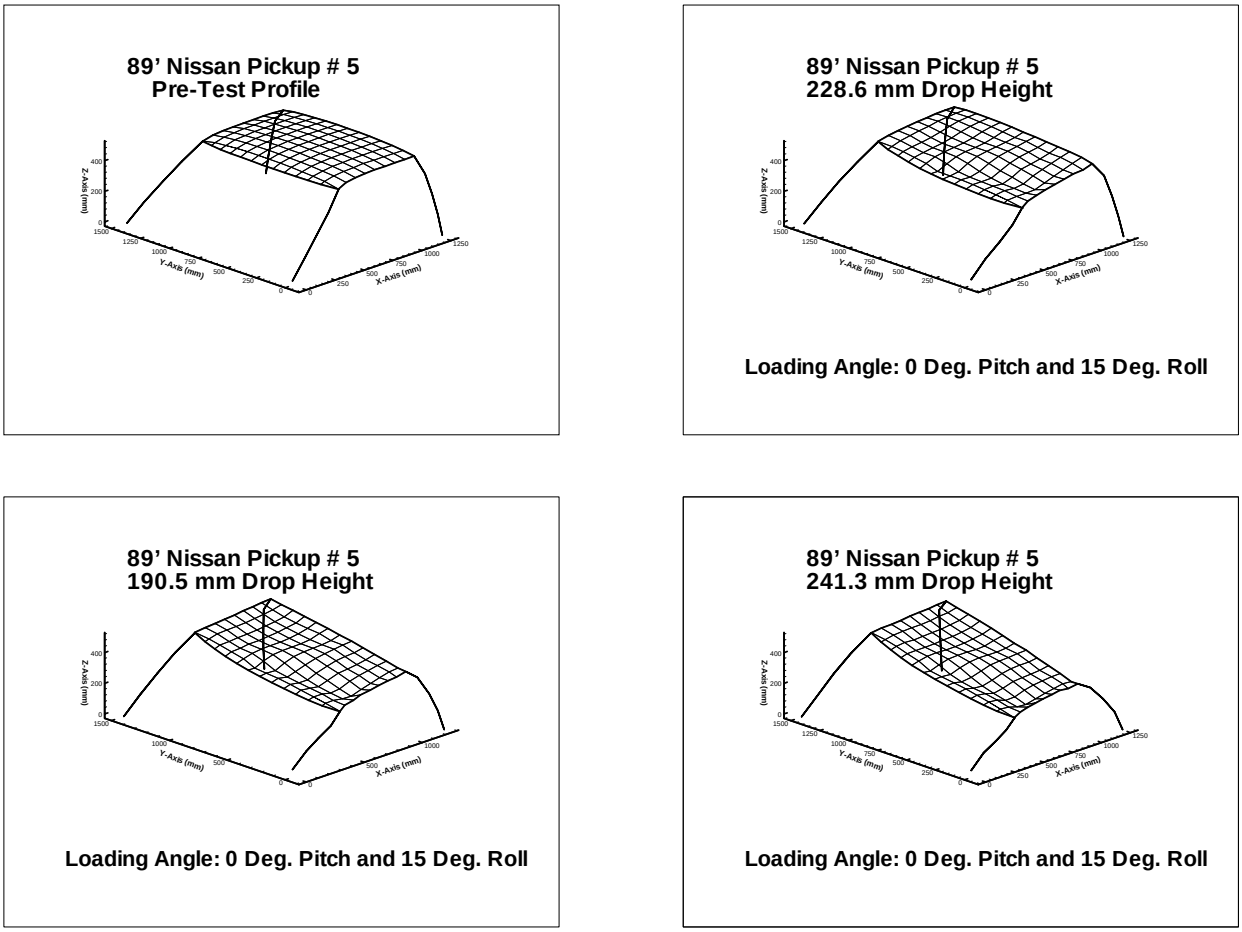


**Figure B(2)-**Nissan #5 multiple floor drop tests roof crush profiles.

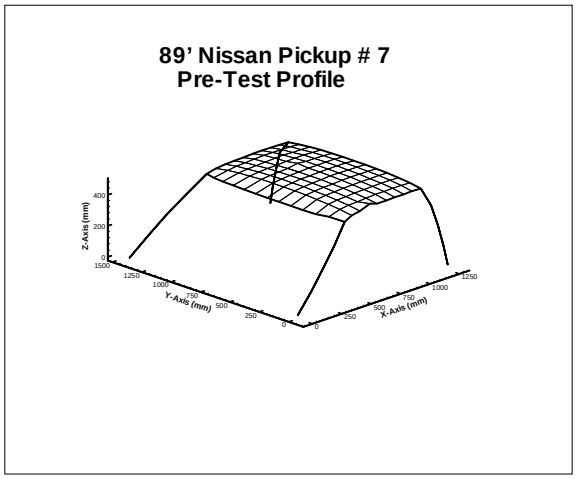


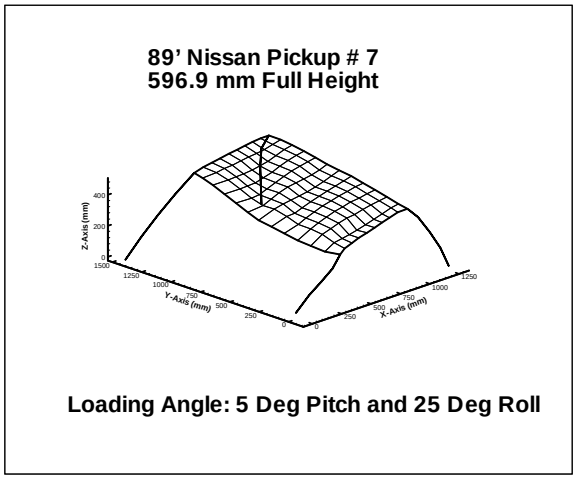


**Figure B(3)-**Nissan #7 floor drop test roof crush profiles.

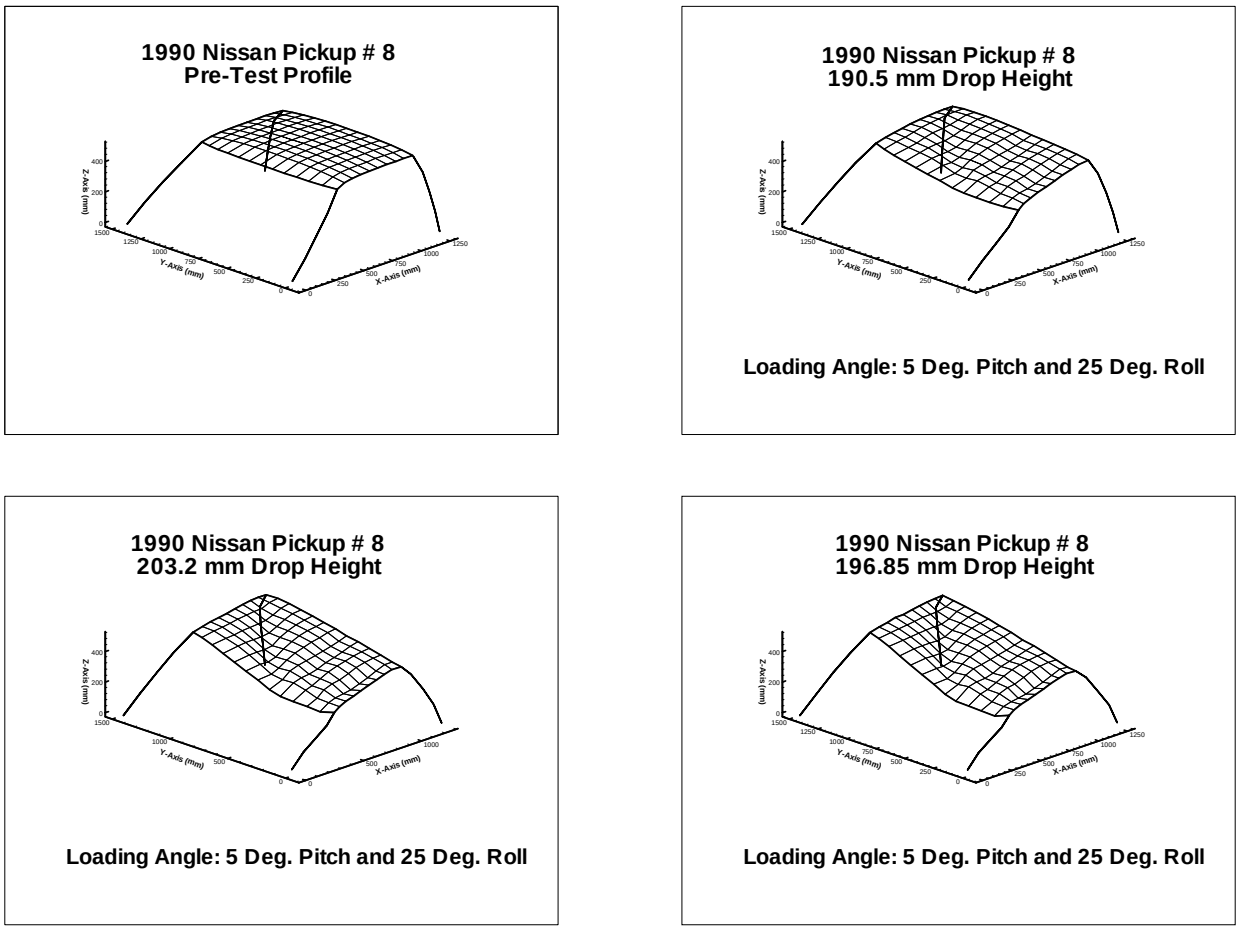


**Figure B(4)-**Nissan #8 multiple floor drop tests roof crush profiles.

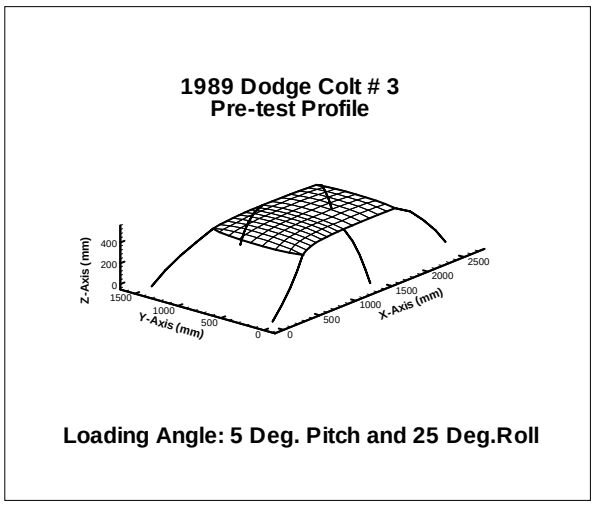


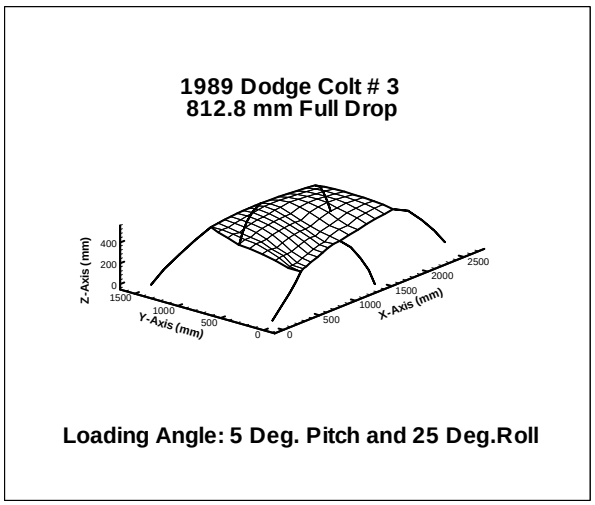


**Figure B(5)-**Dodge Colt #3 floor drop test roof crush profiles.

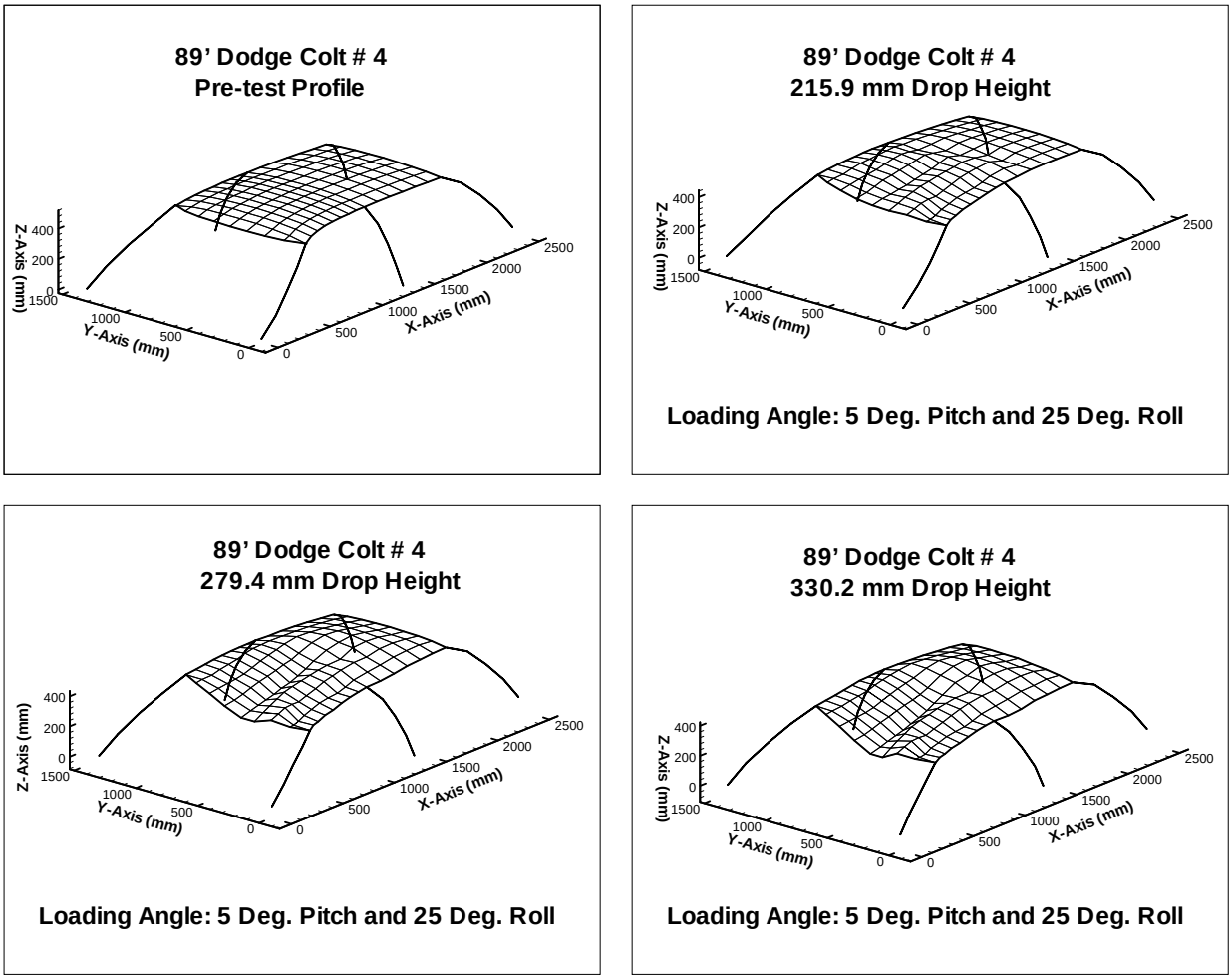


**Figure B(6)**-Dodge Colt #4 multiple floor drop tests roof crush profiles.

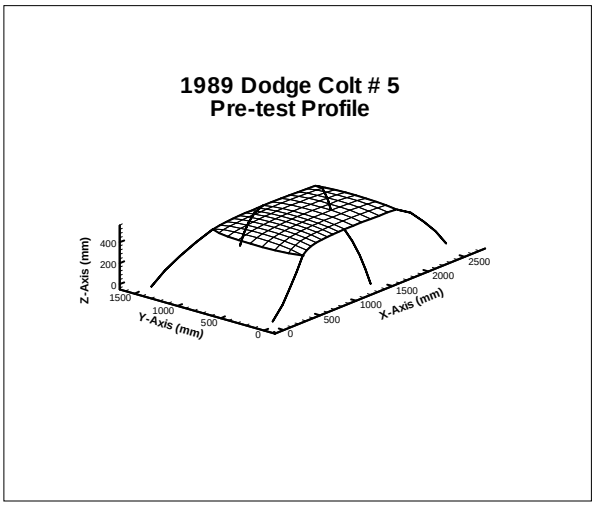


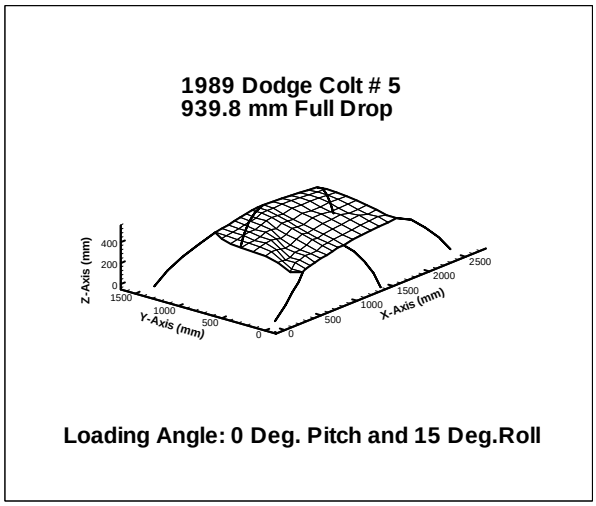


**Figure B(7)-**Dodge Colt #5 floor drop test roof crush profiles.

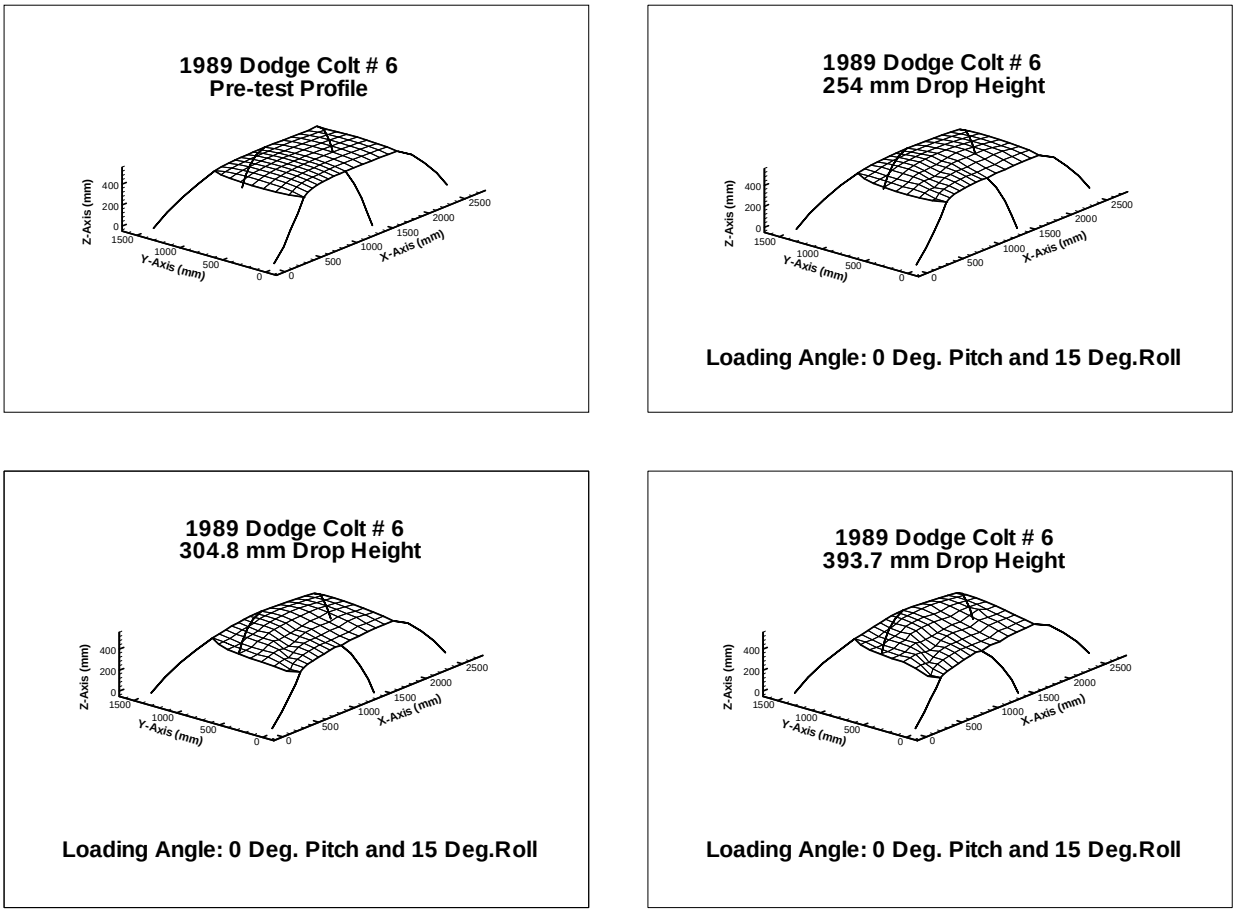


**Figure B(8)**-Dodge Colt #6 multiple floor drop tests roof crush profiles.

## Appendix C

(Roof profiles for all vehicles drop tested onto loadcell  platform.)

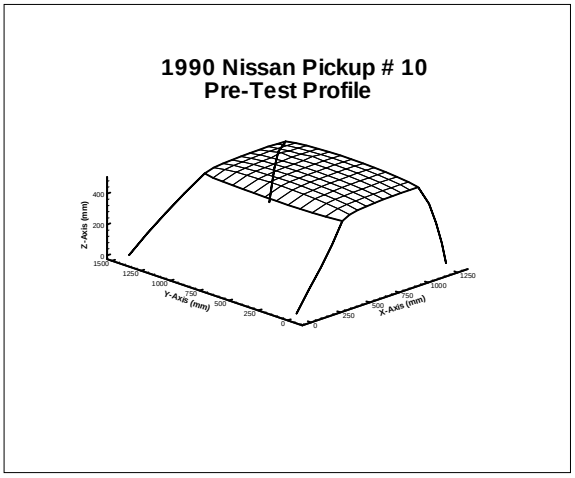


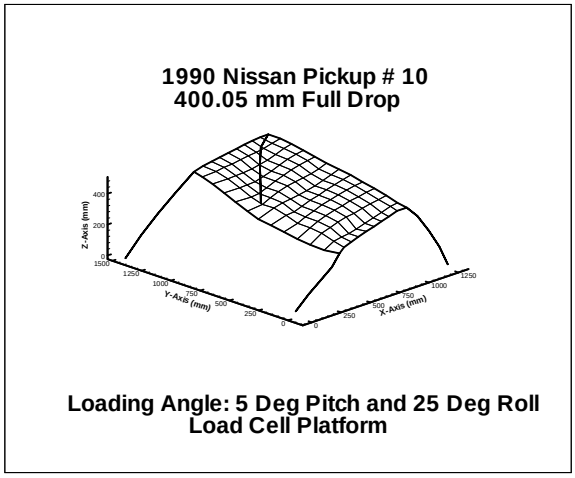


**Figure C(1)-**Nissan #10 load plate drop test roof profiles.

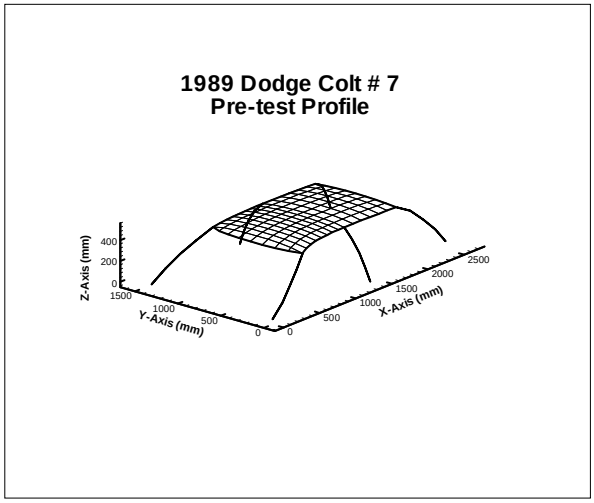


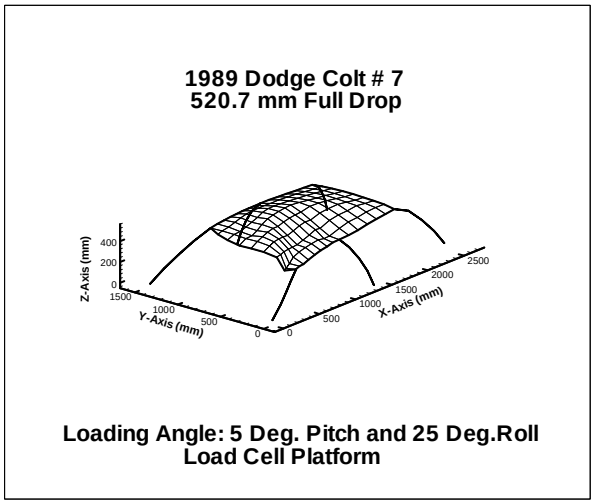


**Figure C(2)**-Dodge Colt #7 load plate drop test roof crush profiles.

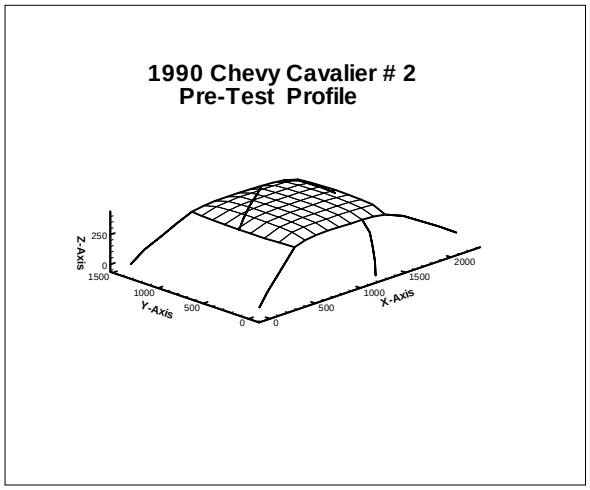


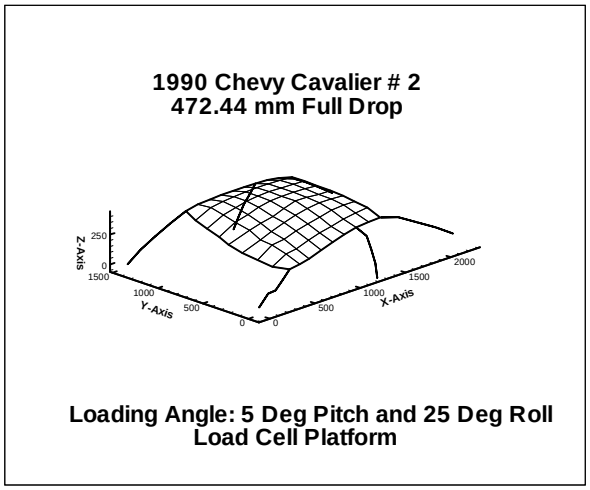


**Figure C(3)-**Chevy Cavalier #2 load plate drop test roof crush profiles.

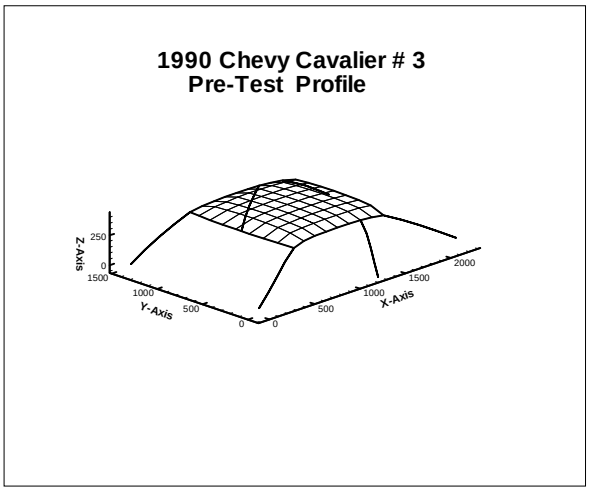


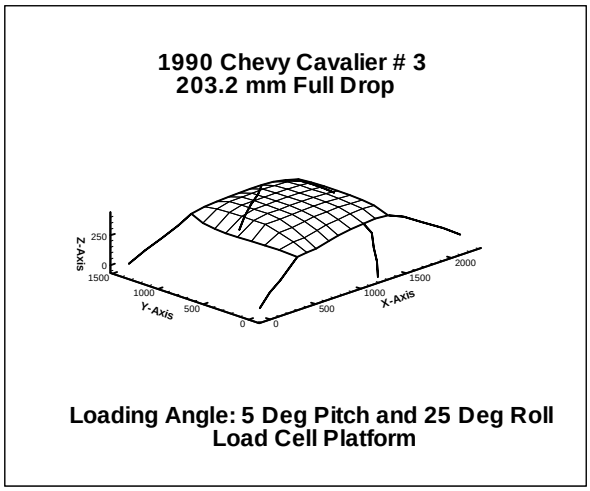


**Figure C(4)**-Chevy Cavalier #3 load plate drop test roof crush profiles.

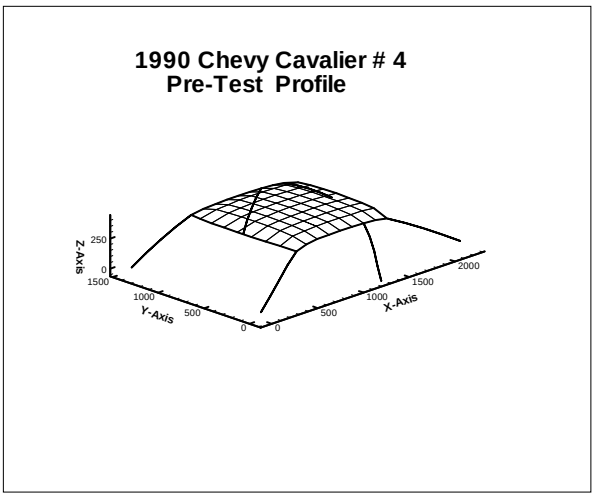


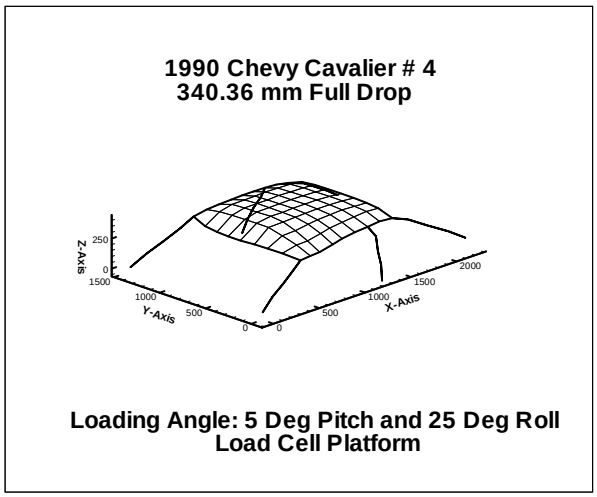


**Figure C(5)**-Chevy Cavalier #4 load plate drop test roof crush profiles.

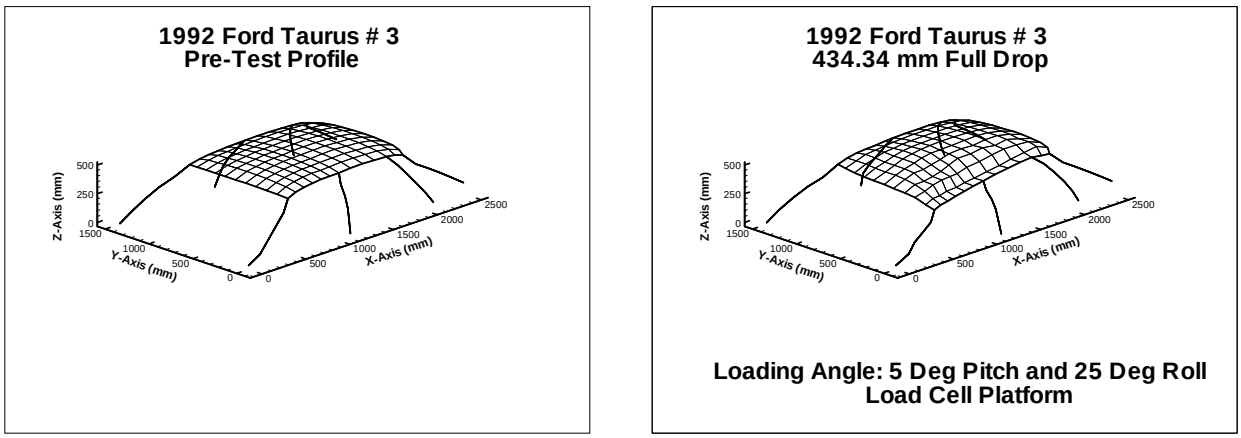


**Figure C(6)-**Ford Taurus #3 load plate drop test roof crush profiles.

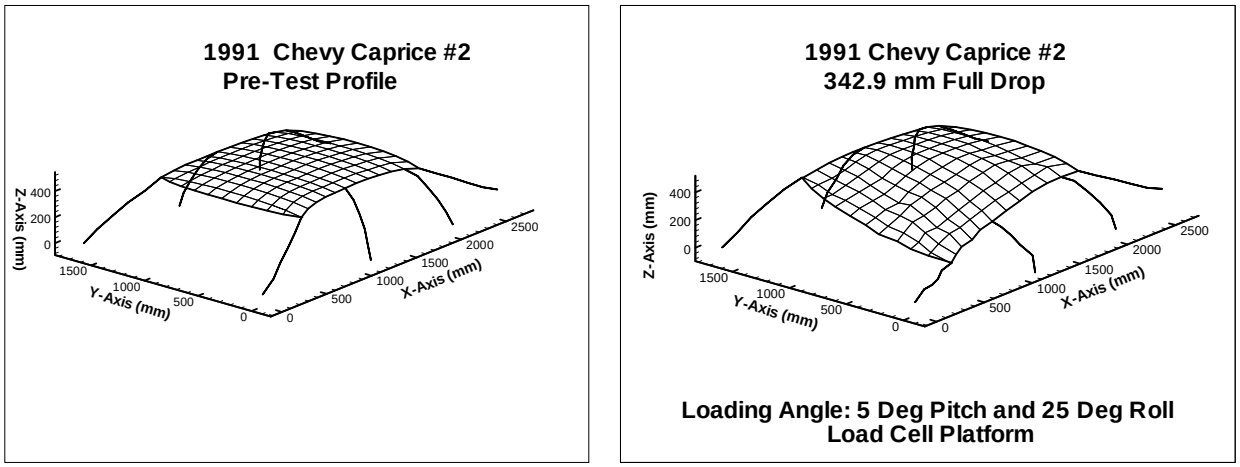


**Figure C(7)-**Chevy Caprice #2 load plate drop test roof crush profiles.

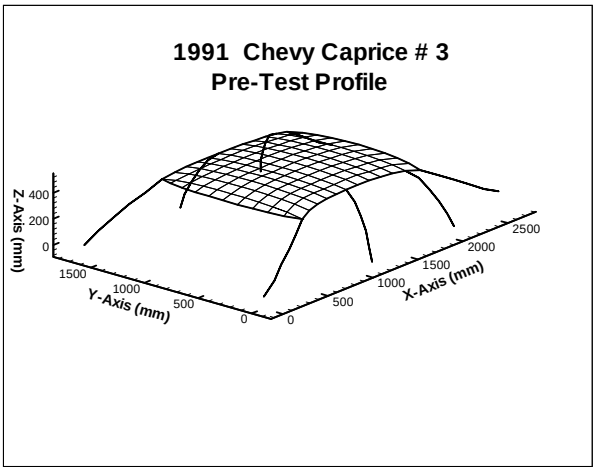


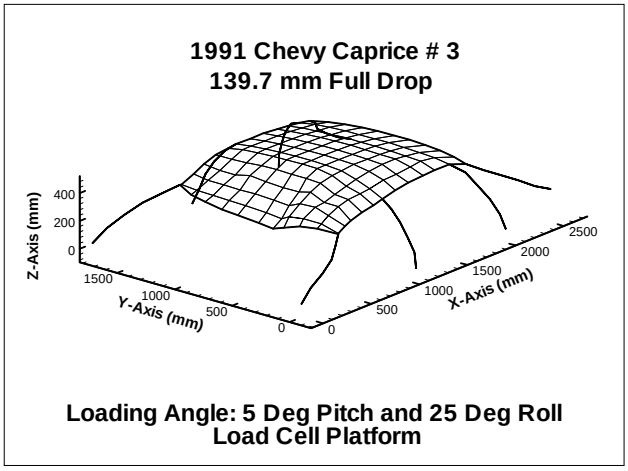


**Figure C(8)**-Chevy Caprice #3 load plate drop test roof crush profiles.

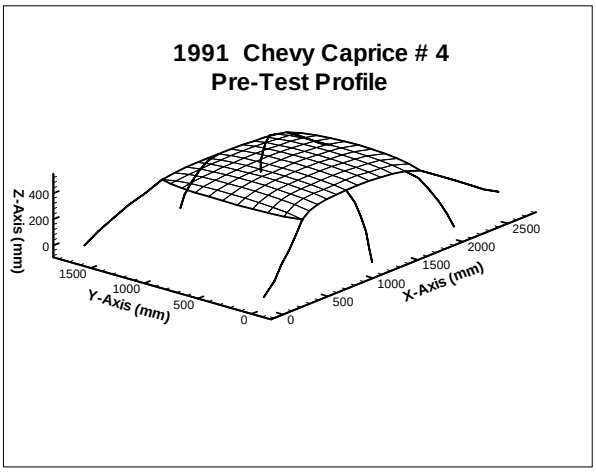


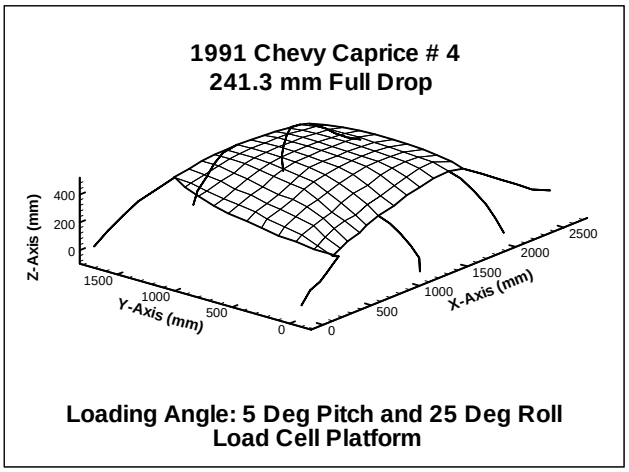


**Figure C(9)**-Chevy Caprice #4 load plate drop test roof crush profiles.

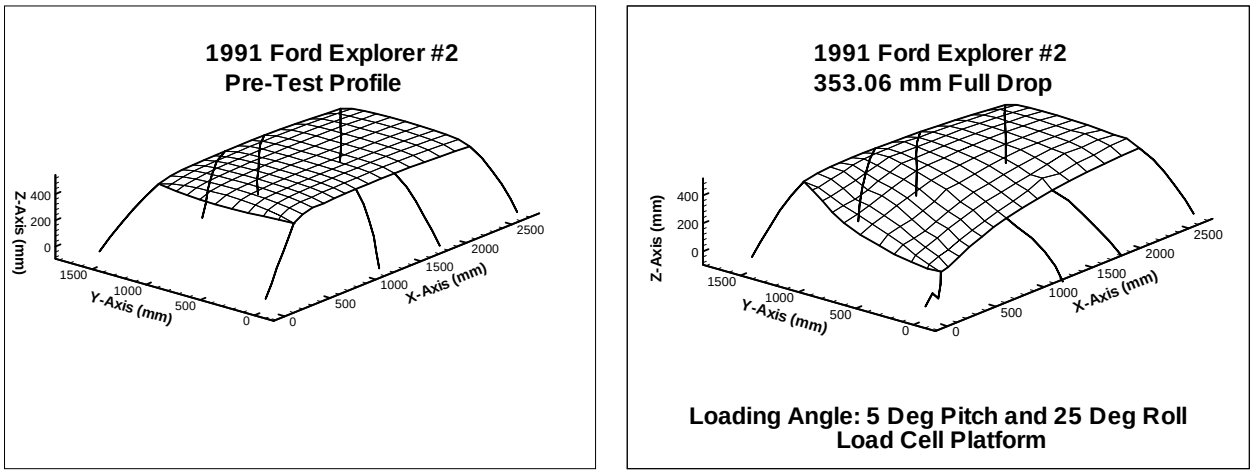


**Figure C(10)**-Ford Explorer #2 load plate drop test roof crush profiles.

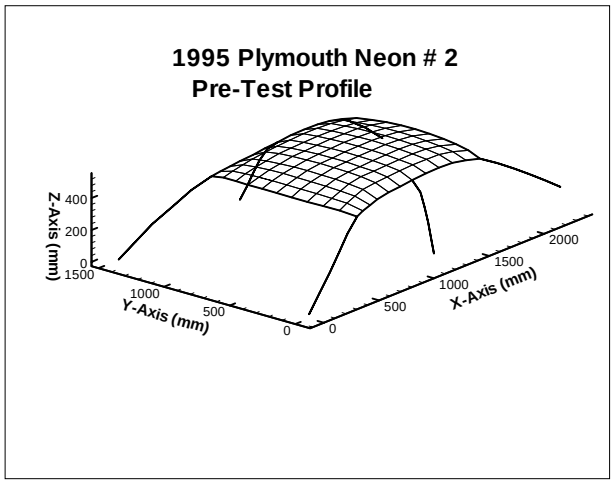


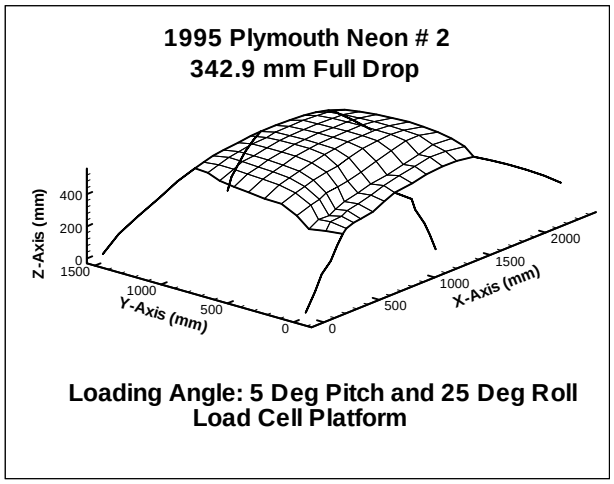


**Figure C(11)**-Plymouth Neon #2 load plate drop test roof crush profiles.

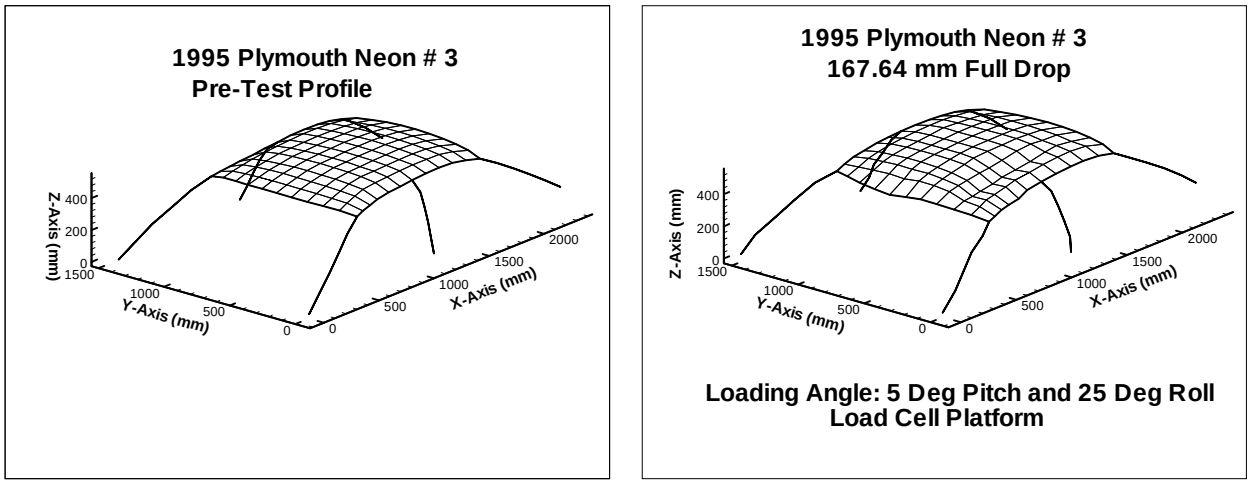


**Figure C(12)**-Plymouth Neon #3 load plate drop test roof crush profiles.

## Appendix D

(Force/Crush and Energy/Crush for all vehicles tested with static roof crush device)

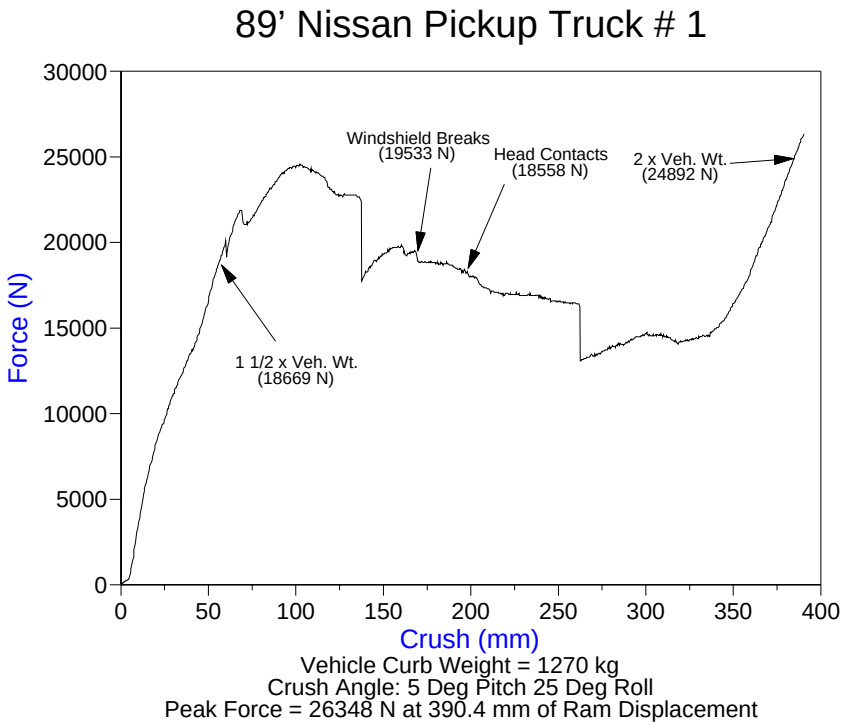


**Figure D(1)**-Nissan #1 quasi-static test force/crush curve.

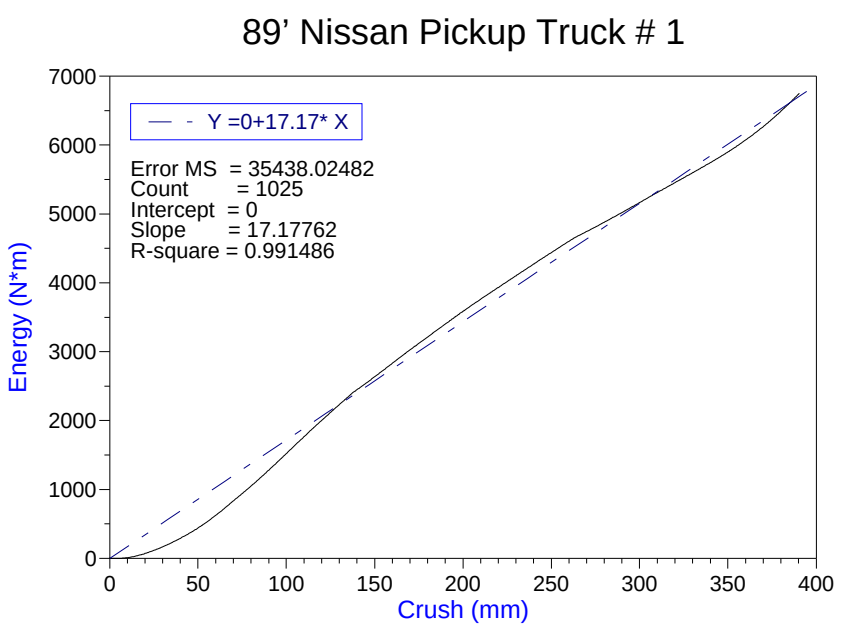


**Figure D(2)**-Nissan #1 quasi-static test energy/crush curve.

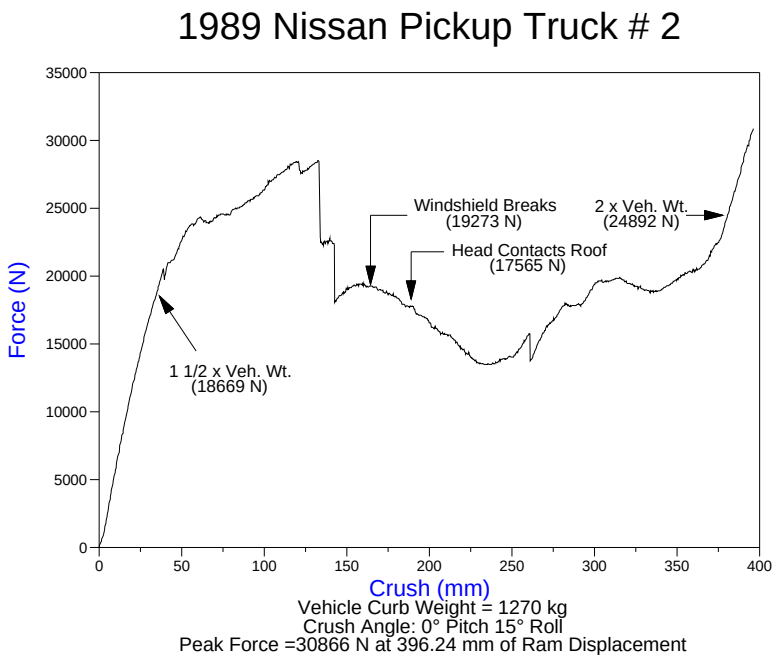


**Figure D(3)**-Nissan #2 quasi-static test force/crush curve.

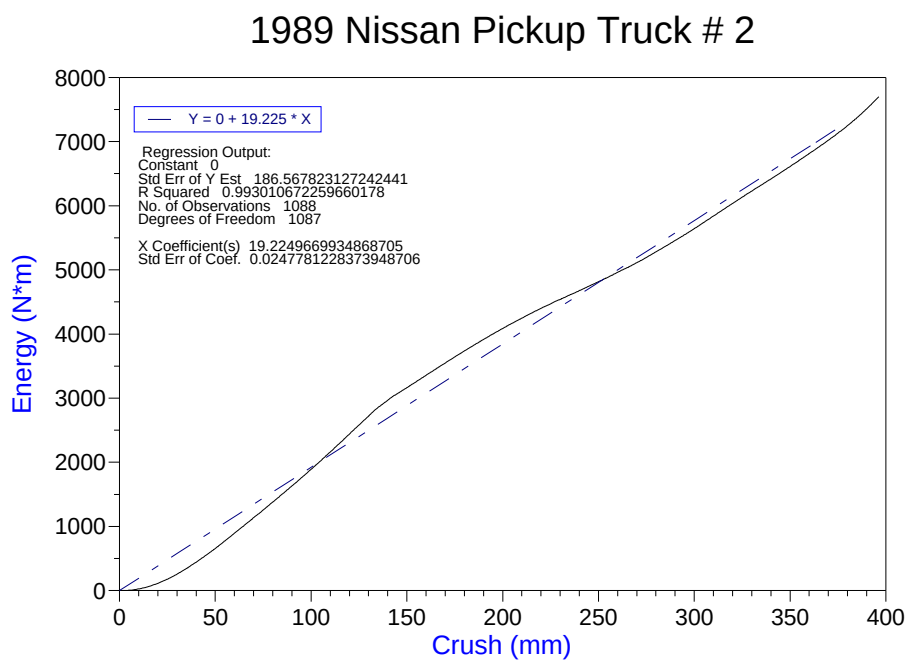


**Figure D(4)**-Nissan #2 quasi-static test energy/crush curve.

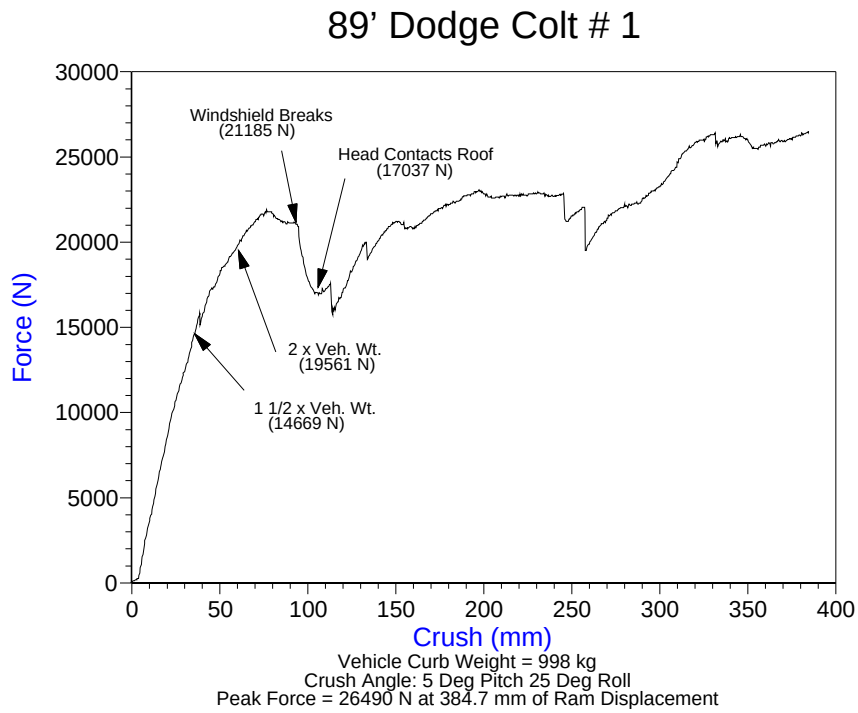


**Figure D(5)**-Dodge Colt #1 quasi-static test force/crush curve.

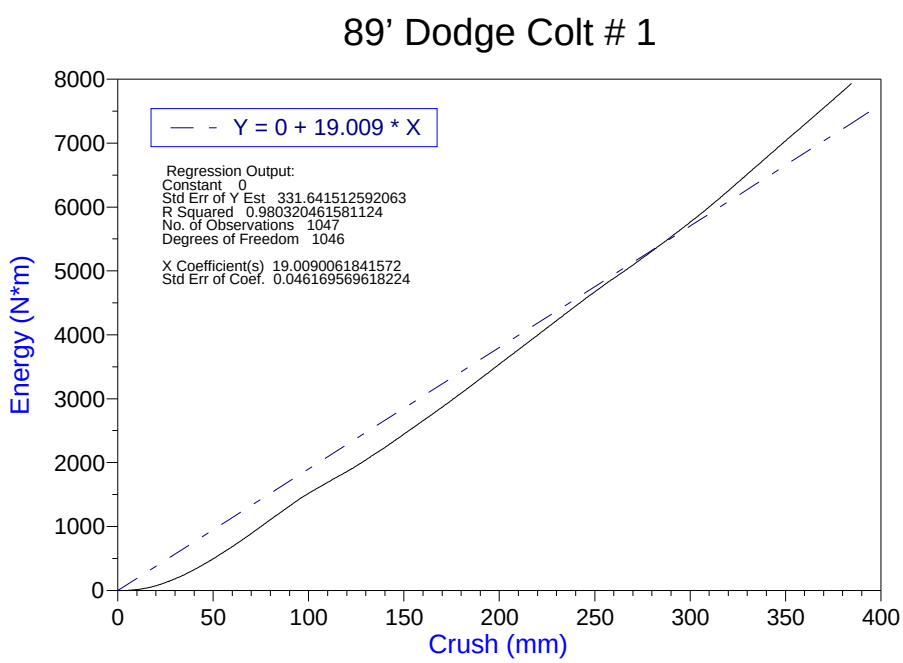


**Figure D(6)**-Dodge Colt #1 quasi-static test energy/crush curve.

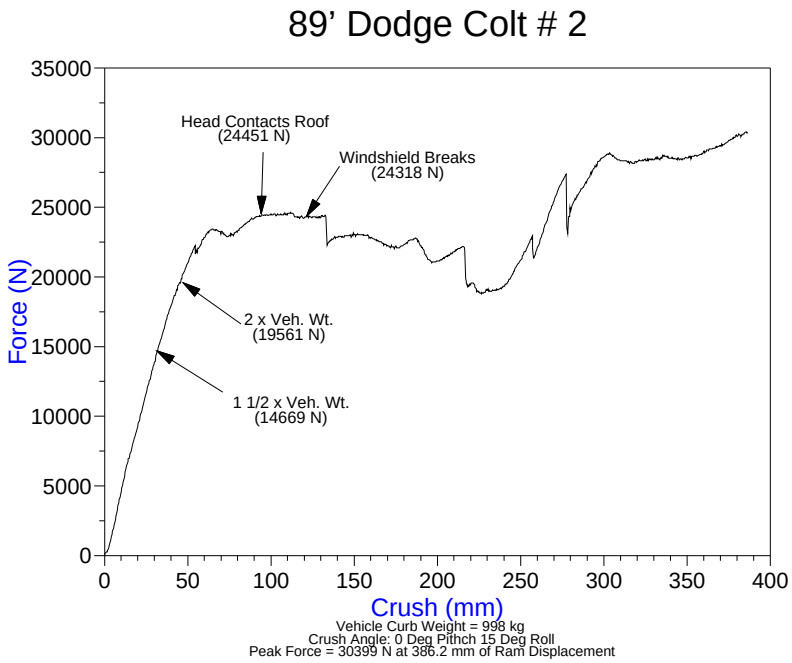


**Figure D(7)**-Dodge Colt #2 quasi-static test force/crush curve.

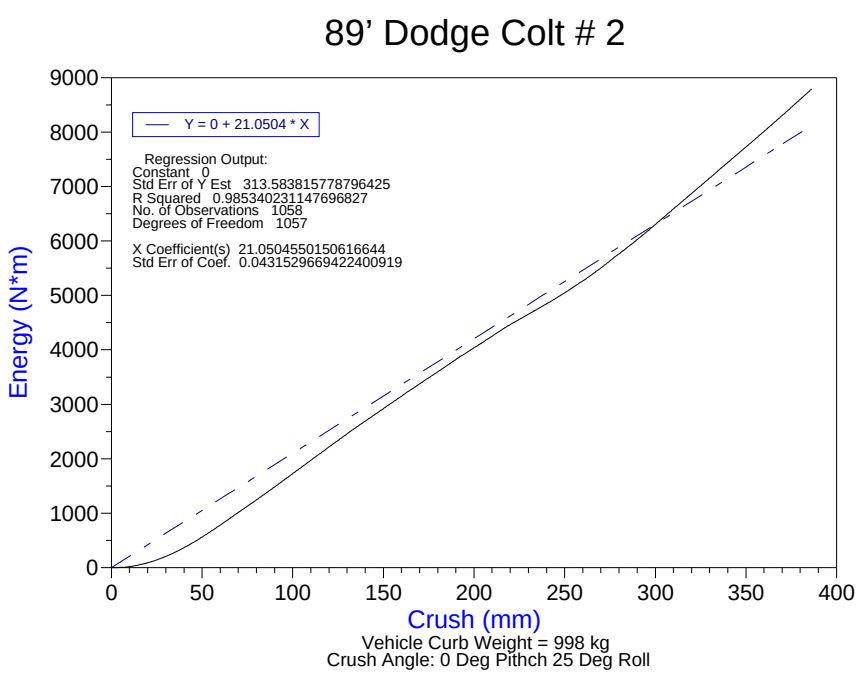


**Figure D(8)**-Dodge Colt #2 quasi-static test energy/crush. curve

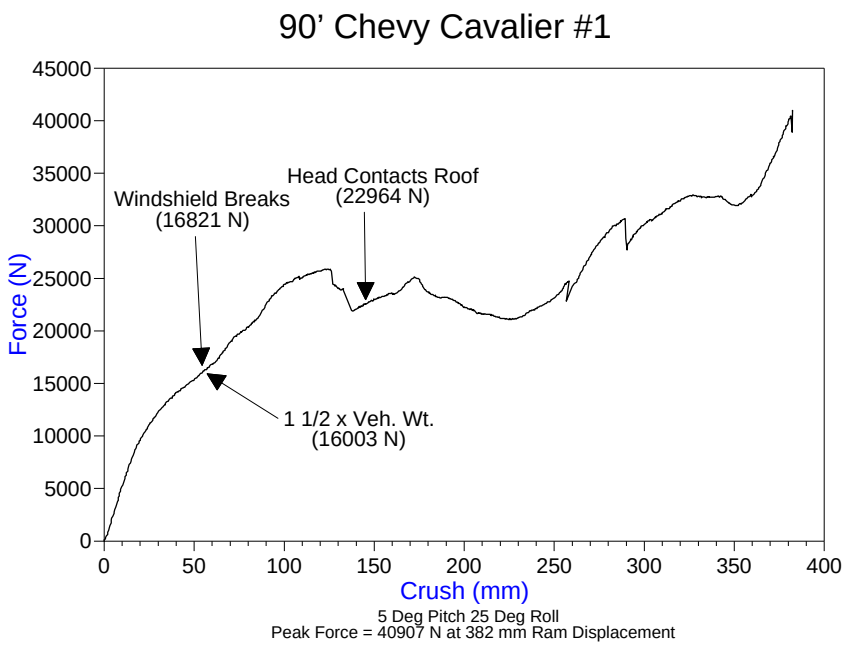


**Figure D(9)**-Chevy Cavalier #1 quasi-static test force/crush curve.

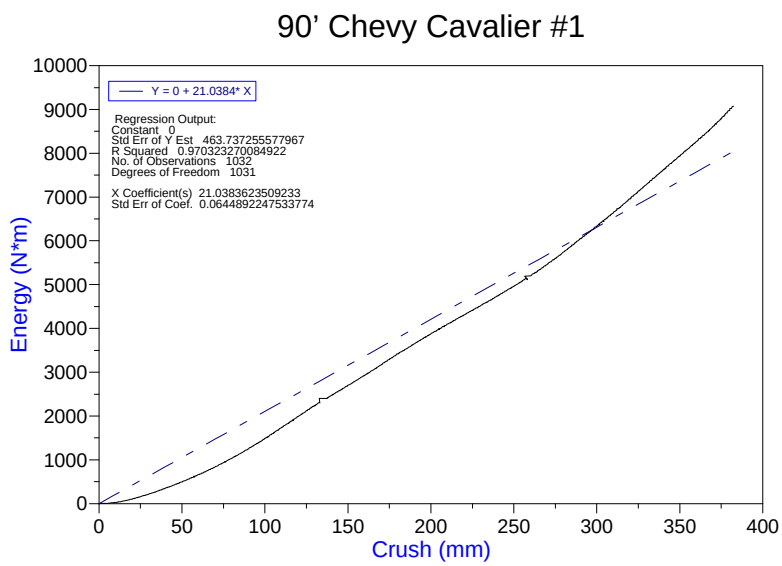


**Figure D(10)**-Chevy Cavalier #1 quasi-static test energy/crush curve.

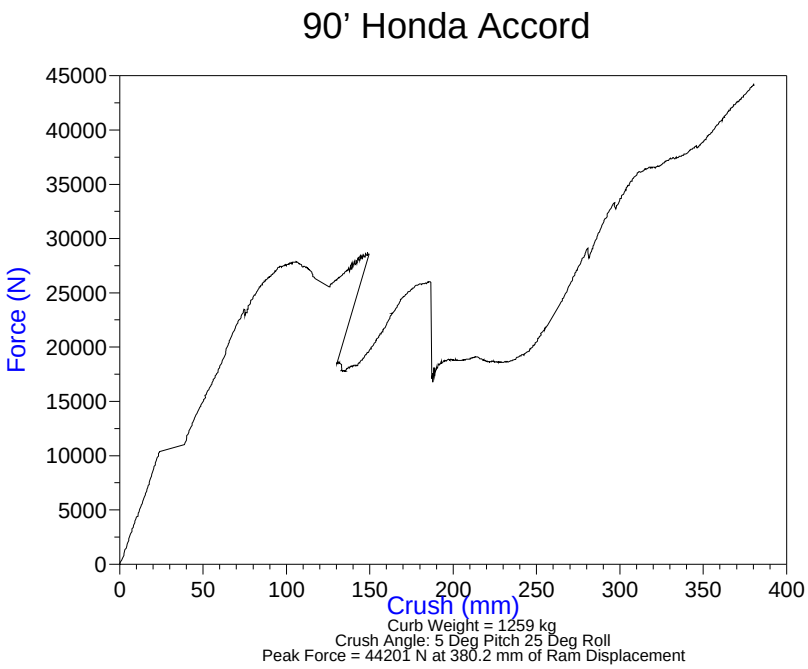


**Figure D(11)**-Honda accord quasi-static test force/crush curve.

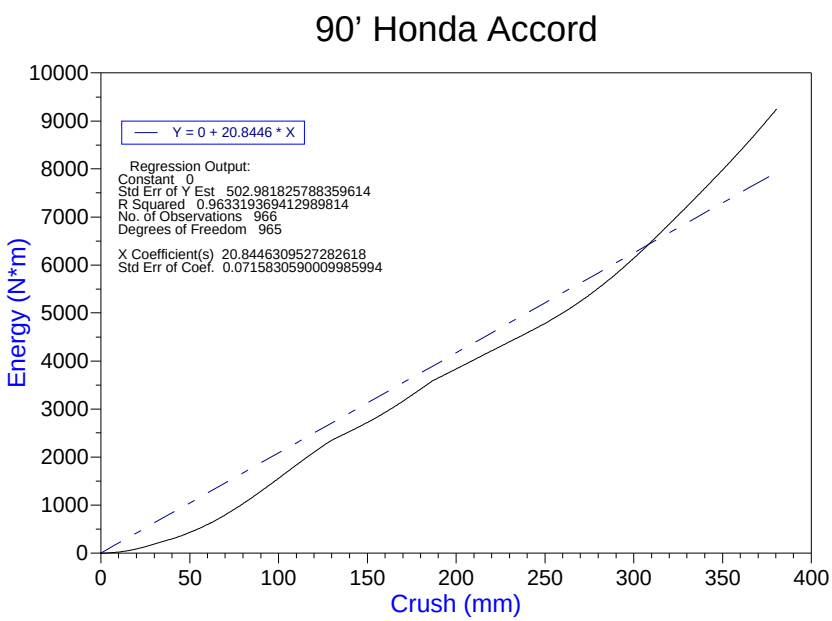


**Figure D(12)**-Honda Accord quasi-static test energy/crush curve.

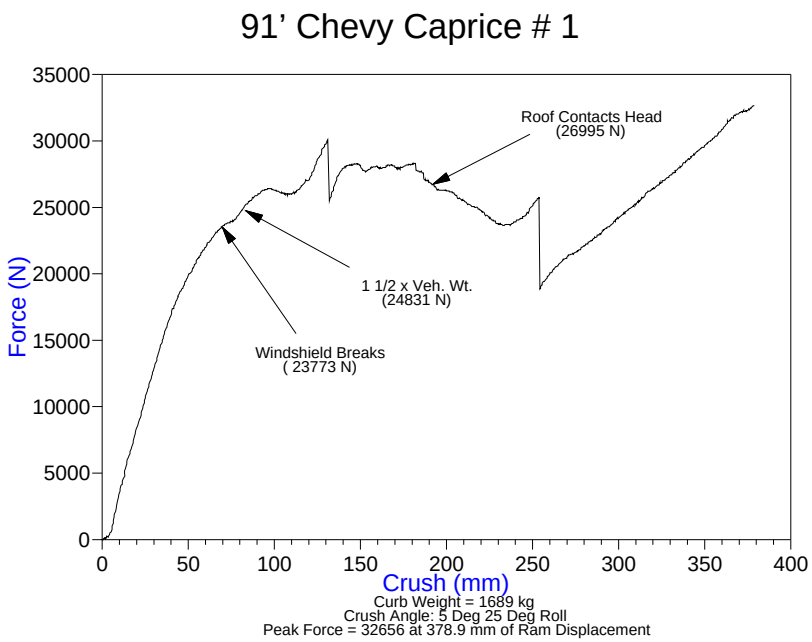


**Figure D(13)**-Chevy Caprice #1 quasi-static test force/crush curve.

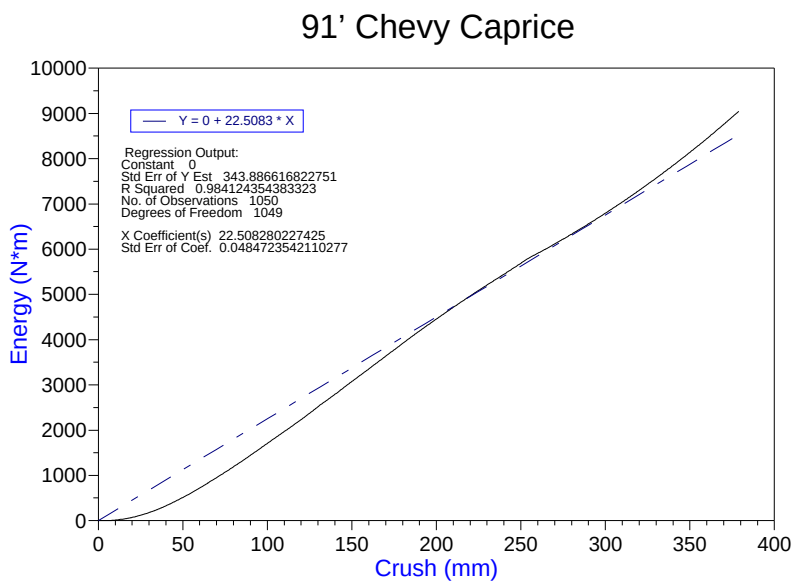


**Figure D(14)**-Chevy Caprice #1 quasi-static test energy/crush curve.

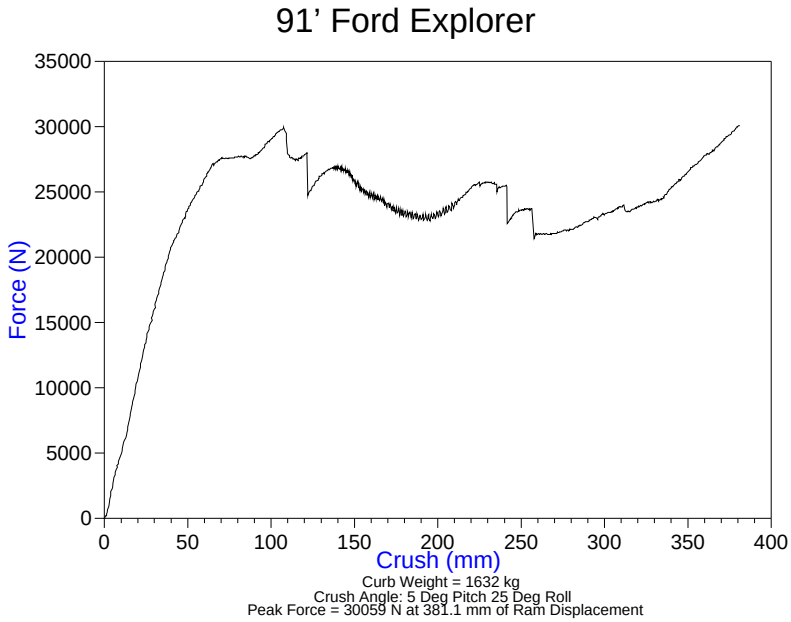


**Figure D(15)**-Ford Explorer #1 quasi-static test force/crush curve.

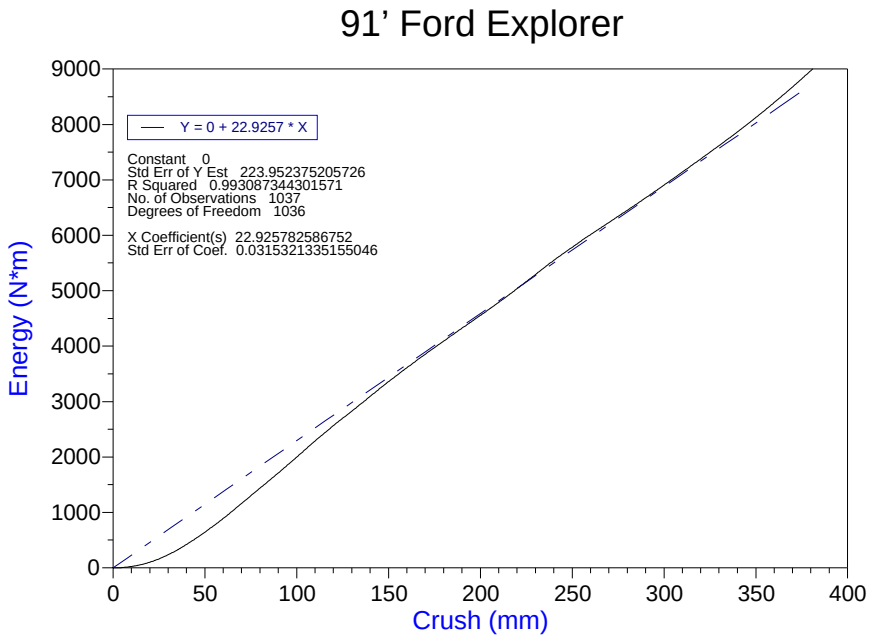


**Figure D(16)**-Ford Explorer #1 quasi-static test energy/crush curve.

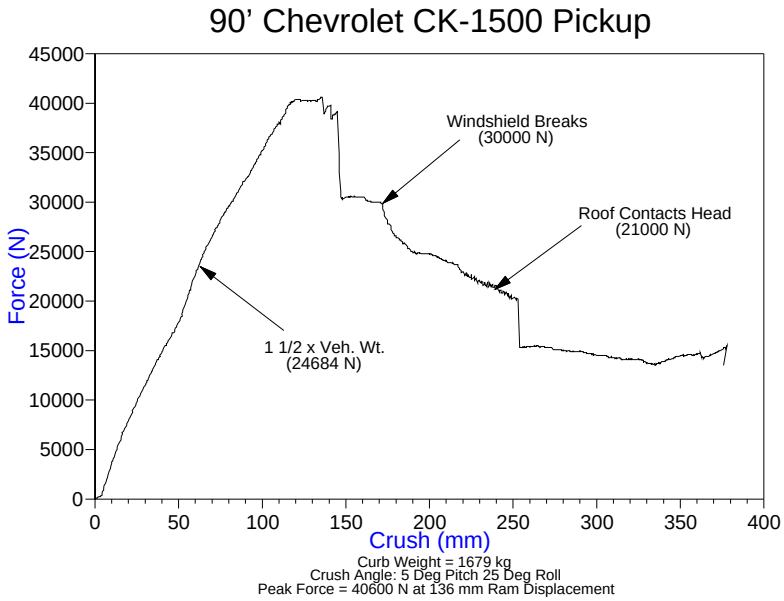


**Figure D(17)**-Chevy CK-1500 PU quasi-static test force/crush curve.

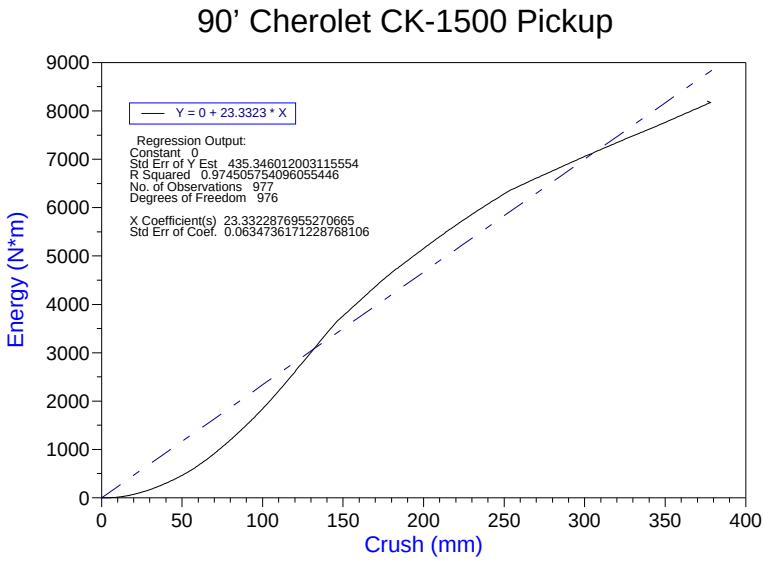


**Figure D(18)**-Chevy CK-1500 PU quasi-static test energy/crush curve

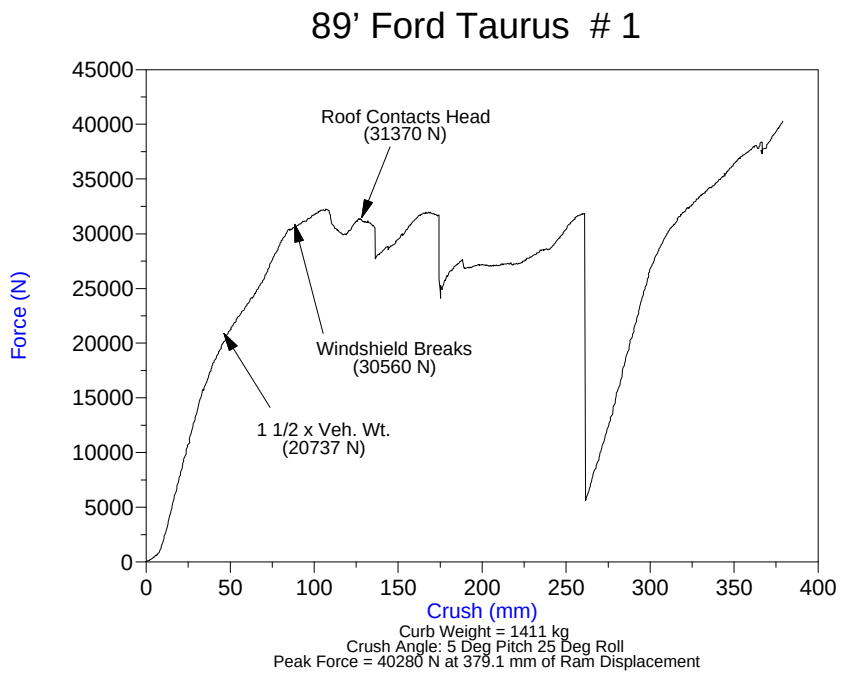


**Figure D(19)**-Ford Taurus #1 quasi-static test force/crush curve.

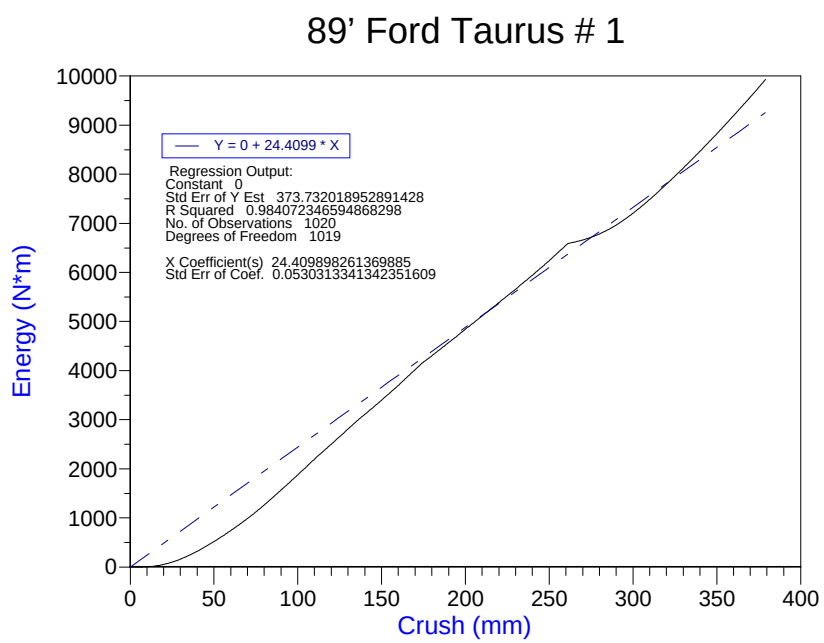


**Figure D(20)**-Ford Taurus #1 quasi-static test energy/crush curve.

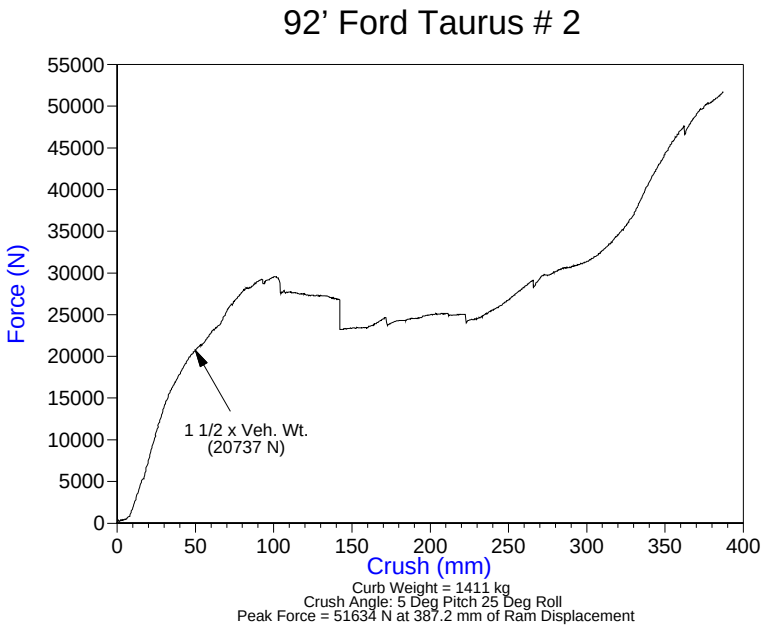


**Figure D(21)**-Ford Taurus #2 quasi-static test force/crush curve.

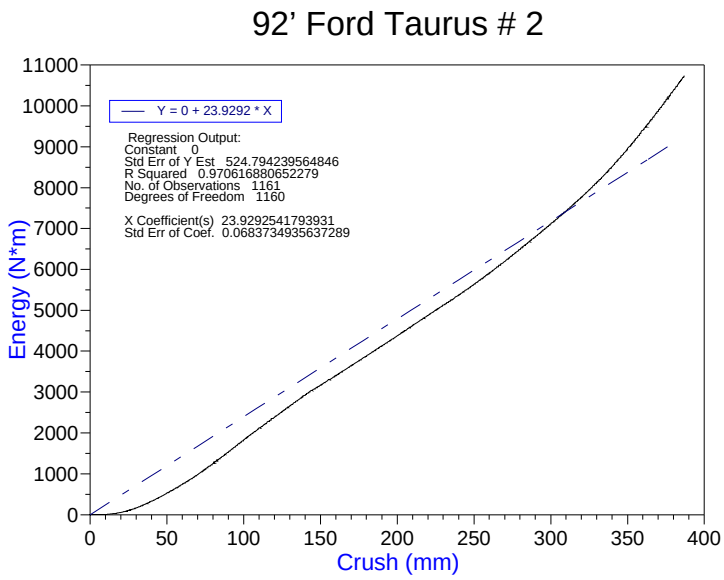


**Figure D(22)**-Ford Taurus #2 quasi-static test energy/crush curve.

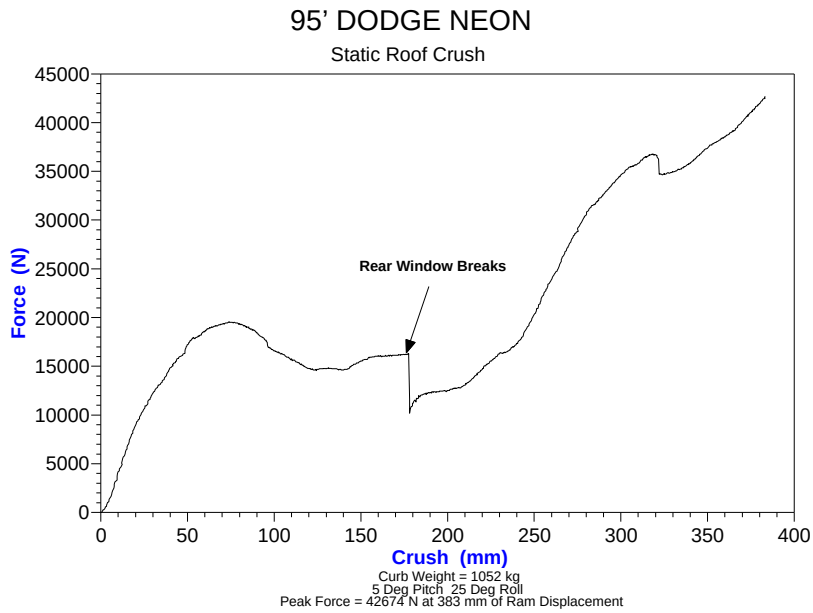


**Figure D(23)**-Dodge Neon #1 quasi-static test force/crush curve.

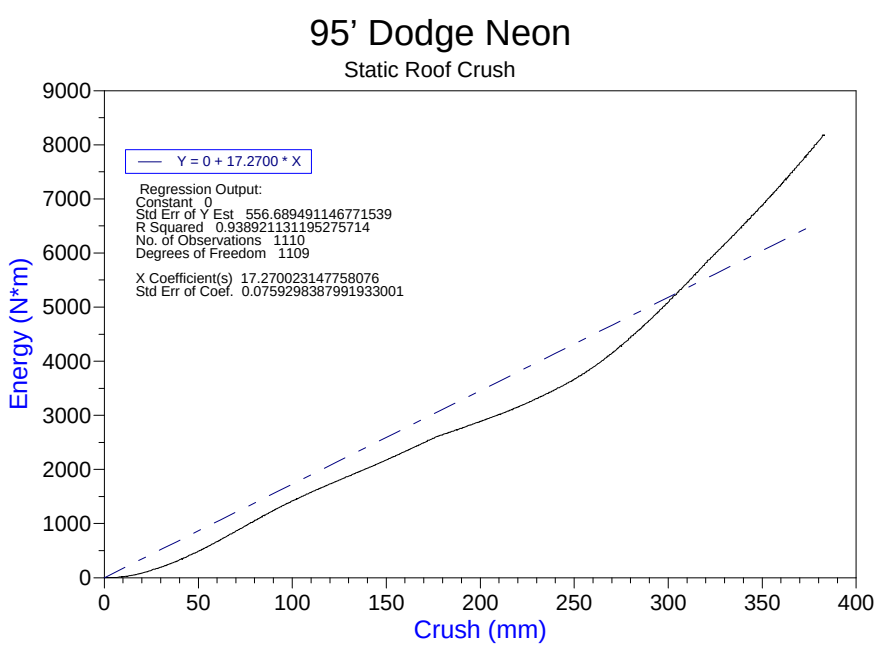


**Figure D(24)**-Dodge Neon #1 quasi-static test energy/crush curve.

## Appendix E

(Force/Crush and Energy/Crush for all vehicles drop tested onto loadcell platform.)

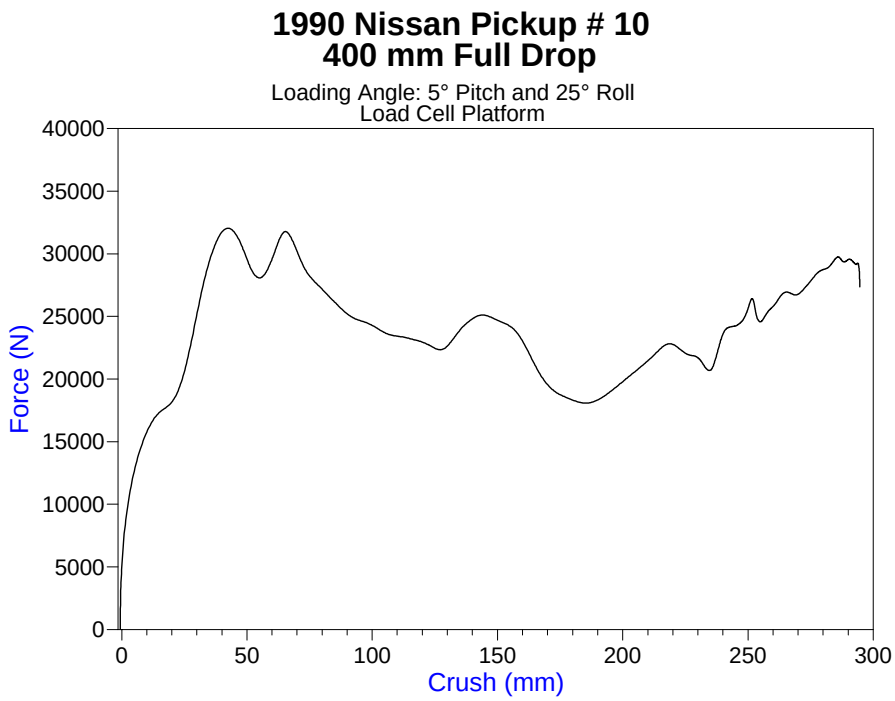


**Figure E(1)**-Nissan #10 load plate drop test force/crush curve.

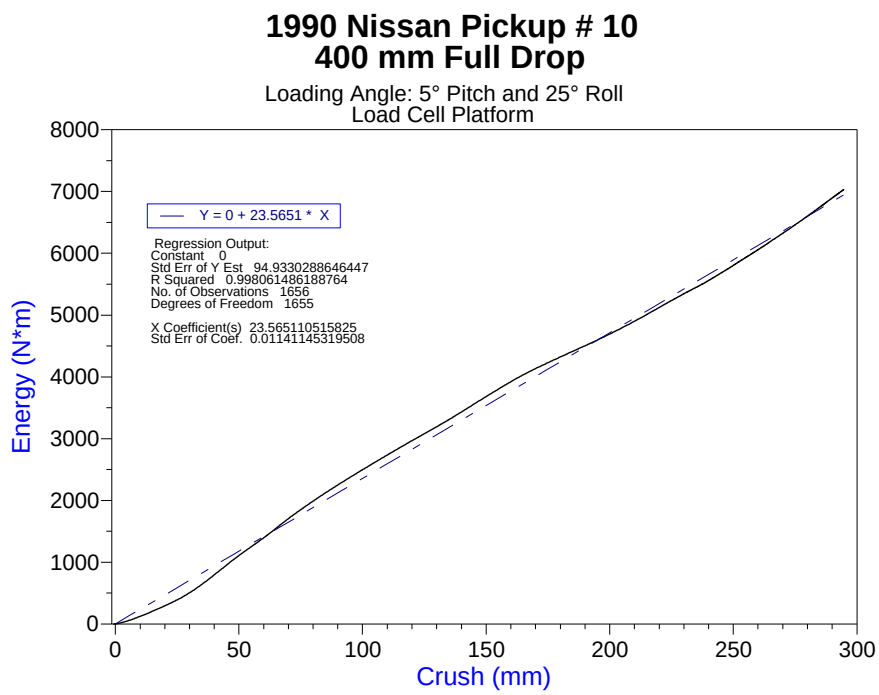


**Figure E(2)**-Nissan #10 load plate drop test energy/crush curve.

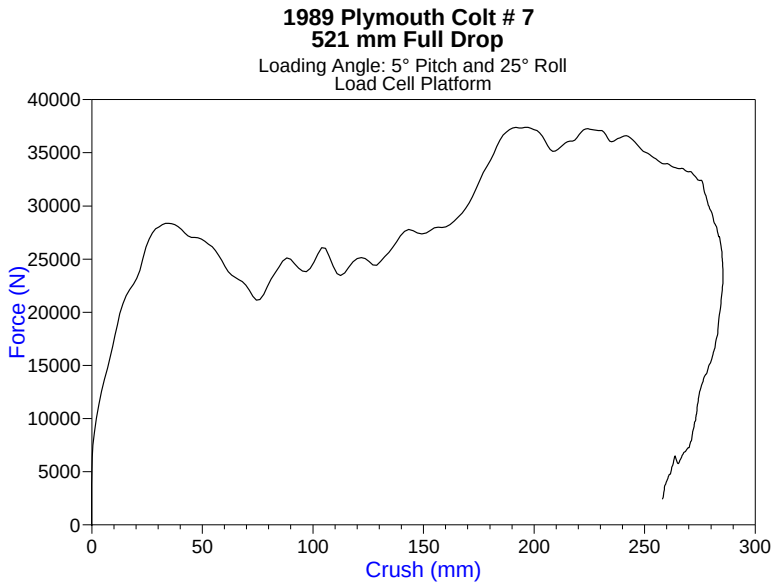


**Figure E(3)-** Plymouth Colt #7 load plate drop test force/crush curve.

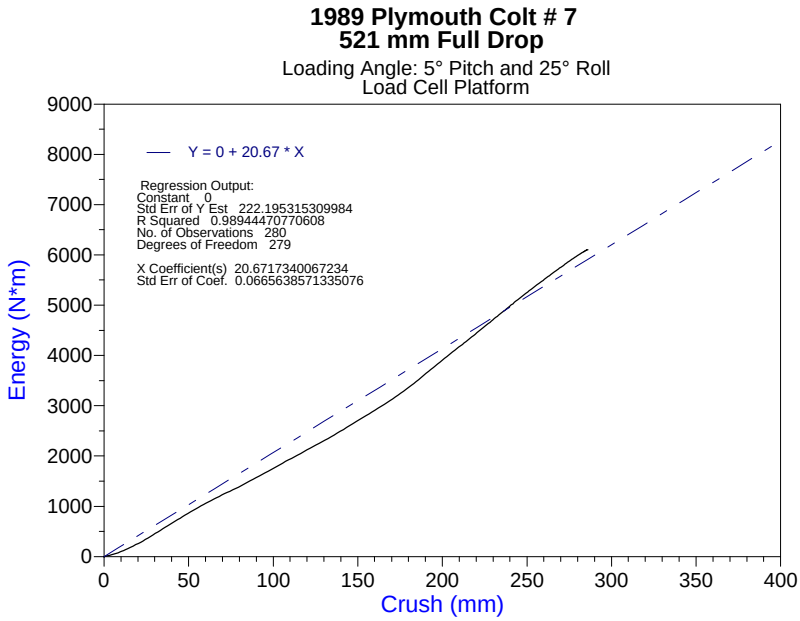


**Figure E(4)-** Plymouth Colt #7 load plate drop test energy/crush curve.

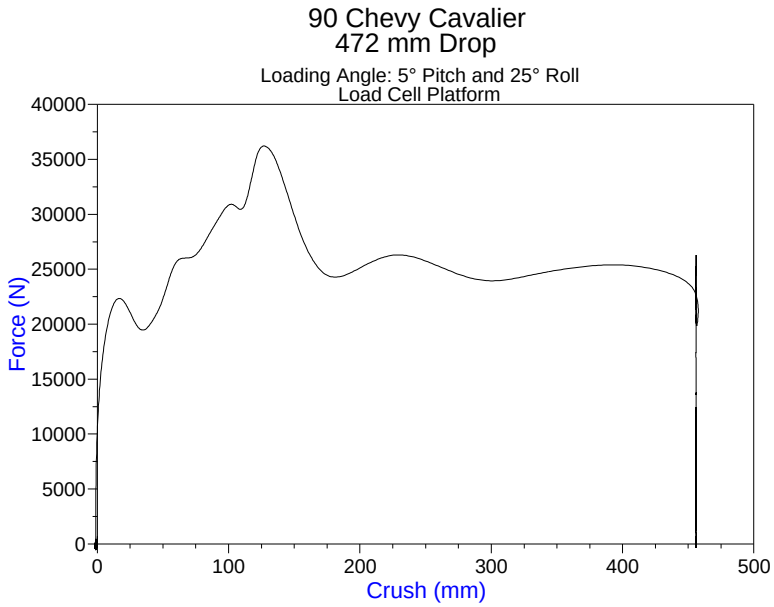


**Figure E(5)**-Chevy Cavalier #2 load plate drop test force/crush curve.

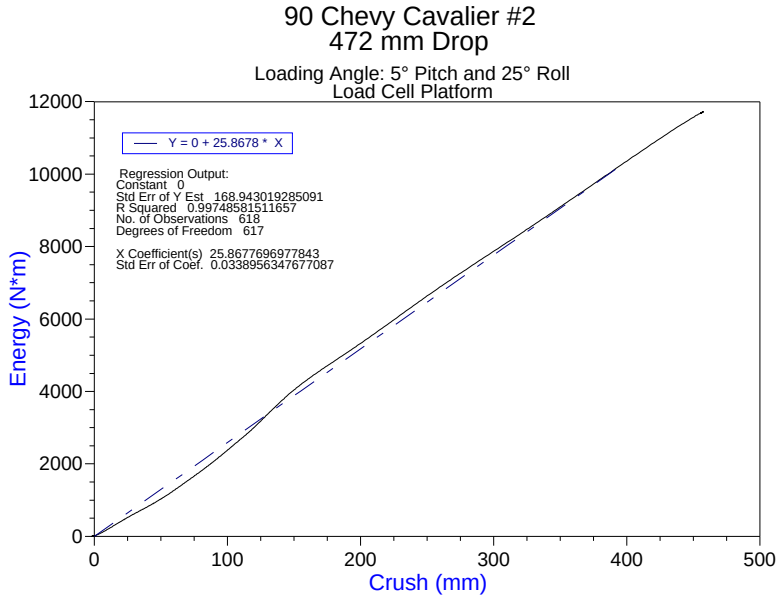


**Figure E(6)**-Chevy Cavalier #2 load plate drop test energy/crush curve.

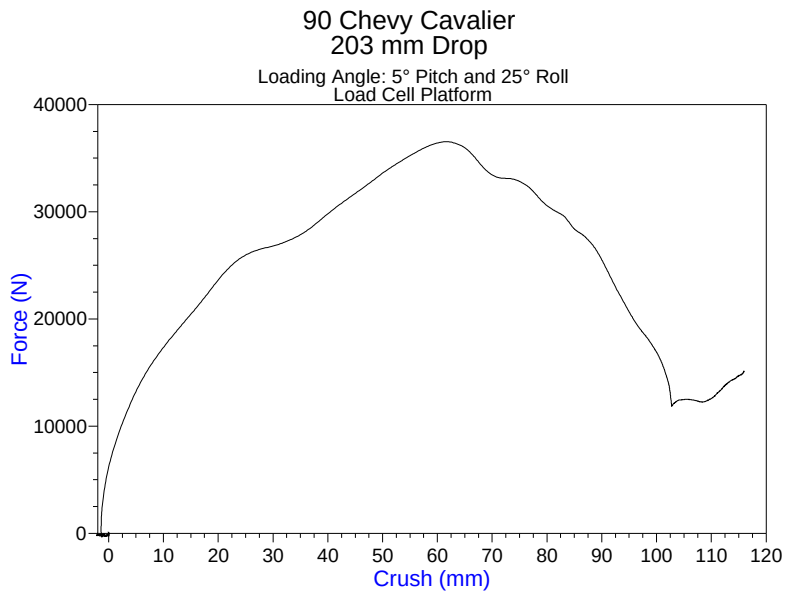


**Figure E(7)**-Chevy Cavalier #3 load plate drop test force/crush curve.

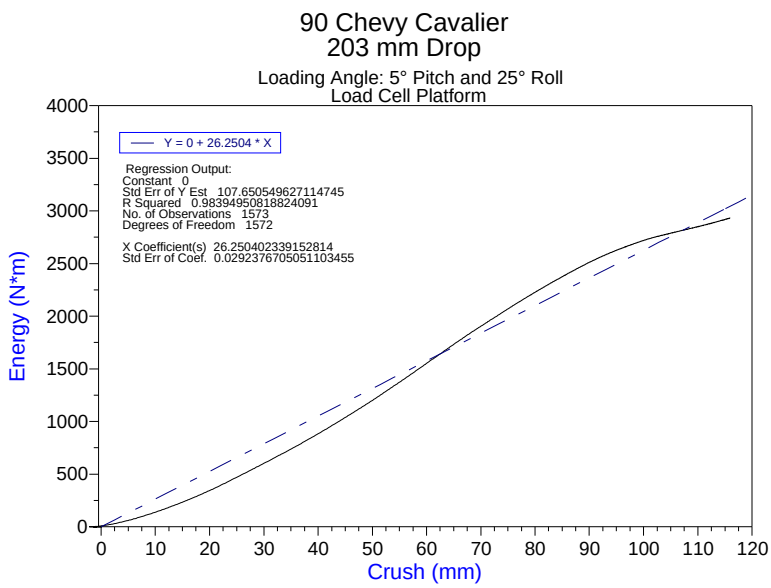


**Figure E(8)**-Chevy Cavalier #3 load plate drop test energy/crush curve.

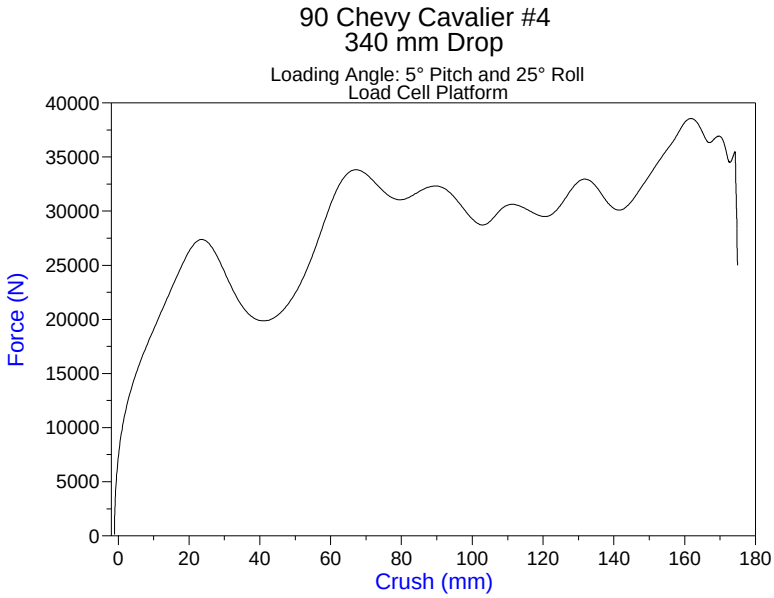


**Figure E(9)**-Chevy Cavalier #4 load plate drop test force/crush curve.

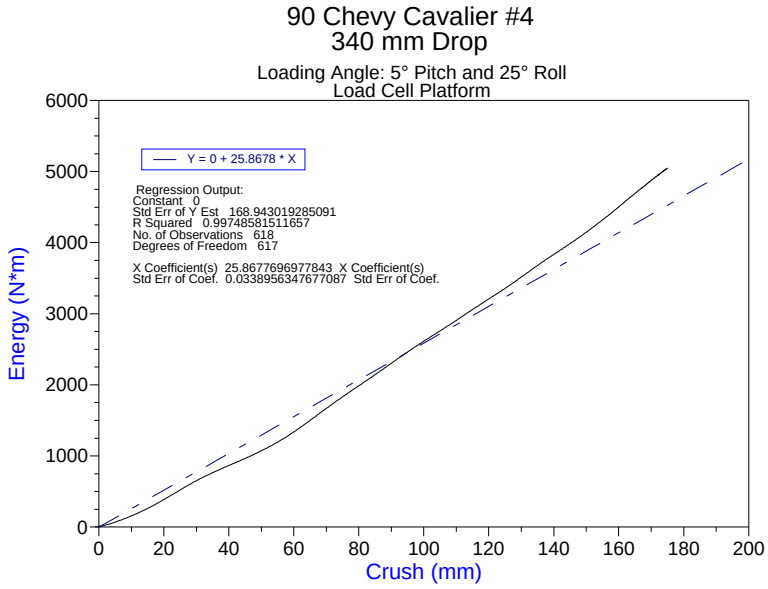


**Figure E(10)**-Chevy Cavalier #4 load plate drop test energy/crush curve

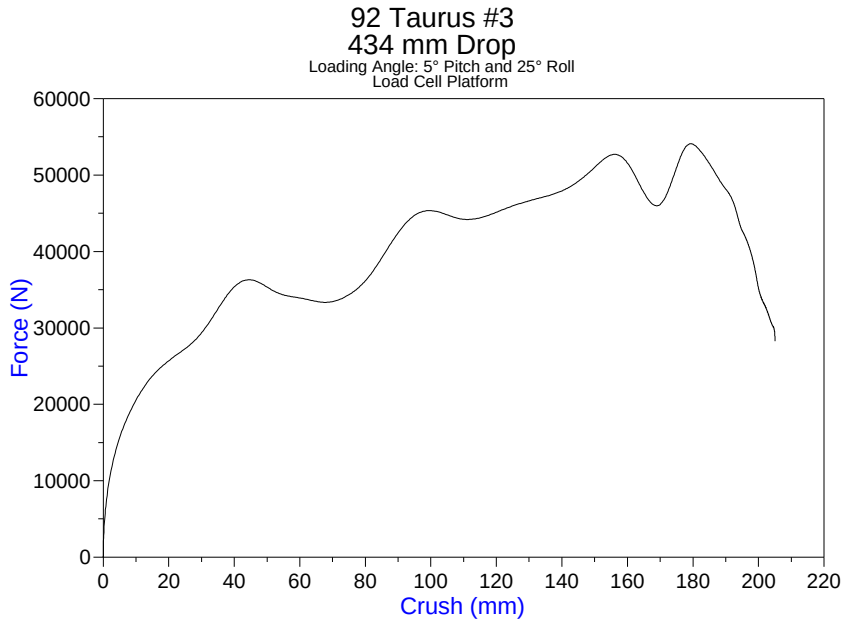


**Figure E(11)**-Ford Taurus #3 load plate drop test force/crush curve.

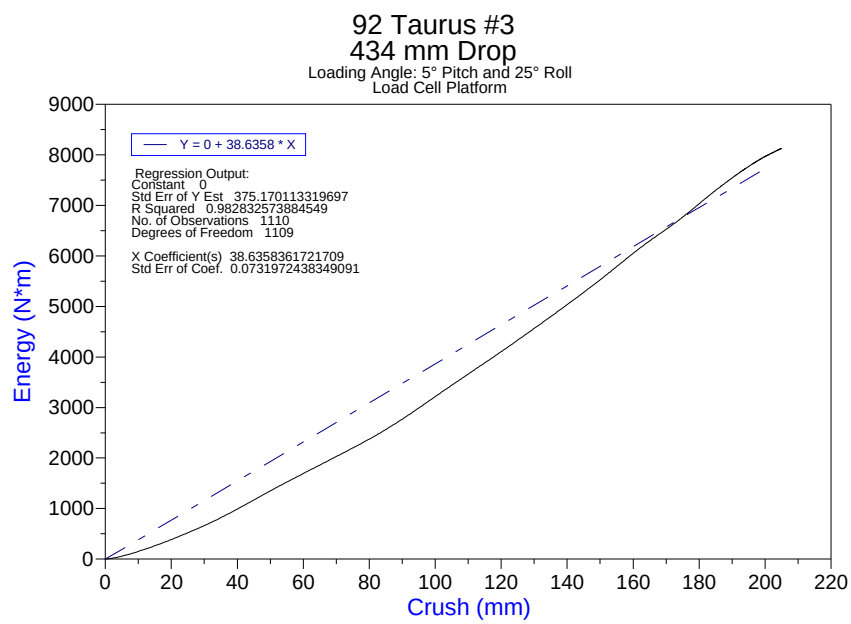


**Figure E(12)**-Ford Taurus #3 load plate drop test energy/crush curve.

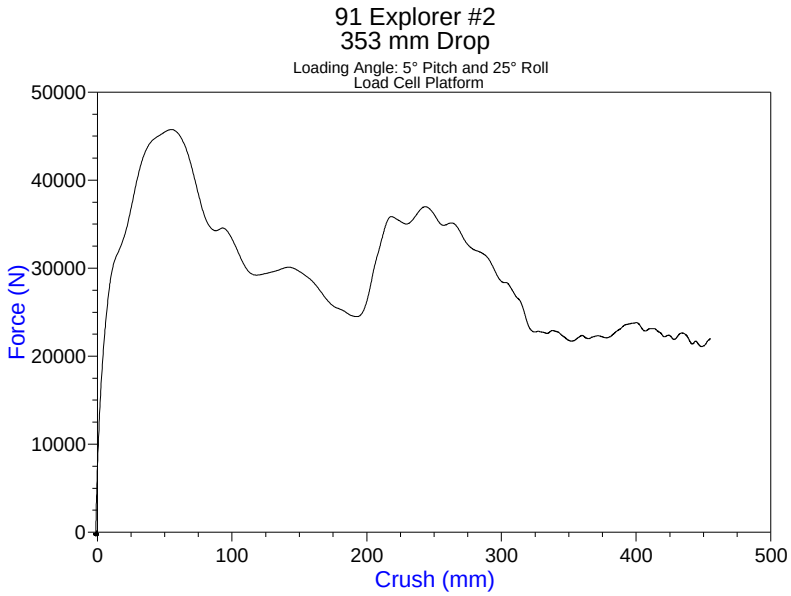


**Figure E(13)**-Ford Explorer #2 load plate drop test force/crush curve

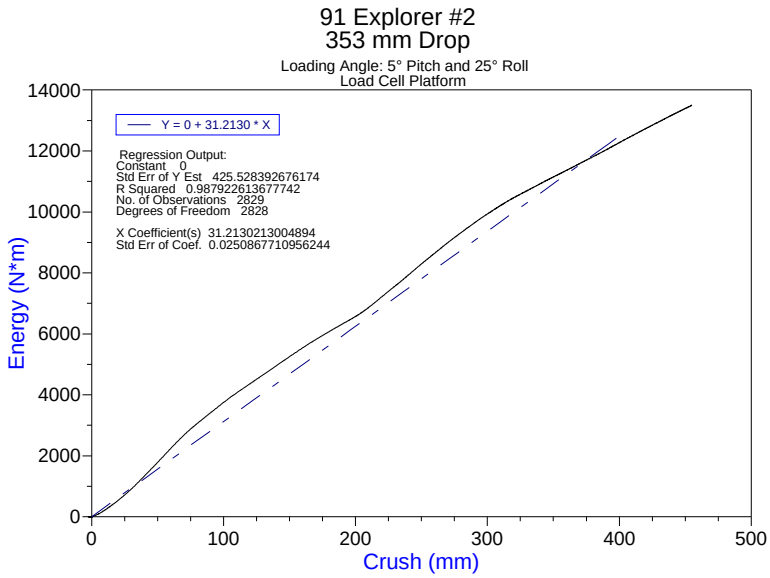


**Figure E(14)**-Ford Explorer #2 load plate drop test energy/crush curve.

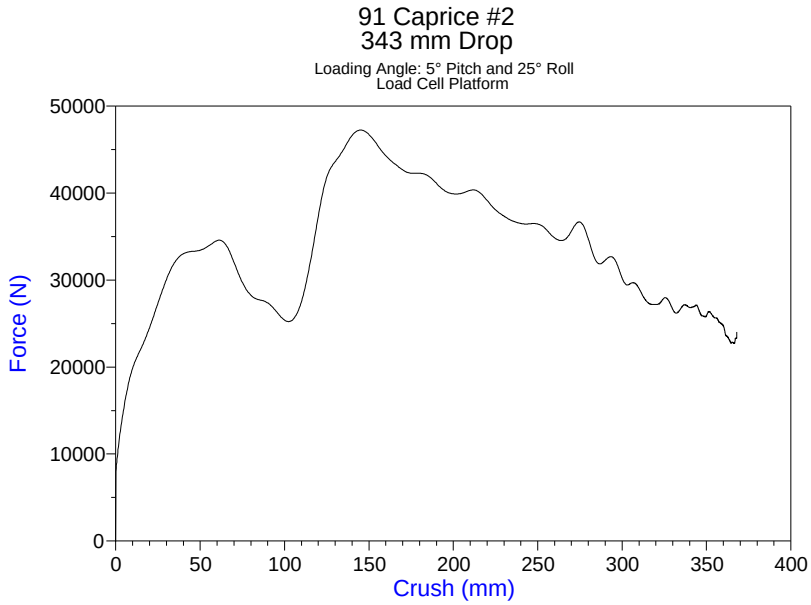


**Figure E(15)**-Chevy Caprice #2 load plate drop test force/crush curve.

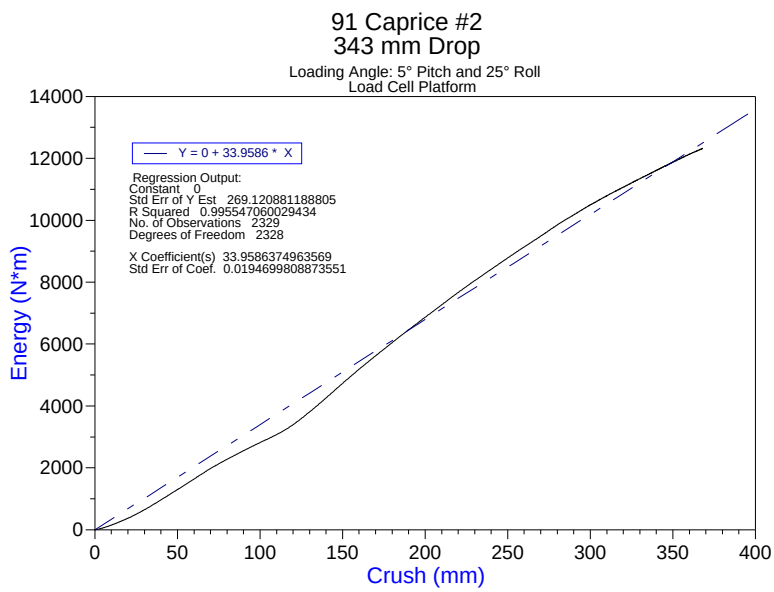


**Figure E(16)**-Chevy Caprice #2 load plate drop test energy/crush curve.

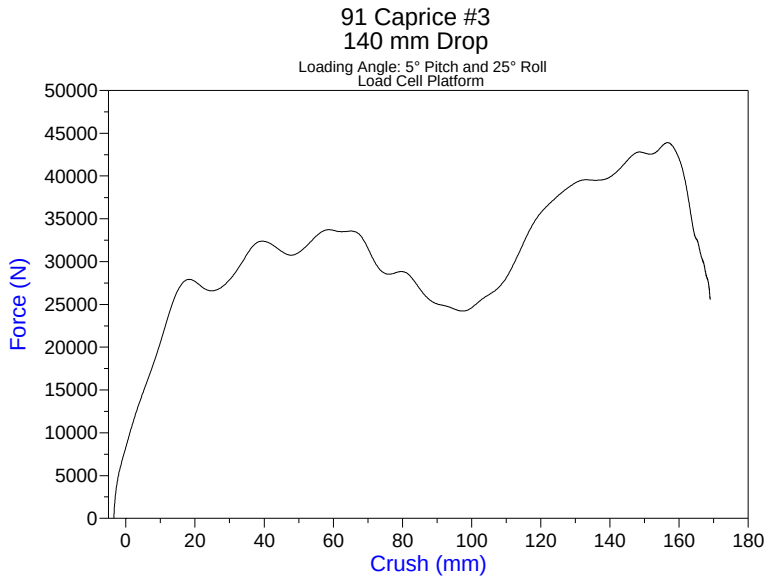


**Figure E(17)**-Chevy Caprice #3 load plate drop test force/crush curve.

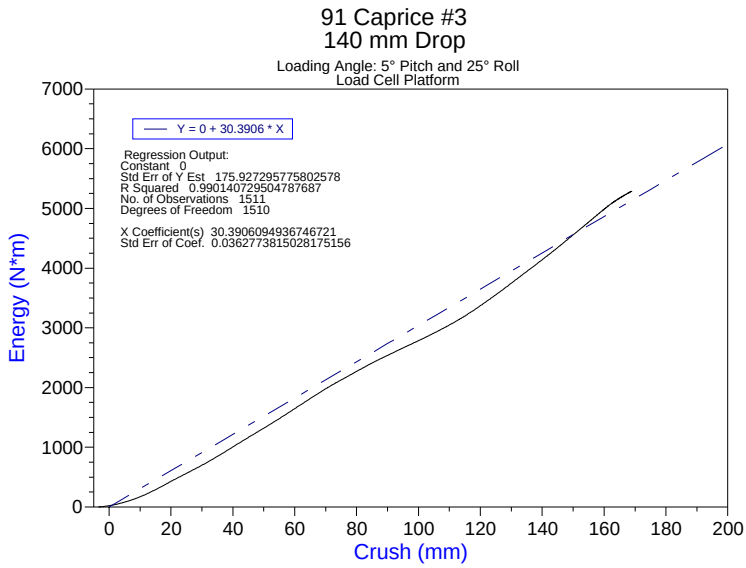


**Figure E(18)**-Chevy Caprice #3 load plate drop test energy/crush curve.

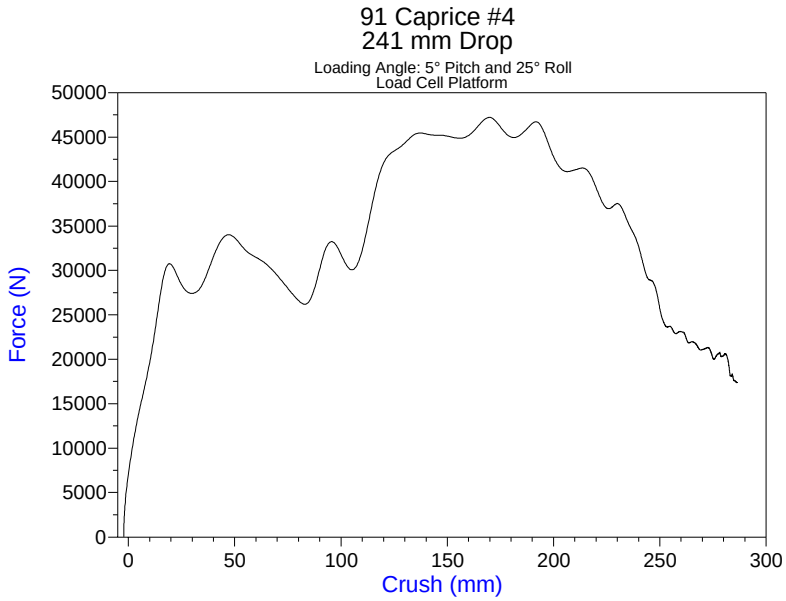


**Figure E(19)**-Chevy Caprice #4 load plate drop test force/crush curve.

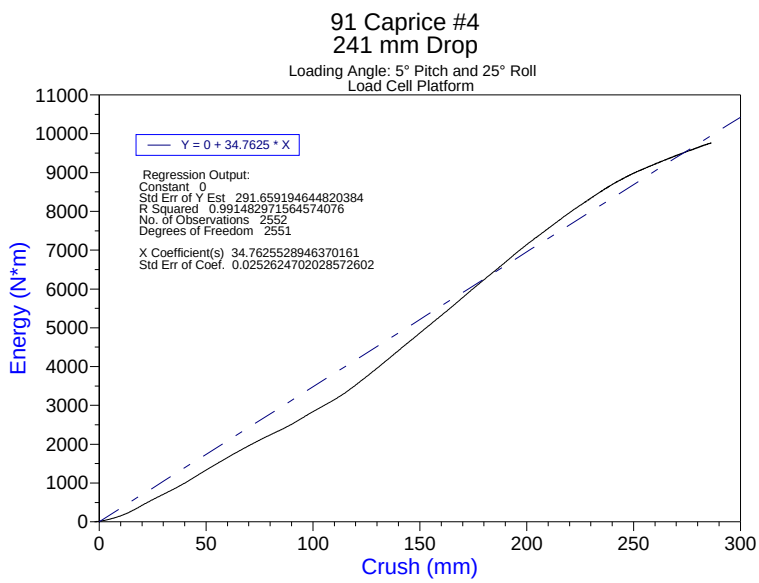


**Figure E(20)**-Chevy Caprice #4 load plate drop test energy/crush curve.

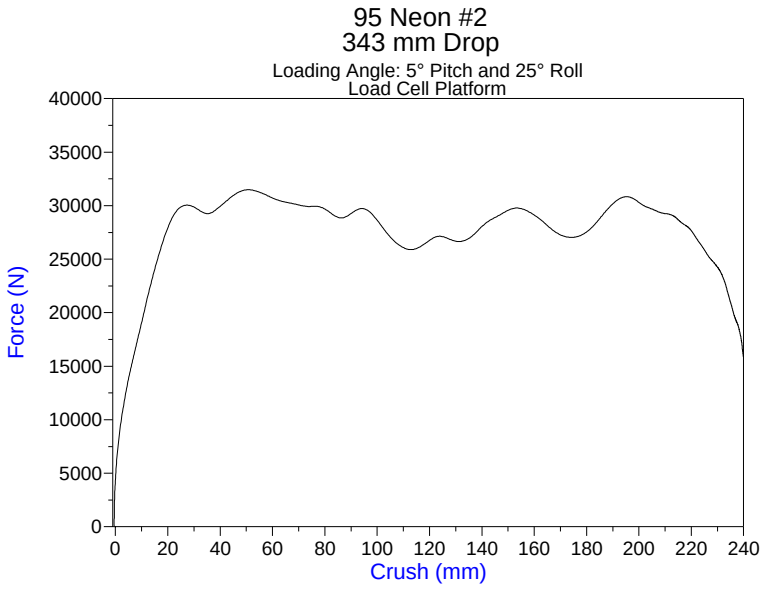


**Figure E(21)-** Plymouth Neon #2 load plate drop test force/crush curve.

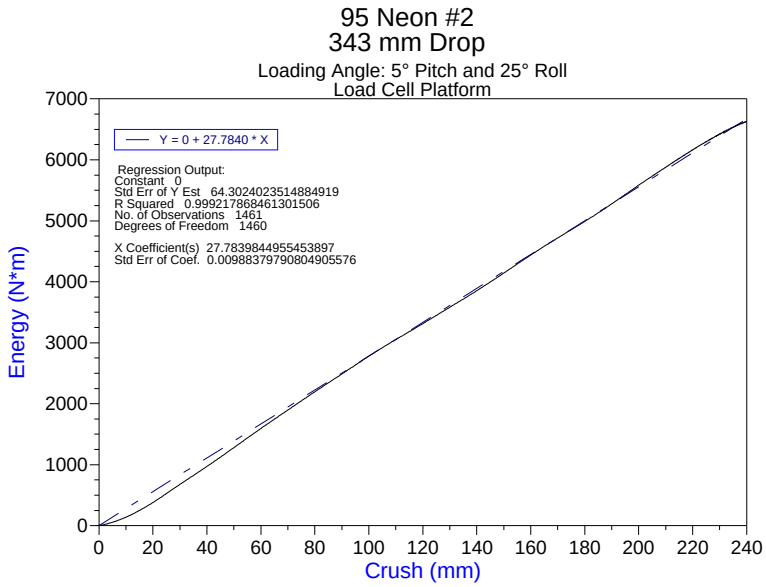


**Figure E(22)-** Plymouth Neon #2 load plate drop test energy/crush curve.

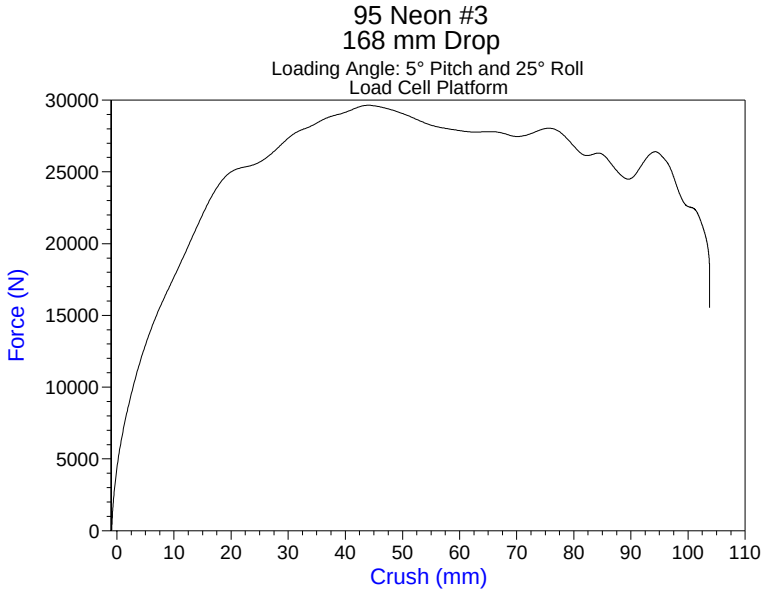


**Figure E(23)-** Plymouth Neon #3 load plate drop test force/crush curve

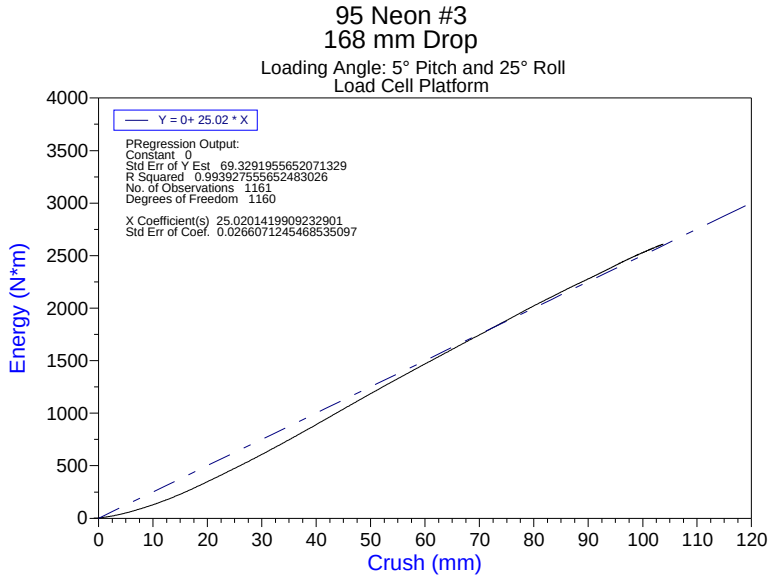


**Figure E(24)-** Plymouth Neon #3 load plate drop test energy/crush curve